# TECHNISCHE UNIVERSITÄT MÜNCHEN

**Pankreas-Forschungslabor/Chirurgische Klinik und Poliklinik**

**Klinikum rechts der Isar**


## Anterior gradient 2 promotes PDAC progression by directing RNA polymerase II nuclear import


Zhiheng Zhang


Vollständiger Abdruck der von der Fakultät für Medizin der Technischen Universität München zur Erlangung des akademischen Grades eines Doktors der Medizin genehmigten Dissertation.

Vorsitzender: Prof. Dr. Jürgen Schlegel

Prüfer der Dissertation:

1. Prof. Dr. Helmut Friess
2. Prof. Dr. Hana Algül


Die Dissertation wurden am 06.04.2020 bei der Technischen Universität München eingereicht und durch die Fakultät für Medizin am 06.10.2020 angenommen.

# Table of Contents

## ABSTRACT

Agr2 (anterior gradient 2) encodes an oncogenic endoplasmic reticulum (ER)-resident protein disulfide isomerase that is universally expressed by human adenocarcinomas. Pancreatic ductal adenocarcinoma (PDAC) is a devastating disease. So far, the function of Agr2 in PDAC is not fully uncovered. We used a well-established mouse model of caerulein-induced pancreatitis and inflammation-accelerated $Kras^{G12D}$-driven PDAC. The dynamic formation of acinar-to-ductal metaplasia (ADM) and pancreatic intraepithelial neoplasia (PanIN) was quantified using immunohistochemistry. To study the function of Agr2 in carcinogenesis, a mouse model with either conditionally ablated or over-expressed Agr2 in pancreatic epithelial cells was used. A set of *in vitro* biochemical assays was carried out to investigate the potential molecular mechanisms. Hereby, we observed that p53 is transiently suppressed during the phenotypic progression from ADM to PanIN lesions. Agr2, a putative p53 inhibitor, is found to be responsible for p53 suppression, as the pancreas-specific Agr2 ablation inhibits this phenotypic progression with concomitant p53 activation while the pancreas-specific Agr2 overexpression impairs p53 activation. Mechanistically, Agr2 binds to Polr2a (RNA polymerase II subunit a), which is the catalytic subunit of the RNA polymerase II (Pol II). As such, Agr2 directs Pol II nuclear import via its C-terminal nuclear localization signal. Loss of Agr2 function causes inadequate Pol II activation, and the resulting transcriptional stress activates p53 in an ATR-dependent manner. Compellingly, it dramatically sensitizes PDAC cell lines with wild-type TP53 to a specific Pol II inhibitor: $\alpha$-amanitin. In summary, the Agr2/Pol II axis constitutes a reasonable target for PDAC containing wild-type p53.

# 1.0 INTRODUCTION

## 1.1 Pancreatic cancer

The pancreas comprises exocrine and endocrine glands which are located in the abdominal cavity. The exocrine gland consists of acinar, ductal, and Centro-acinar cells that synthesize and secrete digestive enzymes (Bardeesy and DePinho 2002, Hezel et al. 2006). The endocrine pancreatic compartment contains five specialized cell types: glucagon-producing α-cells, insulin-producing β-cells, somatostatin-producing δ-cells, pancreatic polypeptides-producing PP-cells, and ghrelin-producing ε-cells. These cells in endocrine pancreatic compartment synthesize hormones which synthesize hormones to regulate metabolism and glucose homeostasis (Bardeesy and DePinho 2002, Hezel et al. 2006).

Depending on cell origin, several types of pancreatic cancers including acinar cell carcinoma, endocrine neoplasm carcinoma, and pancreatic ductal adenocarcinoma (PDAC) have been defined (Aichler et al. 2012). PDAC is one of the deadliest among them. The overall median survival is only six months after first diagnosis, and rate of the 5-year survival remains as low as 7% due to the extraordinary therapeutic resistance, early metastasis, and late detection (Nevala-Plagemann et al. 2020). Most PDAC cases have developed into an advanced stage at the time of diagnosis, with only 20% of patients being eligible for initial therapy (Singhi et al. 2019). The rate of early diagnosis has not been improved during the past 20 years despite intensive efforts have been made. Thus, many patients lose a chance of surgical operation (Nevala-Plagemann et al. 2020). To improve diagnosis and prognosis in patients with PDAC, a better understanding in the molecular mechanisms of pancreatic carcinogenesis is necessary.

### 1.1.1 Epidemiology of PDAC

PDAC ranked as the 7$^{th}$ highest cause of cancer mortality with estimated 458,918 new cases diagnosed in 2018 and associated 432,242 deaths in the same year

(McGuigan et al. 2018). PDAC is predicted to be the second most common cause of cancer-related death in America by 2030 (Singhi et al. 2019). The incidence of PDAC varies significantly between regions and populations. People from European countries (7.3 per 100000 people) and North America (7.4 per 100000 people) have the highest age-standardized incidence. In comparison, people in Africa and South-Central Asia (about 1.0 per 100000 people) have the lowest incidence (Ilic and Ilic 2016). The incidence of PDAC is 37.5% higher in men (5.5 per 100000 people) than women (4 per 100000 people) (McGuigan et al. 2018). In the meantime, PDAC is a typically age-related disease, with 90% of newly diagnosed patients being 55 years and older (Midha et al. 2016).

### 1.1.2 Pathology of PDAC

In general, the majority of PDACs are located in the head pancreas, while tumours located at body and tail are rare (Haeberle and Esposito 2019; Klimstra et al. 2009). PDAC is characterized by the presence of an extensive stroma compartment which mainly comprises fibroblast, pancreatic stellate cells (PSCs), and extracellular matrix (ECM) proteins as well as multiple types of inflammatory cells, including macrophage, endothelial cells, pericytes, and nerve fiber (Hosein et al. 2020). The existence of extensive stroma compartment can cause poor clinical outcome by promoting tumor growth, raising risk of metastasis, and introducing drug resistance (Hosein et al. 2020). Moreover, perineural invasion and vascular are considered as essential factors leading to pain generation, local recurrence, and poor outcome in patients with PDAC (Bapat et al. 2011). Invasive PDAC is also characterized by a high degree of intertumoral cellular and morphological heterogeneity.

### 1.1.3 Developing of neoplastic precursor lesions and genetic mutations

PDAC develops from precursor lesions to advanced malignancy. The precursor lesions include pancreatic intraepithelial neoplasia (PanIN), mucinous cystic neoplasm (MCN), and intraductal papillary mucinous neoplasm (IPMN) (Hruban et

al. 2004). Among these precursor lesions, the PanIN lesions account for more than 90% of precursor lesions and can be subclassified into PanIN1a, PanIN1b, PanIN2, and PanIN3. This morphological progression of PanIN correlates with genetic and epigenetic alterations which are crucially involved in the malignant transformation to PDAC. The point mutations of KRAS (Kirsten rat sarcoma two viral oncogene homolog) are the most common (more than 90%) genetic alterations in PanIN1a and PanIN1b (Caldas and Kern 1995). The activation and overexpression of the ERBB2, epidermal growth factor receptor (EGFR) also occur in PanIN1a and PanIN1b (Bardeesy and DePinho 2002). The loss of function in p16/INK4A can be detected later than KRAS mutation, but the frequency is increasing with the progression of PanIN (PanIN1a:30%, PanIN1b:55%, PanIN2 and PanIN3: 92%) (Day et al. 1996). However, PanIN lesions induced by chronic pancreatitis show rare p16 loss of function (Rosty et al. 2003). Inactivation of TP53, SMAD4/DPC4, and BRCA2 tumour suppressor are also observed in the PanIN3 stage (Bardeesy and DePinho 2002). SAMD4/DPC4 deletion is found around 50% of PDACs, while TP53 mutations can be found in 50-75% of PDACs (Redston et al. 1994).

### 1.2 Current therapeutic methods of PDAC

At present, PDAC treatment includes surgical resection, chemotherapy, radiation therapy, and palliative care (Kamisawa et al. 2016). The selection of treatment depends on the stage of PDAC. Comparing with other treatment options, surgical resection is the only curable treatment and can extend disease-free survival significantly (Kamisawa et al. 2016). Based on the degree of local invasion, PDAC can be divided into three categories: resectable, borderline resectable, and locally advanced. Although surgery can effectively remove the tumour, the 5-year overall survival rates are still around 20% after the operation (Smeenk et al. 2005). To obtain better local control and to improve the survival of PDAC, chemotherapy is combined with surgery, called adjuvant chemotherapy. Adjuvant chemotherapy with gemcitabine significantly improve the survival rate of patients with resected

PDAC (Kondo et al. 2012).

However, approximately 80% of patients are firstly diagnosed with locally advanced and metastasized pancreatic cancer; these patients only have palliative care options to relieve disease-related symptoms (Maitra and Hruban 2008). For example, gemcitabine-based chemotherapy can be given to retard PDAC progression. The combination of gemcitabine and erlotinib, an orally EGFR inhibitor, has been reported to extend progression-free survival and overall survival compared with gemcitabine alone (6.24 months versus 5.91 months); Subgroup analysis of patients with grade 2 or higher skin rash has a better median survival rate benefit (Saif et al. 2008). A regimen called FOLFIRINOX was shown to improve survival compared with gemcitabine, but this regimen is only recommended for patients who are older than 75 years (Kamisawa et al. 2016). For locally advanced pancreatic cancer, there is no significant difference between chemotherapy at 16.5 months (95% CI, 14.5-18.5 months) and chemoradiotherapy at 15.2 months (95% CI, 13.9-17.3 months; hazard ratio [HR], 1.03; 95% CI, 0.79-1.34; P =0.83) (Hammel et al. 2016). In summary, despite of the benefit of gemcitabine and other regimens, novel effective treatments are still needed.

### 1.3 Genetically engineered mouse models of pancreatic cancer

Recently, genetically engineered mouse models (GEMM), which mimic sporadic tumour formation and carcinogenesis, have been developed. The conditional Cre/loxP-based models are the most prevalent GEMMs. The target gene will be activated or inactivated after the activation of Cre recombinase, which leads to the deletion of DNA sequence flanked by specific repeated short repeats (loxP sites). In the pancreas, there are three main epithelial-derived cell types: endocrine, exocrine and ductal (Magnuson and Osipovich 2013). To target the different pancreatic cell types, several different categories of pancreas-specific Cre-driver genes have been developed. As the single point mutation in codon 12 of KRAS

proto-oncogene has been characterized as a driver event during PDAC development; Specific expression of oncogenic $Kras^{G12D}$ induced by Cre/loxP system in pancreas recapitulates the whole spectrum of human PDAC pathologies, from ADM, low-grade PanINs, high-grade PanINs, to advanced PDAC (Hingorani et al. 2003, Collins et al. 2012). Additional genetic changes (e.g. TP53, INK4a/ARF, and SMAD4) significantly accelerates the progression of PDAC (Aguirre et al. 2003, Bardeesy et al. 2006, Bardeesy et al. 2006). We recently characterized the natural course of caerulein-induced pancreatitis and defined three distinctive states termed inflammation, regeneration, and refinement. However, oncogenic Kras alone or in combination with caerulein-induced pancreatitis are not sufficient to initiate early precursor lesions of PDAC (Kong et al. 2018). Thus, we introduced ductal obstruction which induces a severe form of pancreatitis in mice with oncogenic Kras (Watanabe et al. 1995), and it causes a particular proliferative phenotype of oncogenic Kras-expressing ductal cells with nuclear atypia surrounded by proliferating activated fibroblasts and infiltration of immune cells, corroborating the pathological features of pre-neoplastic lesions. Lineage-tracing experiments revealed that these pre-neoplastic cells derived from two distinctive cellular sources: acinar and ductal cells (Cheng et al. 2019).

### 1.4 Anterior Gradient 2 in cancer

Anterior gradient 2 (AGR2) was first identified as a critical gene that is involved in Xenopus laevis forebrain and mucus-secreting cement gland development (Sive et al. 1989). AGR2 is a member of the protein disulfide isomerase (PDI) gene family of endoplasmic reticulum-resident proteins, which contains the thioredoxin-like domain CXXS (Persson et al. 2005). Those active motifs can form mixed disulfides with intestinal mucin. A previous study confirmed that AGR2 interacts with MUCIN2 (MUC2) in the endoplasmic reticulum (ER) of intestinal epithelial cells, which indicate a role in protein folding (Park et al. 2009). AGR2 facilitates protein folding, maturation and translocation in ER, thus maintaining ER homeostasis. (Brychtova

et al. 2011). In addition to its classic thioredoxin fold, other structure-function features of AGR2 are emerging. There is an ER-leader sequence in N-terminus of AGR2, and the C-terminus contains an ER-retention site. There are additional peptide motifs that have an impact on its protein-protein interactions. AGR2 can form a homodimer which is stabilized by an EALYK motif from amino acids 60-64 (Patel et al. 2013), while an N-terminal stretch of amino acids from 21-40 are disordered and destabilize the dimer structure. The deletion of N-terminal from 40 amino acids significantly increases dimer stability (Patel et al. 2013). These results indicate that AGR2 exists in a monomeric state rather than a dimeric state.

### 1.4.1 Role of AGR2 in tumorigenesis

Malignant transformation of normal human tissues during carcinogenesis is associated with a dysregulated machinery of proteins. The involvement of AGR2 in protein maturation, which attenuates abnormal protein production and secretion, suggests its oncogenic role in the cancer initiation. Fessart and co-authors proved that AGR2 converts the non-tumour organoids into tumour organoids and boosts their growth speed (Fessart et al. 2016). AGR2 has been detected in putative precursor lesions of human and mouse pancreas. Furthermore, it has been shown that AGR2 induction precedes preneoplastic lesions formation (Dumartin et al. 2017). In the progression of lung adenomas into invasive mucinous adenocarcinomas, FOXM1 facilitates mucinous characteristics via transcriptionally activating AGR2, which facilitated carcinogenesis in the lung (Milewski et al. 2017). AGR2 expression is also strongly associated with markers of tumour differentiation in breast. (lower tumour grade, estrogen receptor) (Fritzsche et al. 2006). Li and co-authors have shown that AGR2 enhances IGF-1 induced carcinogenesis through interacting with ER-α during breast carcinogenesis (Li et al. 2016).

### 1.4.2 The biological function of AGR2 in cancer

AGR2 has been defined as an oncogene in several cancers. Overexpression of

AGR2 attenuates ultraviolet (UV) light-induced damage by silencing p53 transactivation activity; The deletion of 10 amino acids of the C-terminus of AGR2 inhibited colony survival (Pohler et al. 2004). In oesophageal adenocarcinoma cells, reduced AGR2 expression leads to colony growth inhibition and reduction in tumour xenograft size, highlighting the role of AGR2 in tumour growth and survival (Wang et al. 2008). Similarly, AGR2 silencing inhibits proliferation, invasion, and survival in pancreatic cancer through inhibiting ERK/AKT axis (Liu et al. 2018). In breast cancer, AGR2 knockdown induces cell death and inhibits cancer growth by modulating cyclin D1, estrogen receptor-alpha (Vanderlaag et al. 2010). Furthermore, extracellular recombinant AGR2 increases SK-UT-1 cell proliferation (Hrstka et al. 2017). Conditioned media without AGR2 shows decreased ability to stimulate pancreatic cancer proliferation when comparing with conditioned media with AGR2 (Ramachandran et al. 2008). Knockdown of AGR2 results in the accumulation of cells at the G (0)/G (1) phase and induction of cellular senescence in pancreatic cancer cell lines through elevating γH2AX and inhibition of PI3K/Akt signalling (Hu et al. 2012). In conclusion, AGR2 exhibits dual effects on cell death differing in a variety of cancers.

Increasing evidence shows that AGR2 is essential for the sensitivity of chemo-treatment in cancer cells. patients with breast cancer showing increased AGR2 expression display decreased response to tamoxifen treatment and poor progression-free survival (Hrstka et al. 2013). In hypoxia-induced doxorubicin resistance MCF-7 cancer cells, the knockdown of AGR2 re-sensitizes cells to doxorubicin treatment by binding and stabilizing HIF-1α (Li et al. 2015). A similar result has been observed in another study, in which AGR2 is elevated in fulvestrant-resistant MCF-7cell lines, and silencing of AGR2 significantly increases p27Kip1, p21Waf1/Cip1, and p53 expression and facilitates the fulvestrant-induced ER-α degradation resulting in cell cycle arrest and ER-α pathway activation (Li et al. 2016). In pancreatic cancer cell lines, AGR2 knockdown results in inhibition of the

ERK/AKT axis and reduces chemotherapy resistance (Liu et al. 2018). Taken together, AGR2 is involved in the chemoresistance of human malignancy.

Recent data confirmed that AGR2 could bind to certain oncogenic proteins. AGR2 has been validated to interact with hexametric molecular chaperone and AAA+ superfamily protein Reptin(Rosenbaum et al. 2013). AGR2 also binds to Reptin through a divergent hydrophobic motif (amino acids 104-111), which can be promoted by the deletion of the N-terminal domain of AGR2 (Maslon et al. 2010, Healy et al. 2015). AGR2 protein has been screened for peptide binding aptamers using peptide-phage libraries resulting in the acquisition of two types of peptides that bind to different domains on the protein (Murray et al. 2007). Mohtae and co-authors revealed an AGR2 protein-peptide binding site consensus Tx[IL][YF][YF], which is harboured by several oncogenic proteins (e.g. EpCAM) of the human proteome. A single alanine mutation in EpCAM at the peptide-binding site attenuates its binding to AGR2 *in vitro* (Murray et al. 2007). These findings suggest that AGR2 protein binds to peptides/proteins in a sequence-specific manner. However, the mechanism of AGR2 in pancreatic carcinogenesis remains unclear.

## 2.0 Aims of this study

AGR2 is overexpressed in more than 90% of PDAC (Dumartin et al. 2017, Ferreira et al. 2017). As an ER-resident protein, AGR2 plays a vital role in regulating adaptive changes in cancer cells in response to cellular stress and promoting cell survival and metastasis. Clinical data showed that high AGR2 expression was correlated with unfavourable prognosis in PDAC (Brychtova et al. 2011). AGR2 has been proved as a potential p53 suppressor in Barrett's epithelium and breast cancer (Pohler et al. 2004, Hrstka et al. 2016). At least 28% of PDAC patients still carry wild-type p53, and therefore AGR2 may be a potential p53 target (Cancer Genome Atlas Research Network. Electronic address and Cancer Genome Atlas Research 2017). However, the biological functions of AGR2 in the p53 pathway are unclear. In this study, we aimed to investigate the role of Agr2 in pancreatic carcinogenesis by using *in vivo* and *in vitro* models. Thus, AGR2 deletion and overexpression $Kras^{G12D}$ mouse models were generated and analysed. Murine acini 3D culture and human PDAC cancer cell lines were used. Transcriptional profiling was performed to assess the changes in the pancreas caused by AGR2 deletion.

To this end, the following hypotheses have been formed:

Hypothesis 1: The gene program underlying organ regeneration is also essential for pancreatic carcinogenesis.

Hypothesis 2: AGR2 is essential for murine pancreatic carcinogenesis driven by $Kras^{G12D}$ and caerulein-induced inflammation.

Hypothesis 3: AGR2 plays an essential role in pancreatic carcinogenesis by regulating p53 pathway.

Hypothesis 4: The AGR2 peptide motif is critical for its function in pancreatic carcinogenesis.

Thus, the following questions shall be investigated in this present study:

(1) What is the effect of organ regeneration in early pancreatic carcinogenesis?

(2) What is the impact of AGR2 deletion on murine pancreatic carcinogenesis driven by $Kras^{G12D}$ and caerulein-induced inflammation?

(3) What is the molecular mechanism of AGR2 involvement in pancreatic carcinogenesis?

(4) What is the potential application of AGR2-based interference in pancreatic cancer?

# 3.0 MATERIAL AND METHODS

## 3.1 Material

### (1) Mouse lines

The wild-type (WT; C57BL/6J) mice were obtained from Charles River Laboratory (Sulzfeld, Germany). Ptf1α$^{CreERTM/+}$ (19378), p53$^{flox/flox}$ (00862), Loxp-STOP-Loxp-Kras$^{G12D}$ (LSL-Kras$^{G12D}$; 008179) and LSL-Rosa$^{CAG-tdTomato}$ (007914) obtained from Jackson Laboratory (Bar Harbor, USA). Agr2$^{flox/flox}$ line was obtained from EMMA (EM:04307). p48$^{cre/+}$; LSL-Kras$^{G12D/+}$ mice (hereafter referred to as “KC mice”) were generated by crossing a strain containing the Loxp-STOP-Loxp-Kras$^{G12D}$ (LSL-Kras$^{G12D}$; 008179) gene with mice carrying the pancreas-specific Cre recombinase Ptf1α$^{Cre/+}$ (also known as p48$^{Cre/+}$).

Mice with LSL-Rosa$^{CAG-Agr2}$ were obtained from Cyagen Biosciences (Santa Clara, US). Mouse genomic fragments containing homology arms (HAs) were amplified from BAC clone by using high fidelity Taq and were sequentially assembled into a targeting vector together with recombination sites and selection markers. The linearized vector was subsequently delivered to murine embryonic (ES) cells (C57BL/6) via electroporation, followed by drug selection, PCR screening, and Southern Blot confirmation. Positive clones were chosen for blastocyst microinjection, followed by chimera production. Founders were confirmed as germline-transmitted via crossbreeding with wild-type mice.

### (2) Antibodies

Primary antibodies

| Name | Catalog number | Application* (Reactivity**) | Producer |
|---|---|---|---|
| Rabbit Anti-p53 mAb# | 2524 | WB | Cell Signalling Technology (NEB, Frankfurt/Main, Germany) |

| | | | |
|---|---|---|---|
| Rabbit Anti-Rpb1 CTD (4H8) mAb# | 2629 | WB, IP | Cell Signalling Technology (NEB, Frankfurt/Main, Germany) |
| Rabbit Anti-Phospho-Rpb1 CTD (Ser2/5) (D1G3K) mAb# | 13546 | WB, IHC, IF | Cell Signalling Technology (NEB, Frankfurt/Main, Germany) |
| Phospho-p53 Antibody Sample Kit | 9919 | WB | Cell Signalling Technology (NEB, Frankfurt/Main, Germany) |
| Mouse Anti-Anterior Gradient 2 mAb# | Ab189361 | WB | Abcam |
| Rabbit Anti-Anterior Gradient 2 mAb# | PA585636 | IHC, IF, IP | Thermo Scientific |
| Mouse Anti-Gapdh mAb# | Sc-47724 | WB | Santa Cruz Biotechnology |
| Rabbit Anti-alpha Amylase mAb# | 3796 | WB, IHC, IF | Cell Signalling Technology (NEB, Frankfurt/Main, Germany) |
| Rat Anti-TROMA-III mAb# | 2133570 | IHC, IF | DSHB |
| Mouse Anti-Muc5ac mAb# | MA5-12178 | IHC, IF | Invitrogen |
| Rabbit Anti- | 700178 | IHC, IF | Invitrogen |

| | | | |
|---|---|---|---|
| Claudin18 mAb# | | | |
| Mouse Anti-BrdU (Bu20a) mAb# | 5292 | IHC, IF | Cell Signalling Technology (NEB, Frankfurt/Main, Germany) |
| Rabbit Anti-BrdU mAb | Ab152095 | IF | Abcam |
| Rabbit Anti-Tenascin C (D16C4) mAb# | 12221 | WB | Cell Signalling Technology (NEB, Frankfurt/Main, Germany) |
| Mouse Anti-p21 (WA-1) mAb# | Sc-51689 | WB | Santa Cruz Biotechnology |
| ATR Antibody mAb# | 2790 | WB | Cell Signalling Technology (NEB, Frankfurt/Main, Germany) |
| Phospho-ATR (Ser428) mAb# | 2853 | WB | Cell Signalling Technology (NEB, Frankfurt/Main, Germany) |
| Rabbit Anti-Cleaved Caspase-3 (Asp175) (5A1E) mAb# | 9664 | IHC | Cell Signalling Technology (NEB, Frankfurt/Main, Germany) |
| Rabbit Anti-Phospho-Histone H3 (Ser10) | 53348 | IHC | Cell Signalling Technology (NEB, Frankfurt/Main, |

| | | | |
|---|---|---|---|
| (D7N8E) mAb# | | | Germany) |
| Rabbit Anti-Phospho-ATR(Ser428) mAb# | 2853 | WB | Cell Signalling Technology (NEB, Frankfurt/Main, Germany) |
| Rabbit Anti-ATR (E1S3S) mAb# | 13934 | WB | Cell Signalling Technology (NEB, Frankfurt/Main, Germany) |
| Rabbit Anti-p-p53 (ser15) mAb# | 9248 | WB | Cell Signalling Technology (NEB, Frankfurt/Main, Germany) |
| Chicken Anti-GFP mAb# | Ab13970 | IF | Abcam |
| Rabbit Anti-GFP (D5.1) XP@ mAb# | 2956 | WB | Cell Signalling Technology (NEB, Frankfurt/Main, Germany) |

Secondary antibodies

| Name | Catalog number | Application (Reactivity) | Producer |
|---|---|---|---|
| Rabbit HRP (horseradish peroxidase)-labelled Anti-Rat IgG Ab# | P0450 | IHC (M) | Dako Deutschland GmbH (Hamburg, Germany) |
| Goat HRP- | K4001 | IHC (M) | Dako |

| | | | |
|---|---|---|---|
| Labelled Polymer Anti-Mouse Ab# | | | Deutschland GmbH |
| Goat HRP-Labelled Polymer Anti-Rabbit Ab# | K4003 | IHC (M) | Dako Deutschland GmbH |
| Sheep HRP-labelled Anti-Mouse IgG Ab# | NA931 | WB (M) | GE Healthcare (Little Chalfont, UK) |
| Donkey HRP-labelled Anti-Rabbit IgG Ab# | NA934 | WB (M) | GE Healthcare (Little Chalfont, UK) |
| Goat Alexa Fluor 488 Anti-Mouse IgG Ab# | 115-546-062 | IF | Dianova (Hamburg, Germany) |
| Chicken Alexa Fluor 594 Anti-Rabbit IgG Ab# | A-21442 | IF | Invitrogen |
| Goat Alexa Fluor 594 Anti-rat IgG Ab# | A-11007 | IF | Invitrogen |
| Goat Alexa Fluro 488 Anti-Chicken IgG Ab# | A-11039 | IF | Invitrogen |

*Application Key: WB=Western-blot; IP=Immunoprecipitation; IHC=Immunohistochemistry; **Reactivity key: M=Mouse; #Ab=antibody

**(3) siRNAs and primers**

Human siRNAs were purchased from QIAGEN (Hilden, Germany). All primers used in this study were produced by Sigma-Aldrich (Munich, Germany).

Sequences of siRNA used for gene-silencing experiments:

| Name | Catalog No. | Antisense (5'-3') |
|---|---|---|
| AGR2-siRNA1 | SI04939074 | TTCTGAGTTAGCAACAAGTAA |
| AGR2-siRNA2 | SI04939067 | AAGCTCTATATAAATCCAAGA |
| p53-siRNA1 | SI02623747 | CAGCATCTTATCCGAGTGGAA |
| p53-siRNA2 | SI00011655 | CAGAGTGCATTGTGAGGGTTA |
| ATR-siRNA1 | SI00023114 | TAGCCTATCCTCAACAAGCAA |
| ATR-siRNA2 | SI02664347 | TAGTGACATCTTCTTATTGCAT |
| Control-siRNA | 1022076 | AATTCTCCGAACTGTTCACGT |

Sequences of primers used for qRT-PCR analysis of mouse genes:

| Name | Sense (5'-3') | Antisense (5'-3') |
|---|---|---|
| Agr2 | AGGACTCTCGGCCCAAACTA | GCTTGACTGTGTGGGCATTC |
| α-Amylase | CGAGAACTACCAAGATGCTG | TCCATCCCACTTGCGCATAA |
| Rbpjl | GTATCGAAGTCAGTGGCGGT | GCAGGCTCAGGTGAGTCAAA |
| Krt19 | CCGAGGTCGCCGTCCACTCTGAGCA | GCGTGCCTTCCAGGGCAGGG CAGCTTTCATGC |
| Rbpj | ACTGTAAGTGCCACTGCGAA | ACAACGGAACTGCAAACTGC |
| Try4 | AAGTCCCGCATCCAAGTGAG | CAAAGCTCAAGGTGTTGCCC |
| Ptf1α | TGCCACCATGAACAGTGAGG | GGAATGCGCACGGGTC |
| Ppib | GGAGCGCAATATGAAGGTGC | CTTATCGTTGGCCACGGAGG |
| Tp53 | CGAAGACTGGATGACTGCCA | GAAGCCATAGTTGCCCTGGT |
| Polr2a | CACTGTCATCACCCCTGACC | ATACTGGCTGTTTCCCCTGC |
| Polr2b | GCACCACCGATTGACCTACA | CGAAGGGGCACCATCTCTTT |
| Polr2c | CAGTGCGGATCACGGAACTC | GCGATGAAGACCCTCCGAAT |
| Polr2d | CGCTTCAGCCGGTTCAAAAA | AGTCTCCGGGCAAAGATTGG |
| Polr2e | ACATGGCCCCGAAGTATGTG | ATCGAGCCAGCAGTTCAGTC |
| Polr2f | ATCCCCATCATCATTCGCCG | ATGATAAGCTCGTCCACGCC |
| Polr2g | CATTTCCCTGGAGCACGAGA | GCTTCACCGTGTTGAGCAAG |

| | | |
|---|---|---|
| Polr2h | AGGTCTTGCAGCGAGTTACC | CAACTTCCGGATCGTTGGGA |
| Polr2i | GGTTCCGAAATCGGGAGTGA | ACCGAAGCTGCACCAAACTA |
| Polr2j | GGAGTACCCTGCTTCCGTTC | CGGAGAGGCCCTAAAGCAAT |
| Polr2k | ACTAAGGTTCCCAACGCCTG | GGGTGAGGGACTTTGTAGCC |
| Polr2l | GTAGCACACTCCTGCCATTTG | ACTCCCACATTTCATCGAGCA |

**(4) Plasmid preparation**

The human AGR2 expression vector (RC202023) and the POLR2A expression vector (RC216765) were purchased from Origene (Beijing, China). The POLR2A point mutation (POLR2A$^{Y1177A}$) plasmid and AGR2 partial deletion (AGR2$^{\Delta NSL}$) plasmid were obtained from Genechemo (Shanghai, China). In brief, For the construction of the DNA-plasmid encoding mutant AGR2 without NSL sequence (AGR2$^{\Delta NSL}$), the terminal NSL sequence peptide (138-174aa) was replaced by a stop codon. The template plasmid pCMV6-Entry-AGR2 was amplified by PCR using the following forward primer 5'-CGTCGACTGGATCCGGTACCGAGGAGATCTGCC-3' and reverse primer 5'-GACCGCGGCCGGCCGTTTAAACTTACAAAACTGTCAGAGATGGGTC-3'. The PCR was initialized for 30 seconds at 94℃, followed by an annealing/elongation phase of 22 cycles (94℃ for 30 seconds, 55℃ for 1 minute, 72℃ for the 30s). To generate the POLR2A$^{Y1177A}$ plasmid, the template plasmid pCMV6-Entry-POLR2A was amplified by PCR using the forward primer 5'-ATACCTGGTCACATCAATTGTATCCGTACCCAC-3' and reverse primer 5'-TCGAGCGGCCGCGTACGCGTGTTCTCCTCGTCAC-3'. The PCR was initialized for 30 seconds at 94℃, followed by an annealing/elongation phase of 22 cycles (94℃ for 30 seconds, 55℃ for 1 minute, 72℃ for 30s). All generated plasmids were controlled by nucleotide sequencing after mutagenesis.

**(5) Chemicals and Reagents**

| | |
|---|---|
| 0.25% trypsin/EDTA | Sigma-Aldrich Chemie GmbH (Munich, |

| | |
|---|---|
| | Germany) |
| Acetic acid | Merck Biosciences (Darmstadt, Germany) |
| Acetic anhydride | Sigma-Aldrich Chemie GmbH |
| Acrylamide solution | Carl Roth (Karlsruhe, Germany) |
| Agarose | Carl Roth |
| Albumin Fraction V (BSA) | Carl Roth |
| Ammonium persulfate (APS) | Sigma-Aldrich Chemie GmbH |
| Calcium chloride | Carl Roth |
| Cell lysis buffer (10X) | Cell signalling Technology |
| Chloroform | Merck Biosciences |
| Citric acid monohydrate | Carl Roth |
| Crystal violet | Carl Roth |
| Collagenase | Sigma-Aldrich Chemie GmbH |
| Dimethyl sulfoxide | Carl Roth |
| Diaphorase from Clostridium kluyveri | Sigma-Aldrich Chemie GmbH |
| Dulbecco's MEM | Sigma-Aldrich Chemie GmbH |
| ECL detection reagent | Amersham (Little Chalfont, UK) |
| Ethanol (absolute) | Carl Roth |
| Ethanol 100% | Apotheke TU München (Munich, Germany) |
| Ethanol 96% | Apotheke TU München (Munich, Germany) |
| Ethanol 70% | Apotheke TU München (Munich, Germany) |
| Ethanol 50% | Apotheke TU München (Munich, Germany) |
| Ethidium bromide | Carl Roth |
| Fetal bovine serum | Sigma-Aldrich Chemie GmbH |

| | |
|---|---|
| Formamide | Merck Bioscience |
| Glucose-6-phosphate Dehydrogenase | Sigma-Aldrich Chemie GmbH |
| Glycerol | Merck Biosciences |
| Glycine | Diagnostics |
| Haematoxylin | Merck Biosciences |
| HEPES | Carl Roth |
| Hydrochloric acid (5M) | Apotheke TU München (Munich, Germany) |
| Hydrogen peroxide (30%) | Carl Roth |
| Histo-wax | Leica (Wentzler, Germany) |
| Isopropanol | Carl Roth |
| Kaliumchlorid (potassium chloride) | Carl Roth |
| LB powder | Biolabs |
| SOC medium | Biolabs |
| LDS sample buffer (4X) | Thermo Fisher Scientific |
| L-Glutamine | Sigma-Aldrich Chemie GmbH |
| Liquid nitrogen | Tec-Lab |
| Liquid DAB & chromogen substrate | Dako Cytomation |
| Methanol | Merck Biosciences |
| Molecular weight marker | Thermo scientific |
| MOPS | Carl Roth |
| Dinatriumhydrogenphosphate | Merck Biosciences |
| Natives Repsol | VitaDor |
| Nitrocellulose membranes | GE Healthcare |
| Normal goat serum | Dako Cytomation |
| Para-formaldehyde | Apotheke TU München |
| Phosphate buffered saline (PBS) pH 7.4 | Sigma-Aldrich Chemie GmbH |
| Penicillin-Streptomycin | Sigma-Aldrich Chemie GmbH |

| | |
|---|---|
| Phosphatase inhibitor cocktail | Roche diagnostics |
| Protease inhibitor cocktail | Roche diagnostics |
| Proteinase K | Dako Cytomation |
| Resazurin sodium salt | Sigma-Aldrich Chemie GmbH |
| RNase/DNase-free water | Invitrogen (Karlsruhe, Germany) |
| Rotiphorese Gel 30 (37,5:1) | Carl Roth |
| Sodium borate | Merck Biosciences |
| Sodium chloride | Merck Biosciences |
| Sodium citrate | Merck Biosciences |
| Sodium phosphate | Merck Biosciences |
| Tamoxifen | Sigma-Aldrich Chemie GmbH |
| TEMED | Sigma-Aldrich Chemie GmbH |
| Thiazolyl Blue Tetrazolium Bromide (MTT) | Sigma-Aldrich Chemie GmbH |
| Tris base | Sigma-Aldrich Chemie GmbH |
| Triton X 100 | Carl Roth |
| Tween 20 | Carl Roth |
| PBS powder without $Ca^{2+}$, $Mg^{2+}$ | Biochrom AG (Berlin, Germany) |

**(6) Kits**

| | |
|---|---|
| BCA protein assay kit | Thermo Scientific |
| Qiagen DNA mini kit | Qiagen |
| QIAquick Purification Kit | Qiagen |
| QuantiTect Reverse Transcription Kit | Qiagen |
| RNeasy Plus mini kit | Qiagen |
| SYBR Green master kit | Qiagen |
| Plasmid mini kit | Qiagen |
| Plasmid midi kit | Qiagen |

**(7) Laboratory equipment**

| | |
|---|---|
| Analytic balance | METTLER (Giessen, Germany) |
| Balance | SCALTEC (Göttingen, Germany) |
| Biophotometer | Eppendorf (Hamburg, Germany) |
| Centrifuge | Eppendorf |
| Electrophoresis power supply | Invitrogen |
| Freezer -20℃ | LIEBHERR (Bulle, Switzerland) |
| Freezer -80℃ | Heraeus (Hanau, Germany) |
| Fluorescence reader | Promega |
| Luminescence reader | Promega |
| Microplate reader | Thermo Fisher Scientific |
| Microscope | LEICA (Wetzler, Germany) |
| Microwave oven | SIEMENS (Munich, Germany) |
| Mini-PROTEAN Tetra System | BIO-RAD |
| PH-meter | BECKMAN (Washington, DC, USA) |
| Printer | KYOCERA |
| Refrigerator 4℃ | COMFORT (Buller, Switzerland) |
| Roche Light-Cycler 480 | Roche |
| Roller mixer | STUART (Stone, UK) |
| Scanner | Canon (Tokyo, Japan) |
| Spectrophotometer | Thermo Fisher Scientific |
| SterilGARD Hood | Thermo Fisher Scientific |
| Thermomixer | Eppendorf |
| Vortex Mixer | NEOLAB (Heidelberg, Germany) |
| Water bath | LAUDA (Lauda-Koenigshofen, Germany) |
| Stereomicroscope | Zeiss |
| Tissue embedding machine | Leica |
| Tissue processor | Leica |

**(8) Consumables**

| | |
|---|---|
| Blotting paper | Whatman (Maidstone, Kent, UK) |
| Cell scraper | SARSTEDT (Nuembrecht, Germany) |
| Cell Strainer (100 µm) | FALCON (Durham, USA) |
| CRYO TUBE 20 | TPP |
| Filter (0.2 µm) | NEOLAB |
| Filter-tip (10 µl, 20 µl, 100 µl, 200 µl, 1000 µl) | Starlab |
| Hyper film | GE Healthcare |
| Pure Nitrocellulose membrane (0.45 µM) | BIO-RAD |
| Sterile needles | BD (Franklin Lakes, NL, USA) |
| SEROLOGICAL PIPPETTE (2 ml; 5 ml; 10 ml; 25 ml; 50 ml) | CELLSRAR |
| Tissue culture dishes (60x15 mm; 100x20 mm) | SARSTEDT |
| Tissue culture flasks (25 $cm^2$; 75 $cm^2$; 125 $cm^2$) | GREINER |
| Tissue culture plates (6-well; 24-well; 96-well) | GREINER |
| Tubes (15 ml; 50 ml) | GREINER |

**(9) Human cell lines**

Human pancreatic epithelial ductal cells (obtained from Kerafast) and four Human pancreatic cancer lines-Capan-2, HPAC, PANC-1, SU86.86 (obtained from ATCC, Wesel, Germany) were used for the experiments. DAN-G cell line was kindly provided by Prof. Schneider (Department of Internal Medicine, Technical University of Munich). HEK293 cell line was kindly provided by Prof. Jansson (Department of Surgery, Technical University of Munich).

**(10) Buffers and Solutions**

10x Tris Buffered Saline (TBS)

| | |
|---|---|
| NaCl | 85 g |
| Tris base | 12.1 g |

| | |
|---|---|
| Distilled water | 800 ml |
| Adjust pH to 7.4 with | 5 M HCl |
| Constant volume with distilled water to | 1000 ml |

20x Citrate buffer

| | |
|---|---|
| Citric acid (Monohydrate) | 21.0 g |
| Distilled water | 300 ml |
| Adjust to pH 6.0 with | 5 M NaOH |
| Constant volume with distilled water to | 500 ml |

Washing Buffer (1xTBS+0.1%BSA)

| | |
|---|---|
| 10xTBS | 100 ml |
| BSA | 1 g |
| Constant volume with distilled water to | 1000 ml |

Electrophoresis buffer

| | |
|---|---|
| MOPS | 209.2 g |
| Tris Base | 121.2 g |
| SDS | 20 g |
| EDTA-free acid | 6 g |
| Constant volume with distilled water to | 1000 ml |

Transfer Buffer

| | |
|---|---|
| Tris base | 29.1 g |
| Glycine | 14.7 g |
| Methanol | 1000 ml |
| SDS | 0.1875 g |
| Constant volume with distilled water to | 5000 ml |

Washing buffer

| | |
|---|---|
| 10xTBS | 100 ml |
| Tween 20 | 0.5 ml |
| Constant volume with distilled water to | 1000 ml |

LB medium

| | |
|---|---|
| LB powder | 12.5 g |
| Distilled water | 500 ml |

LB agar plate

| | |
|---|---|
| LB powder | 40 g |
| Distilled water | 1000 ml |

Blocking buffer

| | |
|---|---|
| Dry milk or BSA | 0.5 g |
| Washing buffer | 10 ml |

### 3.2 Methods

#### (1) Mouse breeding and collection of mouse tissue

Mouse breeding was performed at a specific pathogen-free (SPF) mouse facility at the Technical University of Munich. Mouse experiments were performed according to the German Federal Animal Protection Laws and were approved by the Institutional Animal Care and Use Committees of the government of Bavaria and the Technical University of Munich 55.2-1-54-2532-197-2016.

#### (2) Tamoxifen preparation and caerulein treatment

200 µl of ethanol and 1800 µl of autoclaved sunflower oil were added to 80 mg of tamoxifen (Sigma-Aldrich, T5648, St Louis, MO) to obtain 40 mg/ml tamoxifen suspension, followed by 5 minutes of sonication, then stored at 4℃ for a week or at -20℃ for long-term use. Transgenic mice were treated with Tamoxifen (100 µl) at 5-6 weeks of age through oral gavage every 48 hours, for a total of 3 doses over five days. Acute pancreatitis was performed as described previously (Kong et al. 2018). Briefly, 8-10 weeks old WT and transgenic mice were administrated through eight hourly intraperitoneal injections on two consecutive days. The mice in the control group were injected with 0.9% NaCl solution.

#### (3) Immunohistochemistry

Fresh tissues were preserved in 4% paraformaldehyde (PFA) for 24 hours, embedded in paraffin and cut into three µm thick sections. Tissue sections were deparaffinized in roti-clear solution and rehydrated in consecutive ethanol solution. Antigen retrieval was performed with citrate buffer (pH 6.0; 10mM Citric Acid) in a microwave oven for 15 minutes. Sections were incubated in deionized methanol containing 3% hydrogen peroxide at room temperature for 10 minutes and washed with TBS (pH 7.4; 0.1M Tris Base, 1.4M NaCl) containing 3% BSA. Then 10% goat serum was used to blocking of nonspecific reactivity. Sections were incubated with the antibody at 4℃ overnight. Afterward, sections were incubated with horseradish peroxidase-linked goat anti-rabbit or mouse secondary antibodies for 1 hour at room temperature followed by a colour reaction with diaminobenzidine and haematoxylin. Then, sections were dehydrated and mounted.

**(4) Quantification of the nuclear and cellular size of pre-neoplastic cells**

To define the nuclear and cellular size of pre-neoplastic cells, 1000-fold magnification images were acquired from PK-RFP ($p48^{cre/+}$; $Kras^{G12D/+}$; LSL-$Rosa^{CAG\text{-}tdTomato}$) and SK-RFP ($Sox9^{creERT2}$; $Kras^{G12D/+}$; LSL-$Rosa^{CAG\text{-}tdTomato}$) sections. The nuclear and cytoplasmic areas were calculated using the formula πab/4, where a is the longest diameter and b is the shortest diameter. At least 200 cells were measured. Two independent researchers (Tao Cheng; Zhiheng Zhang) counted the images using Image J software (National Institutes of Health, Maryland, US).

**(5) Pancreatic ductal ligation**

The pancreatic duct of 8-10 weeks old mice was ligated as previously described （Watanabe Satoshi et al. 1995）. Generally, mice underwent laparotomy through a midline abdominal incision. The splenic lobe of the wild-type mouse pancreas was ligated. This operation resulted in the obstruction of the pancreas. On each day, Buprenorphine (Temgesic; 1mg/kg body weight) was provided through

subcutaneous injection. Mice were sacrificed at given time points, and organs were collected 2 hours after BrdU injection.

**(6) Venn analysis**

Venn analysis was performed by BioVenn (http://www.biovenn.nl/index.php). Data from Microarray was uploaded to BioVenn. A: genes differentially expressed in wild-type inflammation (compared to wild-type control and wild-type regeneration). B: genes differentially expressed in Kras 3h-d14 (compared to Kras control). A=up: genes from group A but only up-regulated ones. A=down: genes from group A but only down-regulated ones. B=up: genes from group B but only up-regulated genes. B=down: down-regulated genes from group B. (A=up, B=up) & (A=down, B=down): genes that show the same pattern (up/down) in wild-type and Kras cohorts. (A=up, B=down) & (A=down, B=up): genes that show different patterns (up/down) in wild-type and Kras cohorts.

**(7) Co-immunoprecipitation**

For co-immunoprecipitation, tissues or cells were lysed in lysis buffer (50 mM Tris pH 7.4, 150 mM NaCl, 0.25% Na-deoxycholate, 0.5mM EDTA ,10 mM NaF, 0.5% NP-40), containing protease and phosphatase inhibitors. This was followed by centrifugation at 12,000x rpm for 15min. For all experiments, protein concentrations were determined (BCA kit, Pierce) and equal protein amounts were precleared with 15 µl PBS-equilibrated protein G or A beads for 2h at 4°C. The antibody was added and incubated overnight at 4°C while rotating. Afterward, 30 µl beads were added and incubated with rotation for 4h at 4°C. The beads were washed five times with 1 mL lysis buffer, and the SDS loading buffer was added to samples. After incubation at 95°, C for 10 min samples was run on SDS-PAGE followed by immunoblotting.

**(8) Quantitative real-time PCR**

Total RNA was extracted from cells or mouse pancreases tissue with a RNeasy Mini Kit according to the manufacture's protocol. Quantitative real-time PCR (QRT-PCR) was performed using the LightCycler$^{TM}$480 system with the SYBR Green 1 Master Kit (Roche Diagnostics, Penzberg, Germany). Expression of target genes and housekeeping gene Ppib (peptidylprolyl Isomerase B) were analysed.

**(9) Immunoblot**

Total cell protein was extracted by using cell lysis buffer (Cell Signalling Technology) with protease inhibitor and phosphatase inhibitor. Total tissue protein was extracted by using RIPA buffer containing protease inhibitor and phosphatase inhibitor. Protein concentration was determined by BCA protein assay kit. 20 µg protein was loaded onto 10% SDS-PAGE and electro-transferred to PVDF membranes. After incubation with 5% milk or 5% BSA, the membrane was incubated with first antibodies at 4℃ overnight. The membrane was washed and incubated with horseradish peroxidase (HRP)-conjugated secondary antibody at room temperature for 1 hour. Then, signals were detected with Amersham ECL Western Blotting Detection Reagent (GE Healthcare Life Sciences).

**(10) MTT assay**

For the determination of cell proliferation, 2000-5000 cells were seeded in 96 well plates. After 48 or 72 hours, 10ul Thiazolyl Blue Tetrazolium Bromide (MTT, Sigma-Aldrich) was applied to cells and incubated at culture conditions for 4 hours. After the addition of 100ul 2-propanol cell proliferation was determined by measuring absorbance values under 570nm.

**(11) Immunofluorescences**

Fresh tissues were preserved in 4% paraformaldehyde (PFA) for 24 hours, embedded in paraffin and cut into three µm thick sections. Tissue sections were deparaffinized in roti-clear solution and rehydrated in consecutive ethanol solution.

Antigen retrieval was performed with citrate buffer (pH 6.0; 10mM Citric Acid) in a microwave oven for 15 minutes. Sections were incubated in deionized methanol containing 3% hydrogen peroxide at room temperature for 10 minutes and washed with TBS (pH 7.4; 0.1M Tris Base, 1.4M NaCl) containing 3% BSA. Then 10% goat serum was used to blocking of nonspecific reactivity. Sections were incubated with the antibodies at 4℃overnight. Afterward, sections were incubated with secondary antibodies for 1 hour at room temperature.

**(12) Quantification**

For quantification, images were analysed with ImageJ software labelling all positive cells. Five non-overlapping images per animal were taken with a 20x objective lens using a microscope (Carl Zeiss, Munich, Germany). All images from the same experiment were quantified simultaneously to minimize quantification variation.

**(13) Cell culture**

Human cancer cell lines were cultured in DMEM or RPMI-1640 cell culture medium with 10% FBS, 100 μ/ml penicillin and 100 μg/ml streptomycin at 37°, 5% $CO_2$. HPAC cell line was cultured in complete growth medium containing 0.002 mg/ml insulin, 0.005 mg/ml transferrin, 40 ng/ml hydrocortisone, 10 ng/ml epidermal growth factor and 5% Fetal bovine serum.

**(14) Cell siRNA transfection**

Human siRNA oligonucleotides for AGR2, P53, ATR, and negative control siRNA were purchased from Qiagen (QIAGEN, Hilden, Germany). Transfections were carried out according to the manufacturer's instructions. Briefly, siRNA was diluted in culture medium without serum. Hiperfect transfection reagent was added to diluted siRNA and mixed by vortexing. Then, the complexes were added to the cells. The efficacy of siRNA was checked by immunoblot analysis after 72 hours of transfection.

**(15) Mouse acinar cell culture (3D-cultures)**

Mouse acinar cells 3D-culture was carried out as previously described. Briefly, whole pancreatic tissue was removed from the mouse, cut into small pieces with scalpel and collagenase (0.5 mg/ml Collagenase-P, Roche), filtered through a 100 µm nylon cell strainer (BD Biosciences), and washed three times with Hanks balanced salt solution. After centrifugation, the supernatant was removed, and acinar cells were re-suspended in Waymouth's MB 752/1 medium (Life Technologies GmbH) supplemented with 0.1 mg/ml soybean trypsin inhibitor (Sigma Aldrich), streptomycin, penicillin G, and 10% FBS, 20ug/ml dexamethasone (Sigma Aldrich), five mM HEPES (Life Technologies GmbH), and 0.13% $NaHCO_3$. After 24 hours, acinar cells were added to neutralized rat tail collagen type I (1.5 mg/ml, Corning). After solidification, cells were cultured until end time points were reached. Then, proteins or RNA were isolated.

**(16)RNA-sequencing and analysis**

Total RNA extracted from mouse pancreas by the Qiagen RNeasy Mini Kit. Library preparation for bulk 3′-sequencing of poly(A)-RNA was done as described previously (Parekh et al. 2016). Briefly, barcoded cDNA of each sample was generated with a Maxima RT polymerase (Thermo Fisher) using an oligo-dT primer containing barcodes, unique molecular identifiers (UMIs), and an adapter. The 5′ ends of the cDNAs were extended by a template switch oligo (TSO), and full-length cDNA was amplified with primers binding to the TSO-site and the adapter. cDNA was tagmented with the Nextera XT kit (Illumina) and 3′-end-fragments finally amplified using primers with Illumina P5 and P7 overhangs. In comparison to Parekh et al. the P5 and P7 sites were exchanged to allow sequencing of the cDNA in read1 and barcodes and UMIs in read2 to achieve better cluster recognition. The library was sequenced on a NextSeq 500 (Illumina) with 75 cycles for the cDNA in read1 and 16 cycles for the barcodes and UMIs in read2.

Annotations and the reference genome from the Gencode release M15 were derived from the Gencode homepage (https://www.gencodegenes.org/). Dropseq tool v1.12 was used for mapping the raw sequencing data to the reference genome. The resulting UMI filtered count matrix was imported into R v3.4.4, and differential gene expression analysis was conducted with DESeq2 (Love et al. 2014). A gene was called differentially expressed if the adjusted p-value was below 0.05, and the absolute log2 fold change was 0.7. Pathway analysis was conducted with EnrichR (Kuleshov et al. 2016) within the Reactome database. Pathways with an FDR-level of 0.05 were considered to be statistically significant. Gene level differences for genes being regulated between time points and located in selected pathways are shown as a heatmap.

P-values were adjusted with the Benjamini Hochberg procedure. We consider a gene set to be positively associated with a genotype at an FDR level of 0.1. Z-score transformed scores for pathways associated with genotype are displayed as a heatmap.

**(17) Micro-Array analysis**

Gene expression was recorded at different time points after caerulein injections in WT mice, $Kras^{G12D/+}$ mice and control samples in both mouse strains.

A model for differential expression in the wild-type inflammatory phase was generated. A gene was selected if its absolute fold change between the wild-type inflammatory phase samples and the wild-type control samples was higher or equal to 2, and the absolute fold change between the wild-type inflammatory phase samples and the wild-type regeneration phase samples was also higher or equal to 2. Samples from the refinement phase were not included due to the high intra-sample variance and the small number of samples. The analysis yielded a set of 365 genes (254 up-regulated; 111 down-regulated) with significant differential regulation (absolute FC > 2, adjusted $p < 0.05$) in the inflammation phase of Wild-type mice compared to control samples and regeneration samples (two

independent t-tests). As for the $Kras^{G12D}$ samples, the differential expression gene list was generated by comparing all $Kras^{G12D}$ samples (from 3 hours to day 14) treated with caerulein to controls (absolute FC > 2, adjusted p < 0.05).

**(18) Plasmid transformation and transfection**

100 µl of competent E. coli cells, thawed on the ice, were gently mixed with 1 µg of purified plasmid DNA. After 10 minutes of incubation in ice, cells were transferred to 42 ℃ for 50 seconds, followed by 2 minutes incubation on ice. 250 ul SOC medium was added to the cells and incubated at 37 ℃ for 1 hour while shaking. 30 µl of transformed cell suspension was pipetted onto LB agar plates with selection antibiotic and spread using the sterile spreader. Incubate LB agar plate at 37 ℃ overnight. Pick and transfer colonies into sterile polypropylene tubes with 2 ml LB medium and incubate in a shaker incubator at 37 ℃ overnight. Isolate the plasmid DNA with Qiagen plasmid mini kit (No. 12123, Hilden, Germany) from the 1 ml E. coli cells. Digest the plasmid with specific restriction enzymes (Mlu1 or Sgf1), then check the DNA size by gel electrophoresis. Transfer 1 ml E. coli suspension into 250 ml LB medium with selection antibiotic at 37 ℃ overnight. Isolate the plasmid DNA with the Qiagen plasmid midi kit. For long-time use, store the plasmid DNA at -80 ℃.

For the plasmid DNA transfection, plate Hek293 cells in 2 ml of growth medium without antibiotics in 6 well plate and wait until cells reach 70% confluent at the time of transfection. Dilute DNA in 250 µl of MEM I Reduced Serum Medium without serum and mixed gently. In the meantime, dilute 10 ul Lipofectamine 2000 (Thermo Scientific, Frankfurt, Germany) in 250 µl of MEM I Reduced Serum Medium without serum and mixed gently. Incubate for 5 minutes at room temperature. Combine the dilute DNA and Lipofectamine 2000. Mix gently and incubate for 20 minutes at room temperature. Transfer mixed medium to the well-containing cells and medium and mix gently. Incubate cells at 37 ℃ overnight. Change the medium and

incubate for 48-72 hours.

### (19) Statistical analysis

The GraphPad Prism 6 Software (GraphPad, San Diego, California USA) was used. All the experiments were performed as triplicates. Unpaired student's t-test was used for determining statistical significance($p<0.05$). All values are presented as Mean ± Standard Deviation (SD).

# 4.0 RESULTS

## 4.1 Caerulein-induced acute pancreatitis is fully regenerated in wild-type mice while it leads to early carcinogenesis in Kras$^{G12D}$ mice.

To investigate the mechanism of regeneration of the pancreas. As reported previously, the caerulein-induced acute pancreatitis was established in wild-type mice (Kong et al. 2018). 8-weeks-old WT mice were treated with caerulein for two consecutive days (Figure 1a). Histology analysis revealed that the caerulein-induced pancreatitis is a self-limited process (Figure 1b-c), which can be divided into three phases: acute inflammation, regeneration and refinement according to previously published data (Kong et al. 2018). In this study, Krt19 was used to mark the formation of acinar-to-ductal metaplasia (ADM), and α-Amylase was used to label the acinar cells. During the acute inflammation phase infiltration, a lot of immune cells and replacement of acinar cells by ADM lesions could be detected. Thereafter, ADM lesions disappeared and α-Amylase positive acinar cells re-appeared in the regeneration phase (Figure 1d). Within day 7 to day 14, the pancreas compartment was fully regenerated (Kong, Bruns et al. 2018).

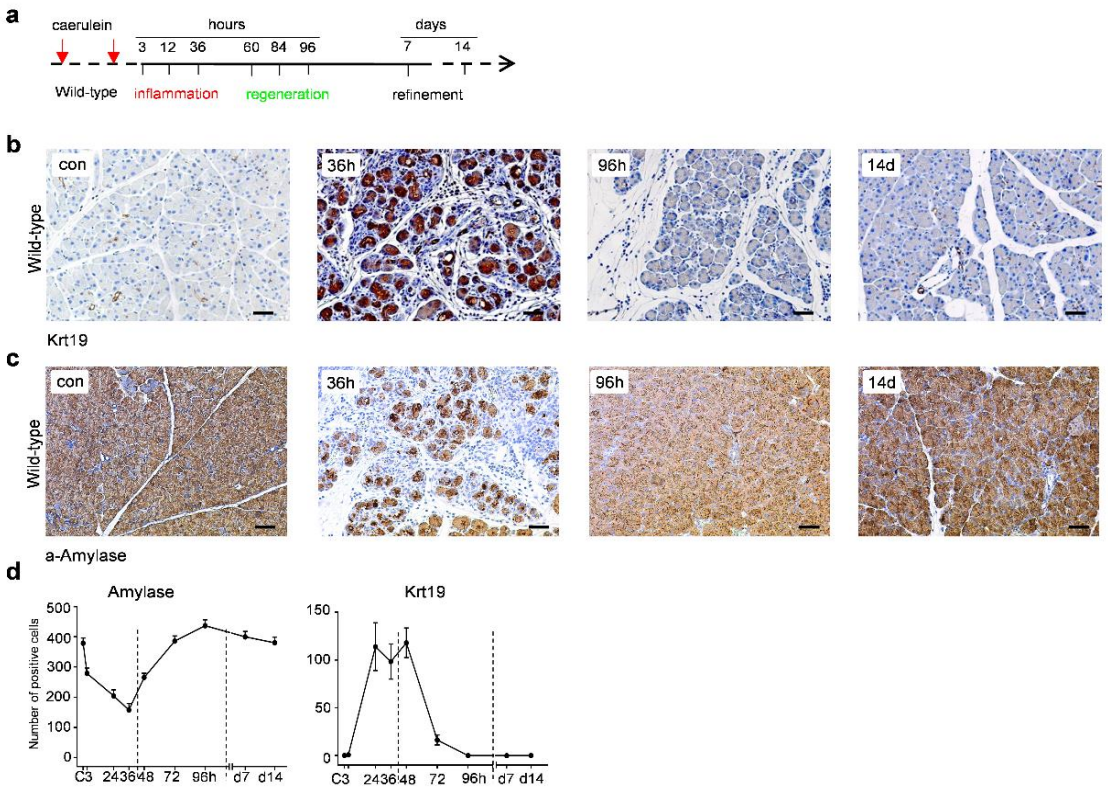

**Figure 1: caerulein-induced acute pancreatitis is fully regenerated in wild-type mice.** (a) Wild-type (WT) mice were sacrificed between 3 hours and 14 days after caerulein-induced acute pancreatitis; (b) Representative IHC pictures show Krt19-positive cells in the different phases of inflammation in WT pancreata; scale bars: 50 mm. (c) Representative IHC pictures show a-Amylase-positive cells in different phases of inflammation in WT pancreata; scale bars: 50 mm. (d) Quantitative data show time-dependent changes in the number of α-amylase and Krt19-positive cells in WT pancreata.

Active point mutations of KRAS are the most common genetic alterations in PDAC (Caldas and Kern 1995), and therefore, $Kras^{G12D}$ mice were used. Similarly, $Kras^{G12D}$ mice were treated with caerulein for two consecutive days at the age of eight weeks. The pancreas was harvested at eight different time points (Figure 2a). In contrast to WT mice, the pancreas with $Kras^{G12D}$ mutation showed an irreversible process. A persistent ADM phenotype was observed in these animals. IHC analysis showed that PanINs lesions increased significantly during the whole process, which suggests the initiation of pancreas carcinogenesis (Figure 2b-e).

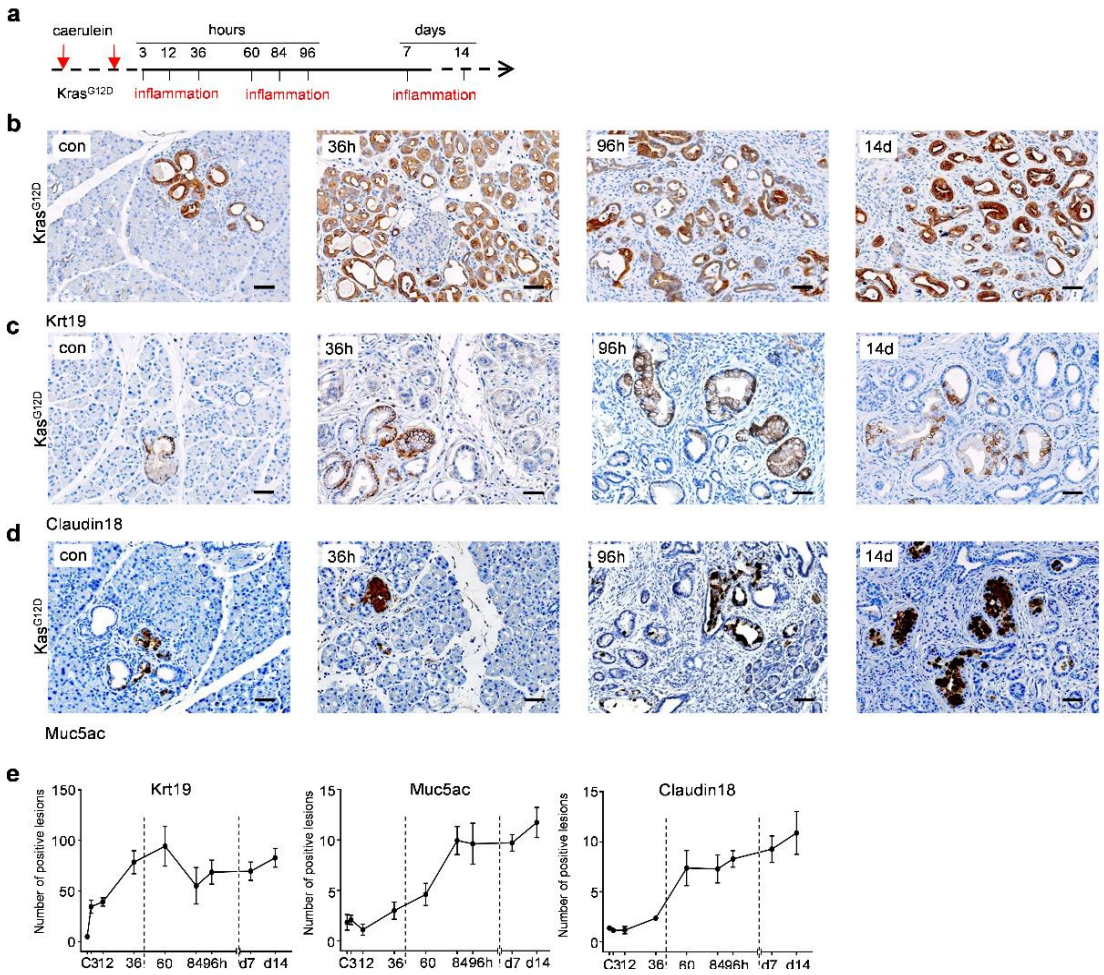

**Figure 2: Caerulein-induced acute pancreatitis leads to early carcinogenesis in Kras$^{G12D}$ mice.** (a) Kras$^{G12D}$ mice were sacrificed between 3 hours and 14 days after caerulein-induced acute pancreatitis; (b) Representative IHC pictures show Krt19-positive cells in the different phases of inflammation in Kras$^{G12D}$ pancreata; scale bars: 50 mm. (c) Representative IHC pictures show Claudin18-positive cells in the different phases of inflammation in Kras$^{G12D}$ pancreata; scale bars: 50 mm. (d) Representative IHC pictures show Muc5ac-positive cells in the different phases of inflammation in Kras$^{G12D}$ pancreata; scale bars: 50 mm. (e) Quantitative data show time-dependent changes in the number of Krt19, Claudin18 and Muc5ac-positive cells in Kras$^{G12D}$ pancreata.

To gain more knowledge of the regeneration, immunofluorescences were used to check the proliferation of different types of pancreatic cells. α-amylase and BrdU double staining showed that there were two waves of proliferation in WT pancreata (Figure 3a, d). One wave at 24 hours and another wave at 96 hours after caerulein treatment. In the presence of oncogene Kras$^{G12D}$, the number of proliferative ADM lesions went up at first 84 hours, thereafter, the proliferation of ADM lesions decreased and then remained persistent (Figure 3c, d). Interestingly, the proliferation of PanIN lesions increased significantly and peaked at 84 hours after caerulein treatment and dropped afterward, which shared the same trend as the proliferation of ADM lesions (Figure 3 b, d).

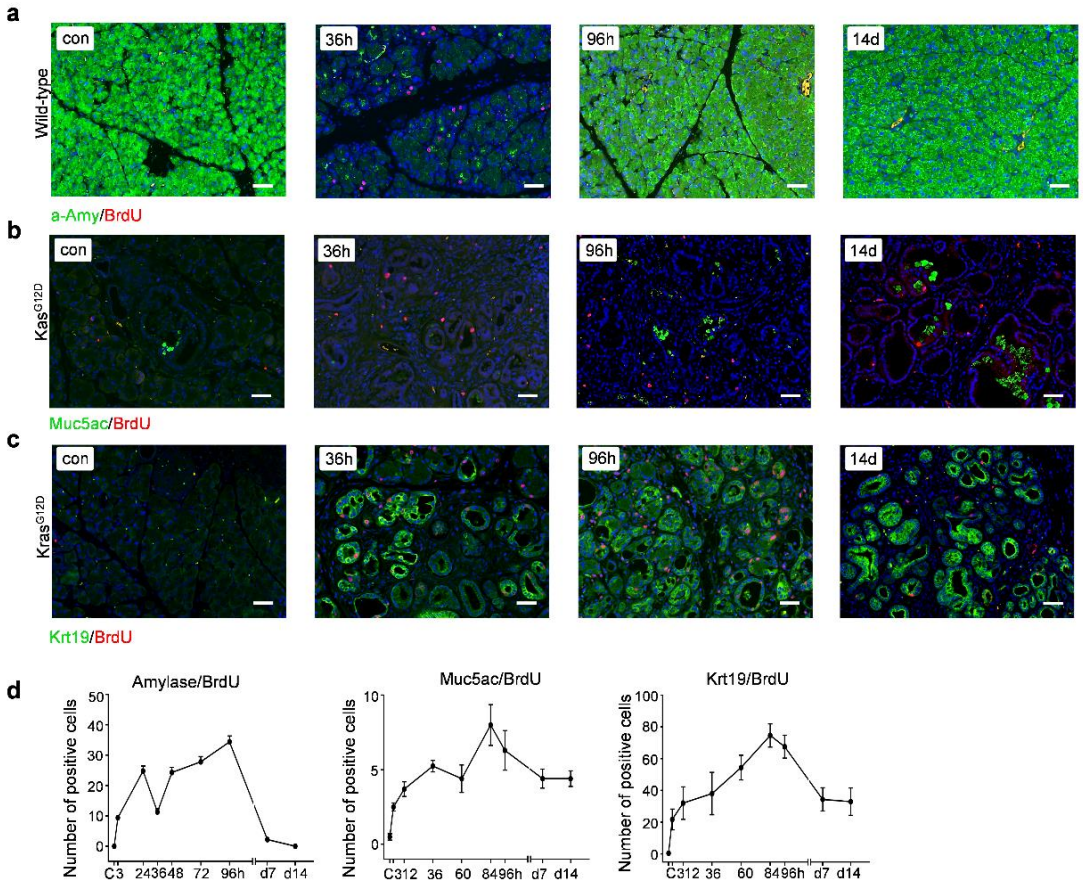


**Figure 3: Quantitative analysis of proliferation in acute pancreatitis and early carcinogenesis.** (a) Representative IF pictures show α-Amylase/BrdU-positive cells in the different phases of inflammation in WT pancreata; scale bars: 50 mm. (b) Representative IF pictures show Muc5ac/BrdU-positive cells in the different phases of inflammation in $Kras^{G12D}$ pancreata; scale bars: 50 mm. (c) Representative IF pictures show Krt19/BrdU-positive cells in the different phases of inflammation in $Kras^{G12D}$ pancreata; scale bars: 50 mm. (d) Quantitative data show time-dependent changes in the number of α-Amylase/BrdU, Muc5ac/BrdU, Krt19/BrdU-positive cells in WT or $Kras^{G12D}$ pancreata.

### 4.2 Ductal obstruction promotes early pancreatic carcinogenesis

Previous data characterized the natural course of caerulein-induced pancreatitis and defined three distinctive states termed inflammation, regeneration, and refinement (Kong et al. 2018). Adult acinar cells were only permissive to oncogenic Kras-mediated transformation during the inflammatory state. Despite compelling evidence of the mechanisms of malignant transformation (to PDAC) in acinar cells, the role of ductal cells in inflammation-promoted PDAC development is less clear. Thus, the pancreatic ductal ligation mouse model was used. To investigate the inflammatory impact of ductal

obstruction on the pancreas, the splenic lobe of wild-type mouse pancreas was selectively ligated, as previously reported (Figure 4a, (Watanabe et al. 1995)). Histological changes in the ligated pancreas at four-time points were analysed (day 1, 3, 7 and 14). Histological analysis revealed that the ligated pancreas was mostly intact between day 1 and 3, which were featured by mild edema, focal immune cell infiltration, and acinar-to-ductal metaplasia (ADMs, less than 10%; Figure 4b, 4c). As the obstructive process progressed, immune cell infiltration and the formation of acinar-to-ductal metaplasia (ADM) became more pronounced. Inceptive atrophy (score: 1/4) and tubular complexes (TCs) with inter- and intralobular fibrosis started to appear on day 7 (Figure 4c). At day 14, strong atrophy (score: 3/4) and a complete loss of the acinar cell compartment with ductal cell replacement were observed (Figure 4b, 4c).

To validate these histological observations, this study determined the proliferation of different cellular compartments after ductal ligation. Indeed, the percentage of proliferating acinar cells (co-labelled by BrdU and α-Amylase) decreased steadily from 62% on day 1 to 0% at day 14 (Figure 4d). In comparison, the percentage of proliferating ductal cells with progenitor-like features (co-labelled by BrdU and Sox9 (SRY-box 9)) increased from 0% on day 1 to 80% at day 14. Next, this study quantified the number of apoptotic cells (labelled by cleaved-caspase 3) and immune cells (marked by CD45) infiltration with increasing acinar cell atrophy (Figure 5). This analysis confirmed that the number of apoptotic cells increased dramatically when the morphological acinar cell atrophy was first detected at day 7 (Figure 6). Finally, immune cell infiltration increased instantly as acinar cell atrophy and death took place (Figure 6).

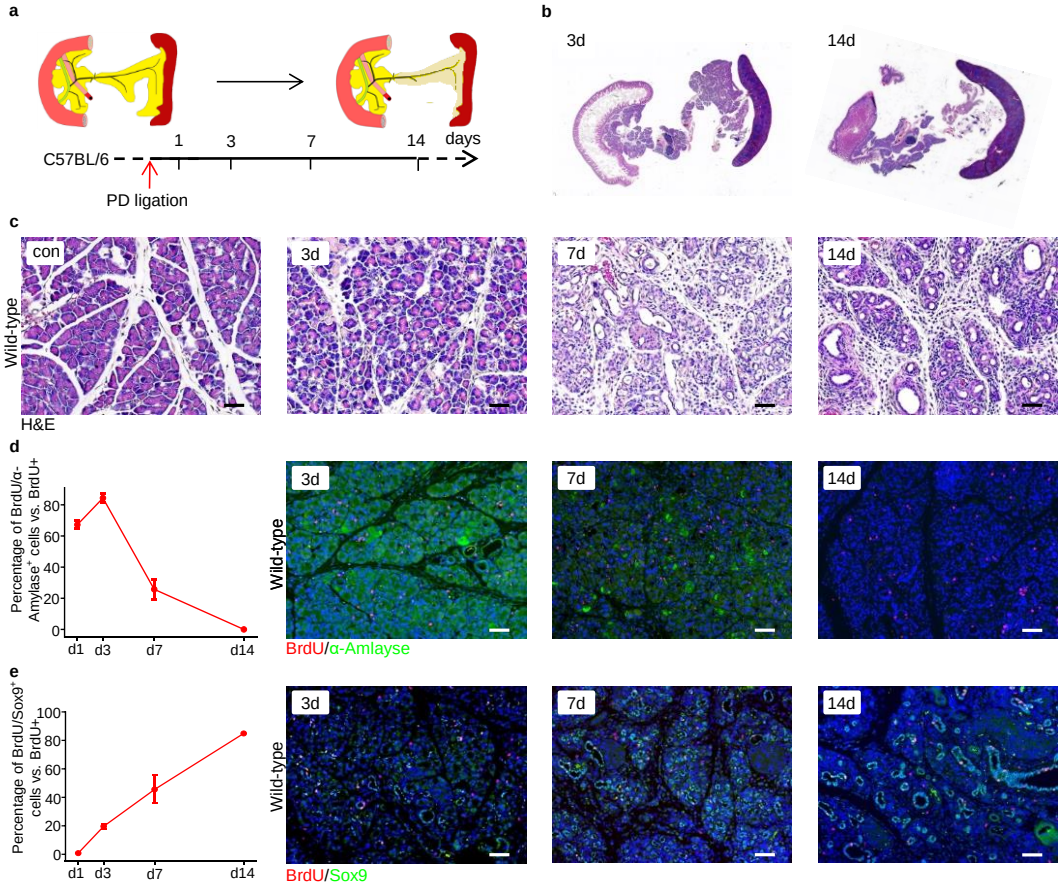


**Figure 4: Ductal obstruction causes acinar compartment atrophy.** (a). WT mice were sacrificed between 1 and 14 days after pancreatic ductal ligation. (b). Representative H&E staining of pancreata 3 and 14 days after ductal ligation. (c). Representative H&E stained sections in WT pancreata 3, 7, and 14 days after ductal ligation (scale bars: 50μm). (d). Quantitative data shows time-dependent changes in the percentages of BrdU/α-Amylase-positive cells in WT pancreata (left); Representative IF pictures show BrdU/α-Amylase-positive cells in WT pancreata 3, 7 and 14 days after ductal ligation (right, scale bars: 50μm). (e). Quantitative data shows time-dependent changes in the percentages of BrdU/Sox9-positive cells in WT pancreata (left); Representative IF pictures show BrdU/Sox9-positive cells in WT pancreata 3, 7 and 14 days after ductal ligation (right, scale bars: 50μm)).

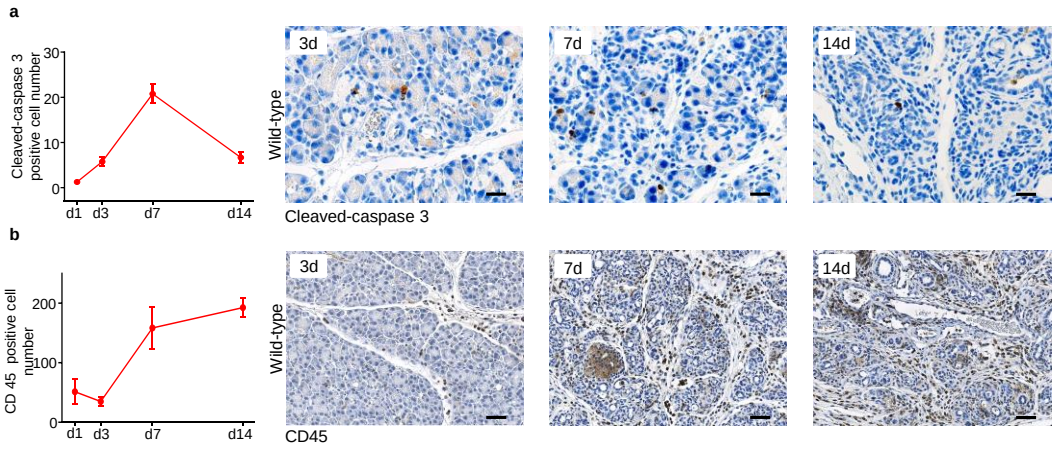

**Figure 5:** (a). Quantitative data shows time-dependent changes in the number of cleaved-Caspase 3-positive cells in WT pancreata (left); Representative IHC pictures show cleaved-Caspase 3-positive cells in WT pancreata 3, 7, and 14 days after ductal ligation (right, scale bars: 50μm). (b). Quantitative data shows time-dependent changes in the number of CD45-positive cells in WT pancreata (left); Representative IHC pictures show CD45-positive cells in WT pancreata 3, 7 and 14 days after ductal ligation (right, scale bars: 50μm).

A previous study demonstrated that p53 activation plays a vital role in mediating acinar cell death (Kong et al. 2015). Inline, p53 is strongly activated in the acinar compartment as acinar cell death starts at day 7 (Figure 6a). To assess the functional relevance of p53 activation, $p48^{Cre}$; $p53^{fl/fl}$ mice were generated in which p53 is specifically ablated in pancreatic epithelial cells (Figure 6b). The pancreas-specific p53 ablation significantly ameliorated the atrophic phenotype of the acinar cell compartment induced by ductal obstruction on day 14 (Figure 6c). Taken together, ductal obstruction causes acinar compartment atrophy but promotes duct compartment proliferation with persistent inflammation. p53 activation is involved in the atrophic response of the acinar compartment after ductal ligation, which is in line with previously published data using global p53-deficient mice (Scoggins et al. 2000).

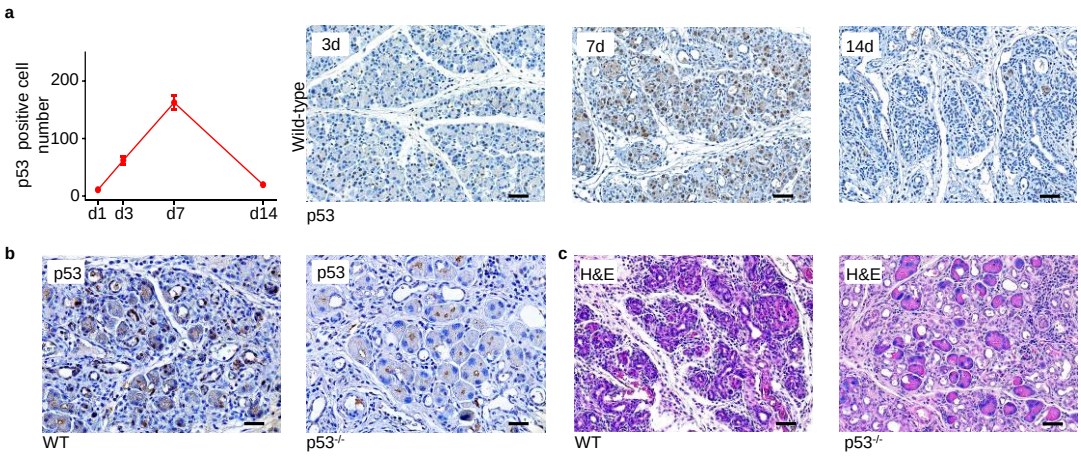


**Figure 6:** (a). Quantitative data shows time-dependent changes in the number of p53-positive cells in WT pancreata (left); Representative IHC pictures show p53-positive cells in WT pancreata 3, 7, and 14 days after ductal ligation (right, scale bars: 50 μm). (b). Representative IHC pictures show p53-positive cells in WT or p48Cre; $p53^{fl/fl}$ pancreata seven days after ductal ligation (scale bars: 50 μm). (c). Representative H&E-stained sections of WT or p48Cre; $p53^{fl/fl}$ mice 14 days after ductal ligation (scale bars: 50 μm, right

panel).

To address the role of ductal ligation in pancreatic carcinogenesis, the well-described $Kras^{G12D}$ was used ((Kong et al. 2018), Figure 6a). Mice were analysed at four time points after pancreatic ductal ligation (day 1, 3, 7, and 14). Notably, the ligated pancreatic lobe was generally less atrophic in $Kras^{G12D}$ mice than that in WT mice at day 14 (Figure 7b vs 4b). Histological analysis revealed that the ADMs, TCs, immune cell infiltration and focal fibrosis were detected at earlier time point-day 3. On day 14, 70-90% of the parenchyma of the ligated pancreas was dominated by TCs, with some of them showing nuclear atypia. Meanwhile, diffuse fibrosis with massive immune cell infiltration was observed, reminiscent of early pancreatic carcinogenesis (Figure 7c). Furthermore, these pathological features were persistent even five months after ductal obstruction; however, no invasive tumours or cells with severe nuclear atypia was observed.

This study thus analysed the dynamic tissue pattern by quantifying the number of different proliferating cellular types in the ligated $Kras^{G12D}$ pancreas. This analysis revealed that the ligated $Kras^{G12D}$ pancreas at day 14 is characterized by I., complete cease of acinar cell proliferation (co-labelled by BrdU and α-Amylase, Figure 8a); II., expansion of proliferating ductal cells with progenitor-like features (co-labelled by BrdU and Sox9 or Pdx1, or Krt19, Figure 8b); III., the proliferation of activated fibroblasts (co-labelled by BrdU and α-SMA, Figure 8c); and IV., persistent immune cells infiltration (labelled by CD45, Figure 9). Finally, the number of apoptotic cells increased steadily until day 7 and then decreased at day 14 in $Kras^{G12D}$ mice, showing a similar tendency as in wild-type mice (Figure 5a, Figure 9b).

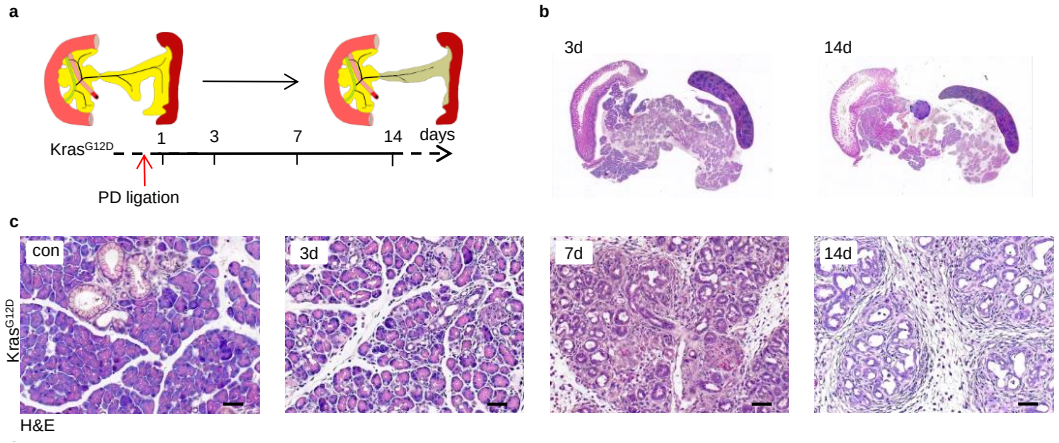


**Figure 7: Ductal obstruction promotes early pancreatic carcinogenesis. (**a). Kras$^{G12D}$ mice were sacrificed between 1 and 14 days after pancreatic duct ligation. (b). Representative H&E stained sections in Kras$^{G12D}$ pancreata 3, 7, and 14 days after ductal ligation. (c). Representative H&E-stained sections in Kras$^{G12D}$ pancreata 3, 7 and 14 days after ductal ligation (scale bars: 50μm).

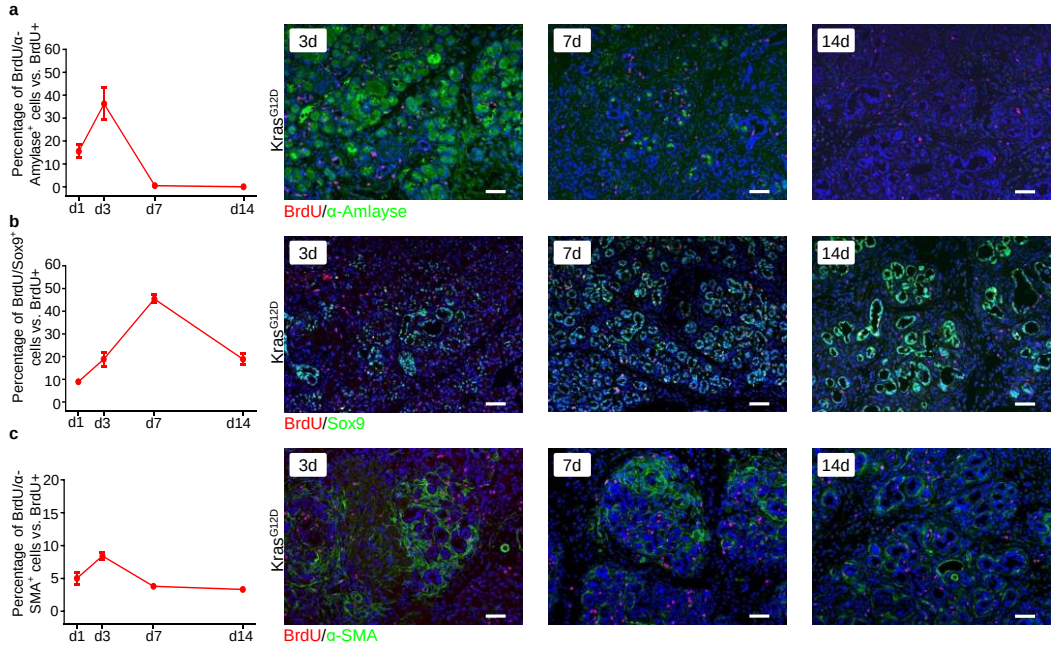


**Figure 8: Ductal obstruction promotes early pancreatic carcinogenesis.** (a). Quantitative data shows time-dependent changes in the percentages of BrdU/α-Amylase-positive cells in Kras$^{G12D}$ pancreata (left); Representative IF pictures show BrdU/α-Amylase-positive cells in Kras$^{G12D}$ pancreata 3, 7, and 14 days after ductal ligation (right, scale bars: 50μm). (b). Quantitative data shows time-dependent changes in the percentages of BrdU/Sox9-positive cells in Kras$^{G12D}$ pancreata (left); Representative IF pictures show BrdU/Sox9-positive cells in Kras$^{G12D}$ pancreata 3, 7 and 14 days after ductal ligation (right, scale bars: 50μm). (c). Quantitative data shows time-dependent changes in the percentages of BrdU/α-SMA-positive cells in Kras$^{G12D}$ pancreata (left); Representative IF pictures show BrdU/α-SMA-positive cells in Kras$^{G12D}$ pancreata 3, 7 and 14 days after ductal ligation (right, scale bars: 50 μm).

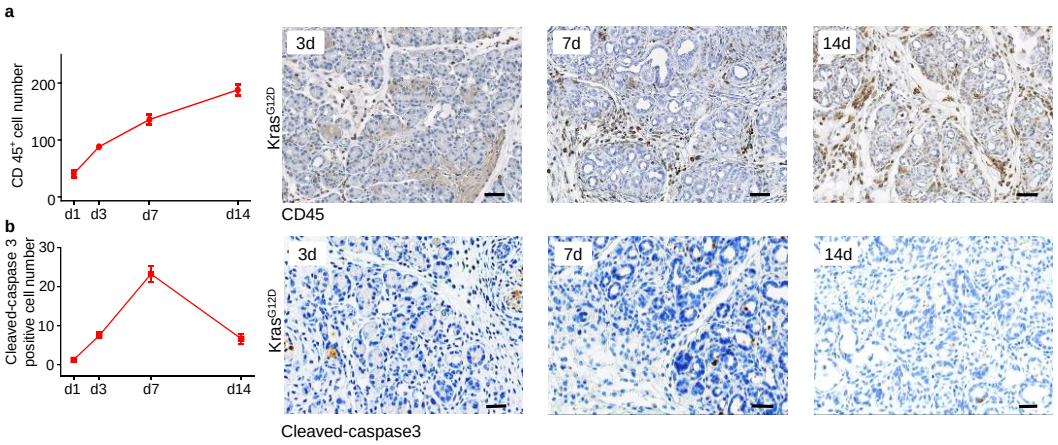


**Figure 9.** (a). Quantitative data shows time-dependent changes in the percentages of CD45-positive cells in $Kras^{G12D}$ pancreata (left); Representative IHC pictures show CD45-positive cells in $Kras^{G12D}$ pancreata 3, 7, and 14 days after ductal ligation (right, scale bars: 50 μm). (b). Quantitative data shows time-dependent changes in the number of cleaved-caspase 3-positive cells in $Kras^{G12D}$ pancreata (left); Representative IHC pictures show cleaved-caspase 3-positive cells in $Kras^{G12D}$ pancreata 3, 7, and 14 days after ductal ligation (right, scale bars: 50 μm).

This pattern was similar to the one that we previously described in early carcinogenesis in caerulein-treated $Kras^{G12D}$ pancreata (Kong et al. 2018). In comparison to the caerulein-treated $Kras^{G12D}$ pancreata, the precursor lesions in the ligated pancreata were negative for PanIN markers (pancreatic intraepithelial neoplasia, Muc5ac and Claudin18) but positive for the ductal marker (Krt19, Figure 10a-10d). Taken together, ductal obstruction promotes the expansion of pre-neoplastic non-mucinous lesions with nuclear atypia in $Kras^{G12D}$ mice, which were distinctive from PanIN lesions observed in the caerulein model.

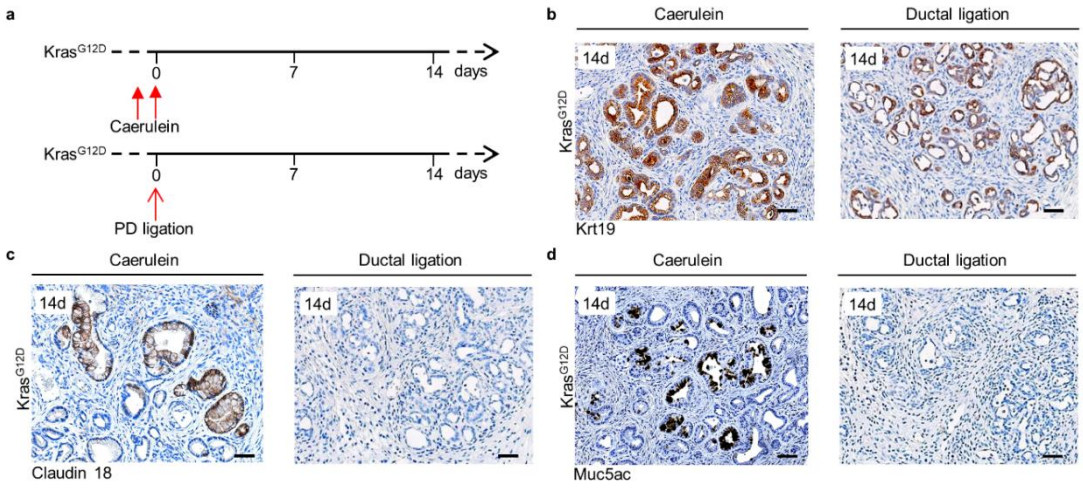

**Figure 10: Pancreatic ductal ligation inhibited PanIN formation.** (a-d). Representative IHC picture show Krt19, Claudin18, and Muc5ac staining in $Kras^{G12D}$ pancreata in 14 days after caerulein injection or ductal ligation.

Taken together, we demonstrate that ductal obstruction causes p53-dependent acinar compartment atrophy but promotes transient ductal compartment proliferation with persistent inflammation in wild-type mice. This transient proliferative response in the ductal compartment and inflammation is co-opted by duct-specific oncogenic Kras to construct a permissive scenario specifying pre-neoplastic lesion formation from the pancreatic ductal compartment.

### 4.3 Anterior gradient 2 (Agr2) is the critical gene during pancreas regeneration and early carcinogenesis.

Then, the microarray was used to analyse the transcriptome data of pancreatic tissues of WT and $Kras^{G12D}$ pancreata (GSE65146). Hundreds of genes were dysregulated in mouse pancreata after caerulein treatment. Those genes which differentially expressed in the inflammation phase of WT mice pancreata when comparing to regeneration and control pancreata were defined as A. Those genes which differentially expressed from 3 hours to 14 days in $Kras^{G12D}$ mice pancreata when comparing to control $Kras^{G12D}$ pancreata were defined as B. Venn diagram and table showed that Agr2 is the only gene which shared by regeneration in WT mice and early carcinogenesis in $Kras^{G12D}$ mice (Figure 11a). WB analysis confirmed this change on protein levels (Figure 11b). Interestingly, Agr2 was highly expressed in $Kras^{G12D}$ pancreata after caerulein treatment when compared to the control group.

As Agr2 has reported as a potential p53 inhibitor (Pohler et al. 2004); The expression of p53 was analysed by WB. In WT pancreata, the p53 was highly expressed at 96 hours; however, the level of p53 decreased significantly at 96 hours (Figure 11b). A similar result was observed in $Kras^{G12D}$ mice, with the high expression of Agr2 at 96 hours, the level of p53 was transiently inhibited (Figure 11c). Several transcripts share the same expression pattern, which is increased or

decreased in both inflammatory samples of wild-type and Kras$^{G12D}$ samples (Figure 11c). Collectively, these data suggest Agr2 might play an essential role in pancreata regeneration and early carcinogenesis.

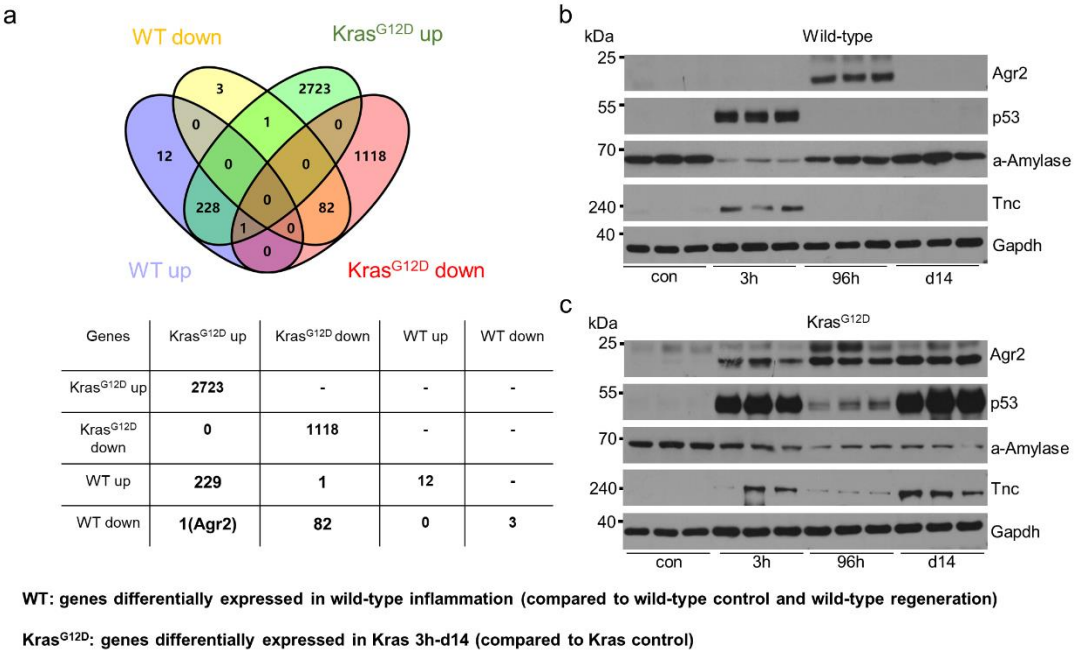


| Genes | Kras$^{G12D}$ up | Kras$^{G12D}$ down | WT up | WT down |
|---|---|---|---|---|
| Kras$^{G12D}$ up | 2723 | - | - | - |
| Kras$^{G12D}$ down | 0 | 1118 | - | - |
| WT up | 229 | 1 | 12 | - |
| WT down | 1(Agr2) | 82 | 0 | 3 |

**WT: genes differentially expressed in wild-type inflammation (compared to wild-type control and wild-type regeneration)**

**Kras$^{G12D}$: genes differentially expressed in Kras 3h-d14 (compared to Kras control)**

**Figure 11: Anterior gradient 2 (Agr2) is induced during acute pancreatitis and early carcinogenesis.** (a) Venn diagram shows the number of genes up- or down-regulated in WT or Kras$^{G12D}$ pancreata by microarray analysis; (b) Western-blot analysis demonstrates levels of Agr2, p53, a-amylase, and Tnc and in WT pancreata 3 hours, 96 hours, and 14 days after caerulein treatment. (c) Western blot analysis demonstrates levels of Agr2, p53, a-amylase, and Tnc and in Kras$^{G12D}$ pancreata 3 hours, 96 hours, and 14 days after caerulein treatment.

### 4.4 Loss of Agr2 decreases the PanIN formation via p53 activation in pancreatic carcinogenesis.

To determine the role of Agr2 deficiency in pancreatic regeneration and carcinogenesis, mice harbouring a floxed Agr2 allele was crossed to an existing PDAC model, p48$^{Cre/+}$; Kras$^{G12D/+}$mice (Kras$^{G12D}$) (Figure 12a). Animals containing Agr2$^{flox/flox}$ and p48$^{Cre/+}$ are referred to as Agr2$^{-/-}$ hereafter, animals carrying all three alleles are referred to as Kras$^{G12D}$; Agr2$^{-/-}$. Agr2 expression was lost entirely in Agr2 deficient mice (Figure 12b and c).

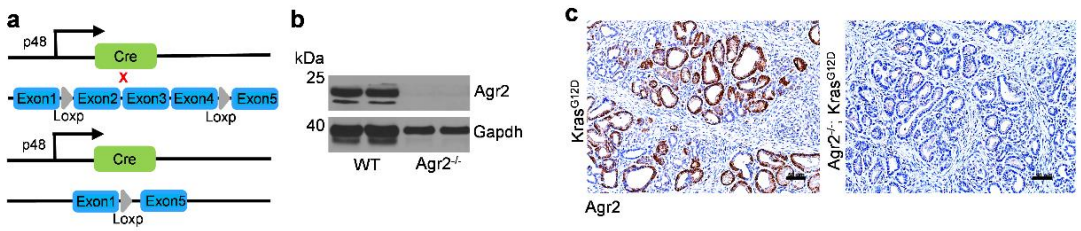


**Figure 12: The establishment of Agr2 knockout mice.** (a) Schematic model of generating pancreas-specific Agr2 knock out mouse. (b) Western blot analysis shows levels of Agr2 in WT and Agr2$^{-/-}$ pancreata; (c) IHC analysis shows Agr2 staining in Kras$^{G12D}$ and Kras$^{G12D}$; Agr2$^{-/-}$ mice. Scale bars: 50 mm.

Thus, the function of Agr2 in pancreatic regeneration was investigated. H&E analysis showed that Agr2 deletion leads to the delayed regeneration of acinar cells, there still some inflammatory cells infiltration and ADM lesions remained at 96 hours in Agr2$^{-/-}$ mice (Figure 13a), while the pancreas in WT mice was regenerated. Then, acinar cell markers (α-amylase, Rbpjl, Pnlip, Try4, and Ptf1α) and ductal cell marker (Rbpj) were analysed by quantitative real-time PCR, Agr2 deletion leading to the downregulation of acinar cell markers and upregulation of ductal cell marker (Figure 13b). Interestingly, increased proliferation and apoptosis of acinar cells were observed in Agr2 knockout mice (Figure 13c). The increased proliferation and apoptosis might cause by the delayed acinar regeneration.

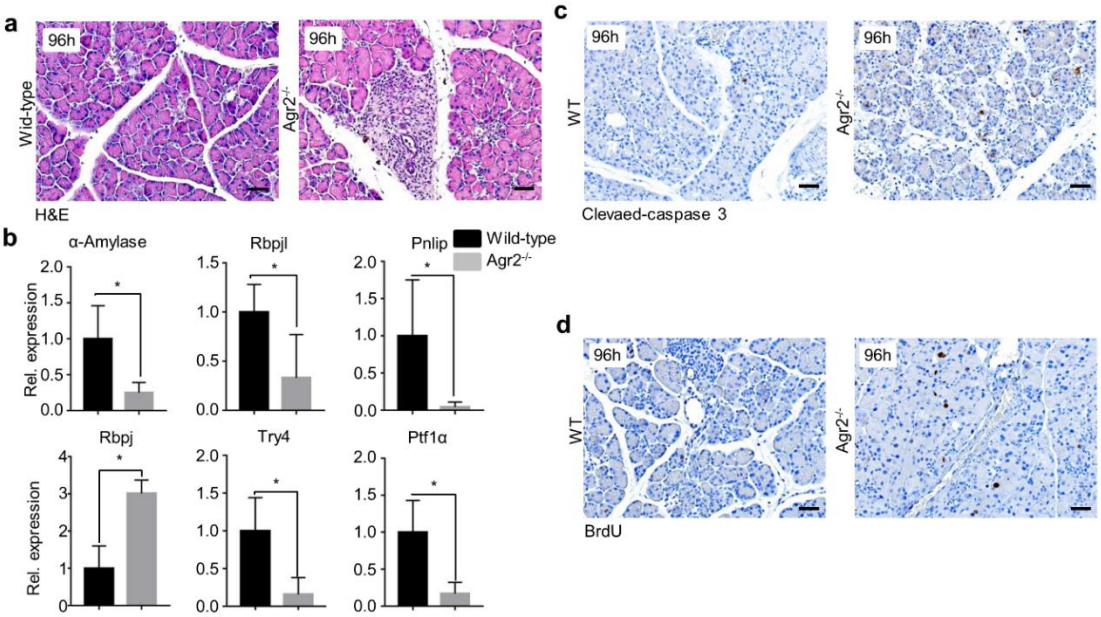


**Figure 13: Loss of Agr2 leading to the delay of pancreas regeneration after acute pancreatitis.** (a) Representative H&E pictures in WT and Agr2$^{-/-}$ mice 96 hours after

caerulein-induced acute pancreatitis. scale bars: 50 mm. (b) Quantitative real-time PCR analysis shows the relative mRNA expression of α-Amylase, Rbpj1, Pnlip, Rbpj, Try4, and Ptf1a between WT and $Agr2^{-/-}$ mice. (c) Representative IHC pictures show cleaved-caspase3 and BrdU-positive cells at 96 hours after caerulein-induced acute pancreatitis in WT pancreata; scale bars: 50 mm.

Emerging evidence indicates that Agr2 is overexpressed in several solid tumours (Brychtova et al. 2015); its role in PDAC has not been fully studied to date. Hypothesizing that Agr2 is also critically involved in pancreatic tumorigenesis. Thus, the $Kras^{G12D}$; $Agr2^{-/-}$ mice were treated with caerulein, IHC analysis showed that loss of Agr2 significantly decreased the number of Claudin18- and Muc5ac-positive PanIN lesions, while Agr2 deficiency has no effect on the formation of ADM lesions (Figure 14 a, b, c, e, f, and g). To further understand how Agr2 deficiency affect the pancreatic carcinogenesis, co-staining of krt19 and BrdU showed Agr2 knockout impaired PanIN lesion proliferation (Figure 14 d, h). Taken together, Agr2 deletion did not affect ADM formation but significantly suppressed $Kras^{G12D}$ and pancreatitis-induced formation of PanIN. These results suggest an essential role of Agr2 in the progression from ADM to PanIN.

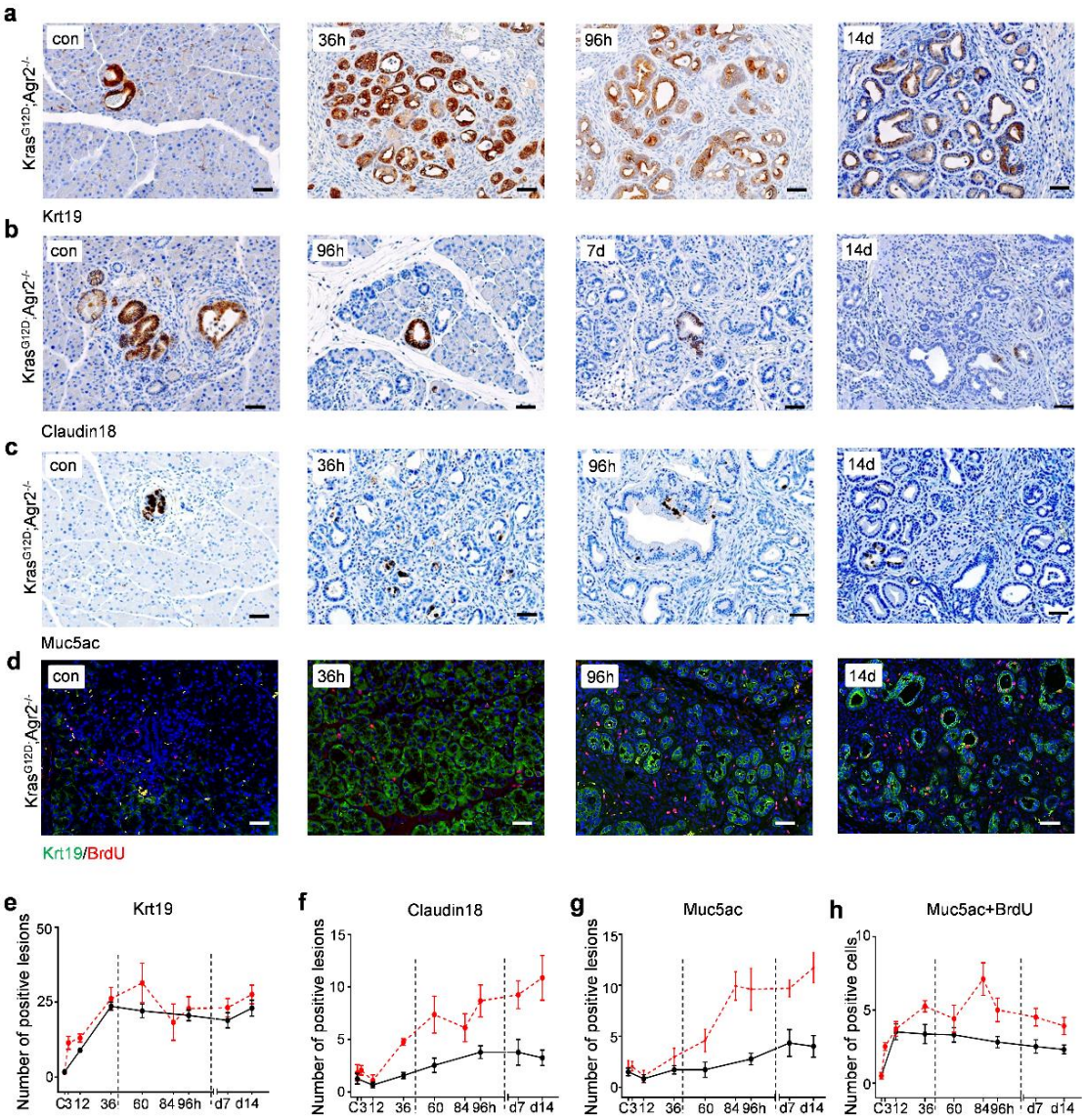


**Figure 14: Loss of Agr2 decrease the PanIN in the early carcinogenesis of Kras$^{G12D}$ mice.** (a) Representative IHC pictures show Krt19-positive cells in the different phases of inflammation in Kras$^{G12D}$ pancreata; scale bars: 50 mm. (b) Representative IHC pictures show Claudin18-positive cells in the different phases of inflammation in Kras$^{G12D}$ pancreata; scale bars: 50 mm. (c) Representative IHC pictures show Muc5ac-positive cells in the different phases of inflammation in Kras$^{G12D}$ pancreata; scale bars: 50 mm. (d) Representative IF pictures show Krt19/BrdU-positive cells in the different phases of inflammation in Kras$^{G12D}$ pancreata; scale bars: 50 mm. (e-h) Quantitative data show time-dependent changes in the number of Krt19, Claudin18, Muc5ac, Muc5ac/BrdU-positive cells in WT or Kras$^{G12D}$ pancreata.

The previous study has proved that Agr2 could inhibit p53 activity (Hrstka et al. 2016). Thus, IF and WB were used to analyses the expression of p53 in the WT pancreas with Agr2 knockout. IF showed less α-Amylase and p53 double-positive

cells in WT pancreas comparing to Agr2 knockout pancreas (Figure 15a, Figure 16a),

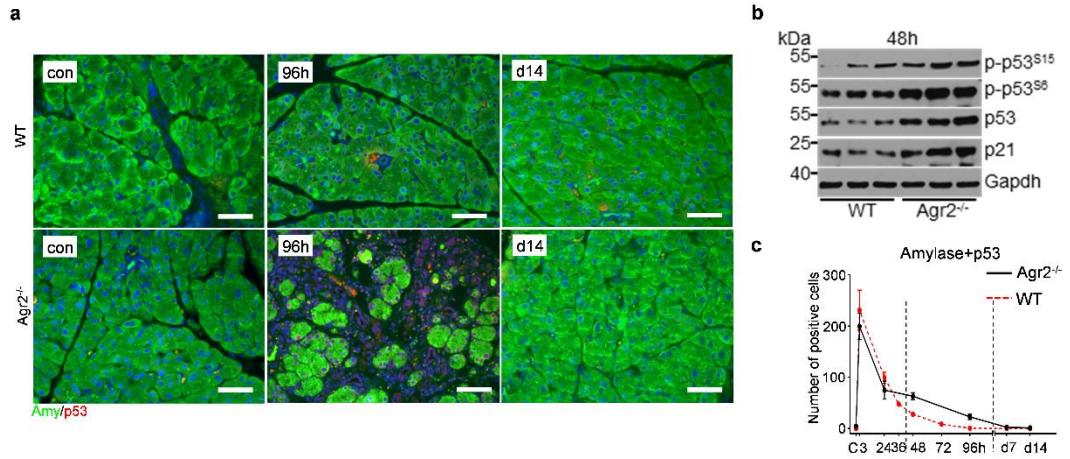


**Figure 15: Agr2 ablation leads to p53 activation.** (a) Representative IF shows α-Amylase/p53 staining in the different phases of inflammation in WT pancreata; scale bars: 50 mm. (b) Western blot analysis shows levels of p53, p21, p-p53$^{ser6}$, and p-p53$^{ser15}$ in WT and Agr2$^{-/-}$ pancreata; (c) Quantitative data analysis indicates the number of α-Amylase/p53, in WT and Agr2$^{-/-}$ pancreata.

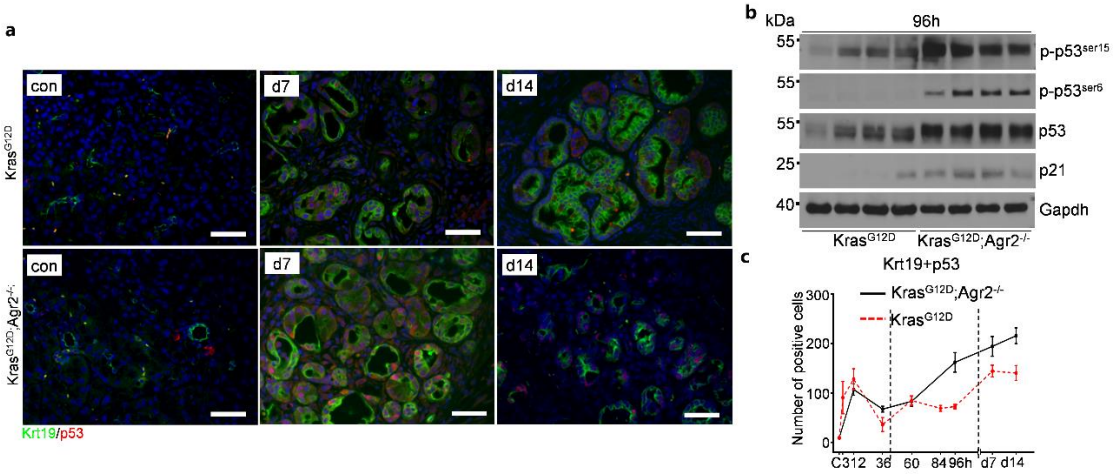


**Figure 16.** (a) Representative IF shows Krt19/p53 staining in the different phases of inflammation in Kras$^{G12D}$ pancreata; scale bars: 50 mm. (b) Western blot analysis shows levels of p53, p21, p-p53$^{ser6}$, and p-p53$^{ser15}$ in Kras$^{G12D}$ and Kras$^{G12D}$; Agr2$^{-/-}$ pancreata; (c) Quantitative data analysis indicates the number of Krt19/p53 in Kras$^{G12D}$ and Kras$^{G12D}$; Agr2$^{-/-}$ pancreata.

WB confirmed Agr2 knockout leading to p53 activation, total p53 was upregulated and p53 phosphorylation at serine 15 and 6 were upregulated after Agr2 knockout (Figure 15 b). In the presence of Kras$^{G12D}$, Agr2 knockout significantly activated

p53 in Krt19-positive cells (Figure 15 c, Figure 16c), which was also confirmed by WB (Figure 16b).

P53 induces cell growth arrest in the G1 phase of the cell cycle (Yang et al. 1996). And progenitor-like cell proliferation is essential for $Kras^{G12D}$-induced pancreatic carcinogenesis (Kong et al. 2018). IF results showed that Agr2 knockout decreased acinar cell proliferation and decreased Krt19-positive lesions proliferation in the presences of $Kras^{G12D}$ (Figure 17a-d).

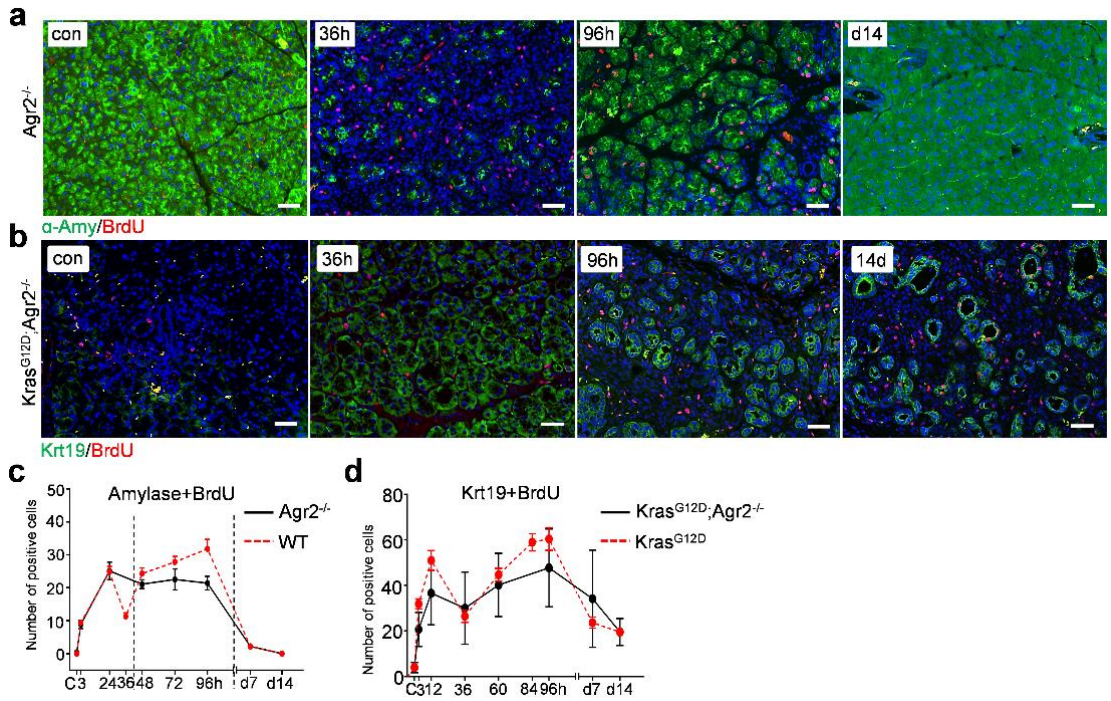


**Figure 17: Agr2 ablation decreased ADM proliferation.** (a) Representative IF shows α-Amylase/BrdU staining in the different phases of inflammation in $Agr2^{-/-}$ pancreata; scale bars: 50 mm. (b) Representative IF shows Krt19/BrdU staining in the different phases of inflammation in $Kras^{G12D}$; $Agr2^{-/-}$ pancreata; scale bars: 50 mm. (c-d) Quantitative data analysis shows the number of α-Amylase/p53, Krt19/p53 in $Agr2^{-/-}$ or $Kras^{G12D}$; $Agr2^{-/-}$ pancreata.

### 4.5 Agr2 overexpression significantly accelerated PanIN formation.

Then, the role of Agr2 overexpression in the initiation of pancreatic tumorigenesis was explored. The LSL-$Rosa^{CAG\text{-}Agr2}$ conditional knock-in mouse line was generated; Out of 160 drug-resistant clones, only 19 potentially targeted clones were confirmed. Eight clones were expanded for Southern Blotting, and seven ES clones (1F3, 1F5, 2A2, 2B12, 2D7, 2E6, and 2G12) showed correct insertion of the

target (Figure 18 b), 1F5 clone was finally used for generating mouse line. The mouse brings the knock-in gene was confirmed by PCR screening (Figure 18 c).

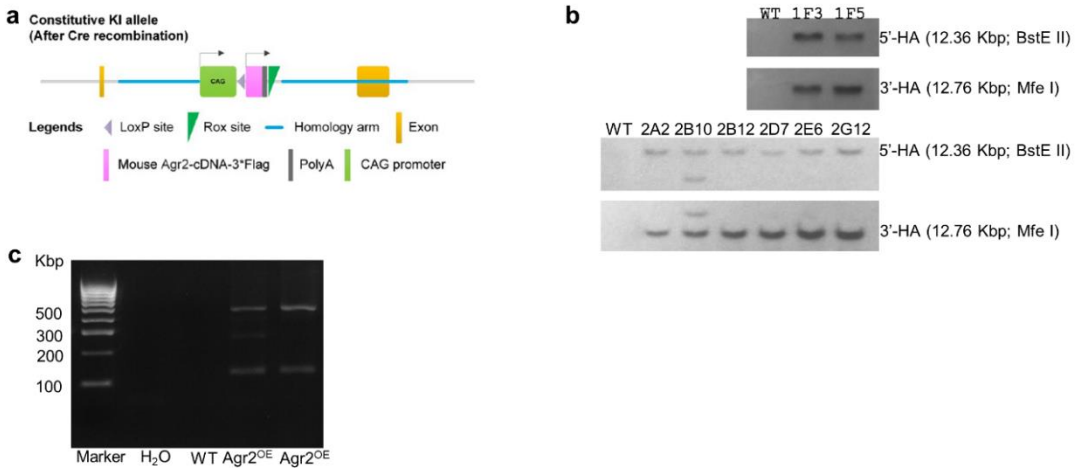


**Figure 18: Schematic representation of the establishment of Agr2 overexpression mice.** (a) Schematic model of generating pancreas-specific Agr2 over-expression mouse. (b) Seven of the eight ES clones (1F3, 1F5, 2A2, 2B12, 2D7, 2E6 and 2G12) were confirmed correct by southern blot analysis. (c) PCR screening shows the expression of Agr2 in the mouse.

Next, the $p48^{Cre/+}$; $Kras^{G12D/+}$; LSL-$Rosa^{CAG\text{-}Agr2}$($Kras^{G12D}$; $Agr2^{OE}$) mice were generated. $Kras^{G12D}$; $Agr2^{OE}$ mice have administrated caerulein at eight weeks of age and evaluated at 14 days after the administration. Interestingly, Agr2 overexpression significantly accelerated the ADM and PanIN formation in the presence of $Kras^{G12D}$ without caerulein treatment (Figure 19 a, b, d), and significantly decreased mice life span (data not shown). Also, at 14 days after caerulein administration, Agr2 overexpression accelerated PanIN formation, while did not affect ADM formation (Figure 19 c, d).

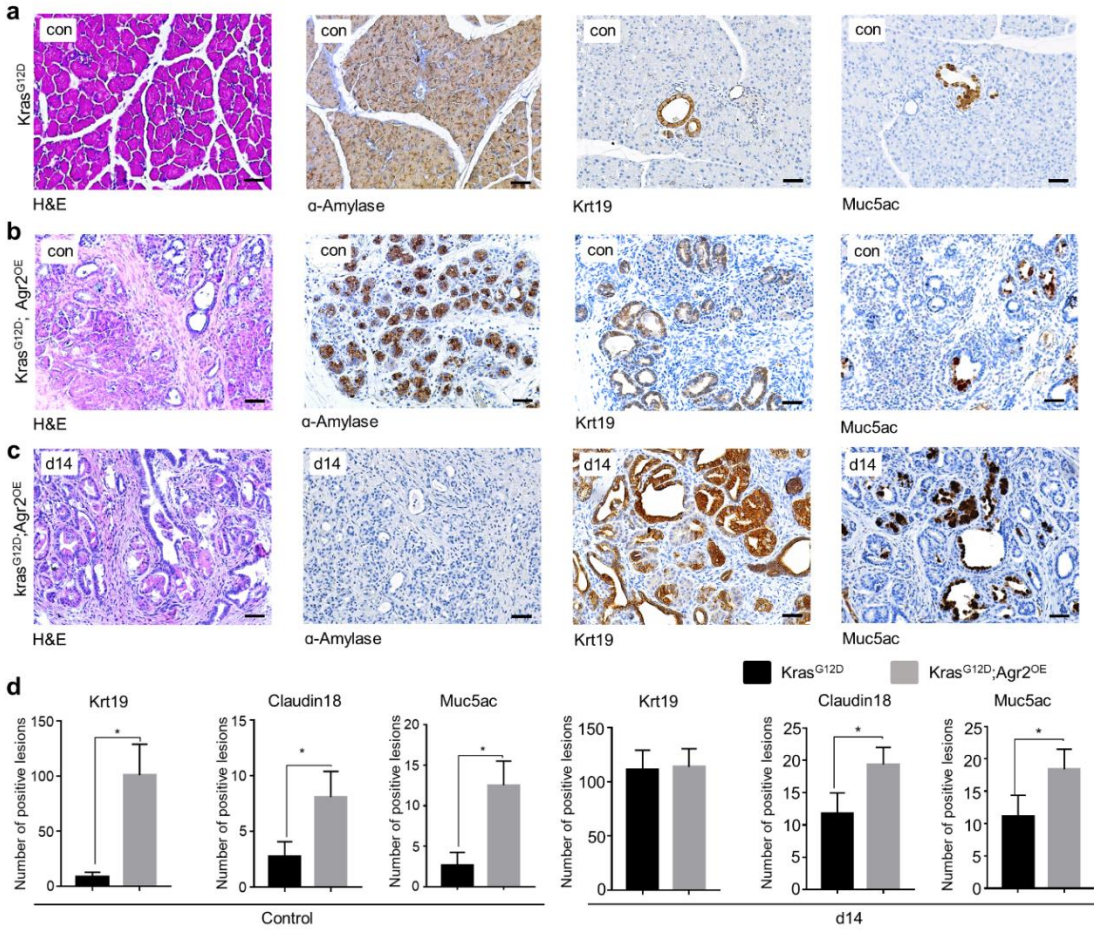


**Figure 19: Agr2 overexpression promotes early carcinogenesis.** (a) Representative pictures show H&E, α-Amylase, Krt19, and Muc5ac staining in 8 weeks old $Kras^{G12D}$ mice without caerulein treatment. scale bars: 50 mm. (b) Representative pictures show H&E, α-Amylase, Krt19 and Muc5ac staining in $Kras^{G12D}$; $Agr2^{OE}$ mice without caerulein treatment. scale bars: 50 mm. (c) Representative pictures show H&E, α-Amylase, Krt19 and Muc5ac staining in $Kras^{G12D}$; $Agr2^{OE}$ mice 14 days after caerulein treatment. scale bars: 50 mm. (d) Quantitative data show the number of Krt19, Claudin18, Muc5ac, -positive cells in $Kras^{G12D}$; $Agr2^{OE}$ and $Kras^{G12D}$ pancreata.

As $Kras^{G12D}$; $Agr2^{OE}$ mice have a relatively short life span, so an inducible system with $P48^{CreERTM/+}$ was used to generate $P48^{CreERTM/+}$; $Kras^{G12D}$; $Agr2^{OE}$ mice ($iKras^{G12D}$; $Agr2^{OE}$) (Figure 20 a). $iKras^{G12D}$; $Agr2^{OE}$ mice were administrated tamoxifen at five weeks of age and injected with caerulein for two consecutive days at three weeks after the tamoxifen administration, and pancreatic tissues were harvested at day 14 (Figure 20 b). In $iKras^{G12D}$; $Agr2^{OE}$ mice without caerulein administration, Agr2 overexpression does not affect tumorigenicity (Figure 20 c). On day 14 after Caerulein administration, PanIN lesions positive for Muc5ac were

observed in iKras$^{G12D}$; Agr2$^{OE}$ (Figure 20 d), quantification data showed that more PanIN lesions were observed in iKras$^{G12D}$; Agr2$^{OE}$ compared to iKras$^{G12D}$ mice (Figure 20 e). These results indicate an essential role of Agr2 in pancreatic carcinogenesis.

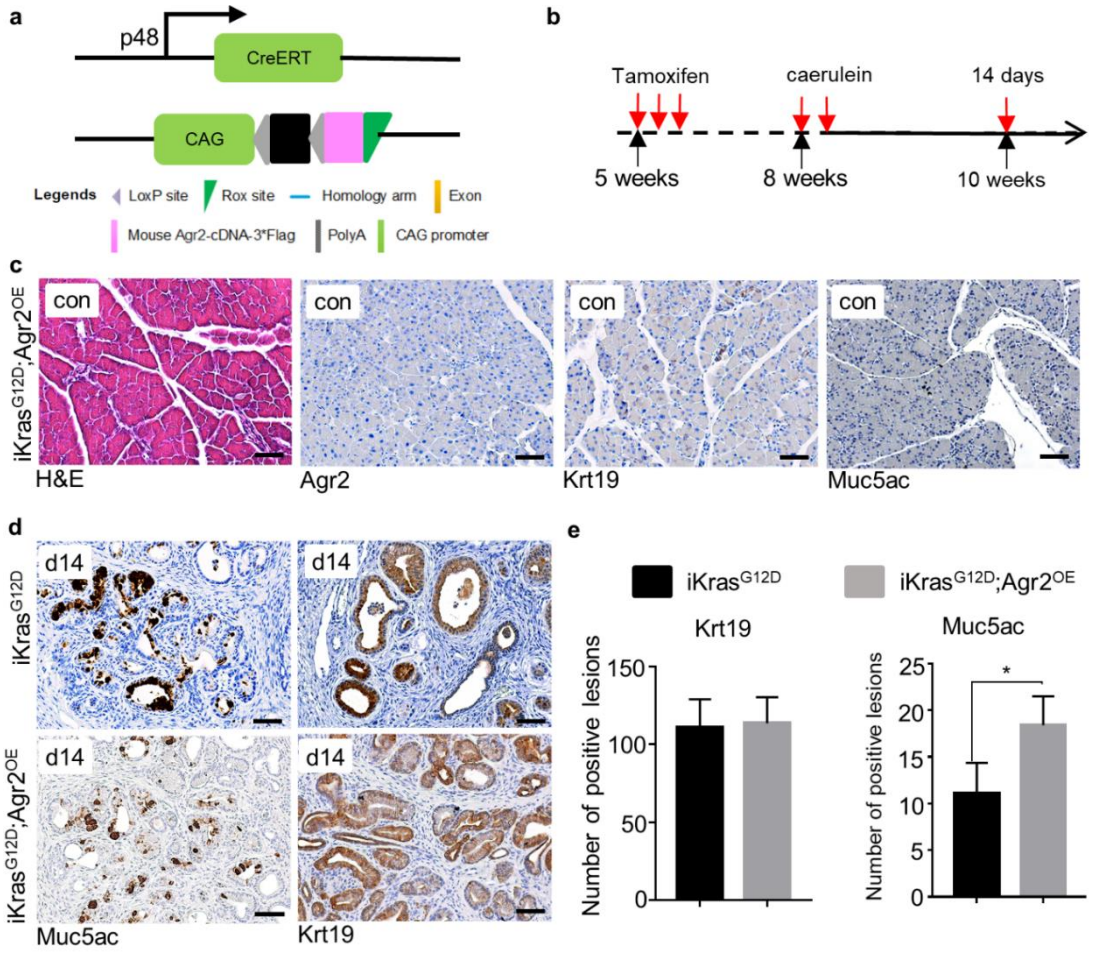


**Figure 20: Agr2 accelerates the pancreas early carcinogenesis in Kras$^{G12D}$ mice with an inducible Cre system.** (a) Schematic model of generating pancreas-specific Agr2 overexpression mouse. (b) Mice were treated with tamoxifen at 5-6 weeks old and sacrificed at 14 days after caerulein-induced acute pancreatitis. (c) Representative pictures show H&E, Agr2, Krt19 and Muc5ac staining in 8 weeks old iKras$^{G12D}$; Agr2$^{OE}$ mice. scale bars: 50 mm. (d) Representative pictures show Krt19 and Muc5ac staining in iKras$^{G12D}$ and iKras$^{G12D}$; Agr2$^{OE}$ mice 14 days after caerulein treatment. scale bars: 50 mm. (e) Quantitative data shows the number of Krt19, and Muc5ac positive lesions among iKras$^{G12D}$; Agr2$^{OE}$ and iKras$^{G12D}$ mice.

Then, we investigated the expression of p53 with Agr2 overexpression 14 days after caerulein treatment. IF analysis showed that there were more krt19 and p53-double-positive cells in iKras$^{G12D}$ mice then iKras$^{G12D}$; Agr2$^{OE}$ mice (Figure 21 a).

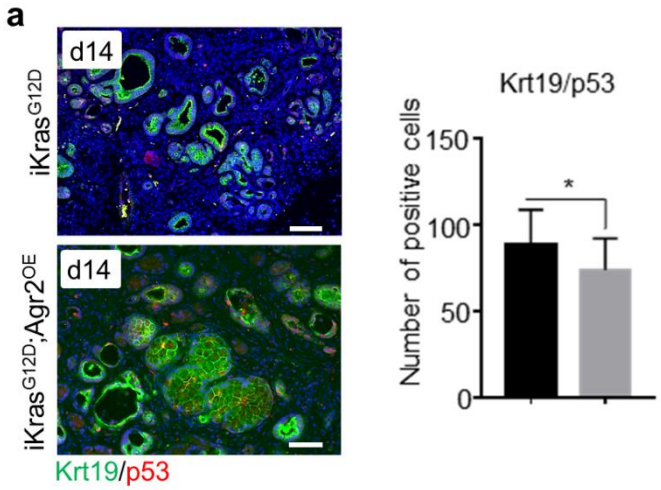


**Figure 21: Agr2 overexpression impairs p53 activation.** (a) Representative IF pictures show Krt19/p53 staining in iKras$^{G12D}$ and iKras$^{G12D}$; Agr2$^{OE}$ mice 14 days after caerulein treatment. scale bars: 50 mm.

As ex vivo 3D culture mimicked the differentiation of acinar cells to ductal cells during pancreatitis(Liou et al. 2015). So acinar cells were isolated from mouse pancreases, at 96 hours after culture, the condition of Agr2 does not affect the number of ADM, while Agr2 overexpression increased the percent of ADM area comparing to Agr2 knockout group (Figure 22 a, b).

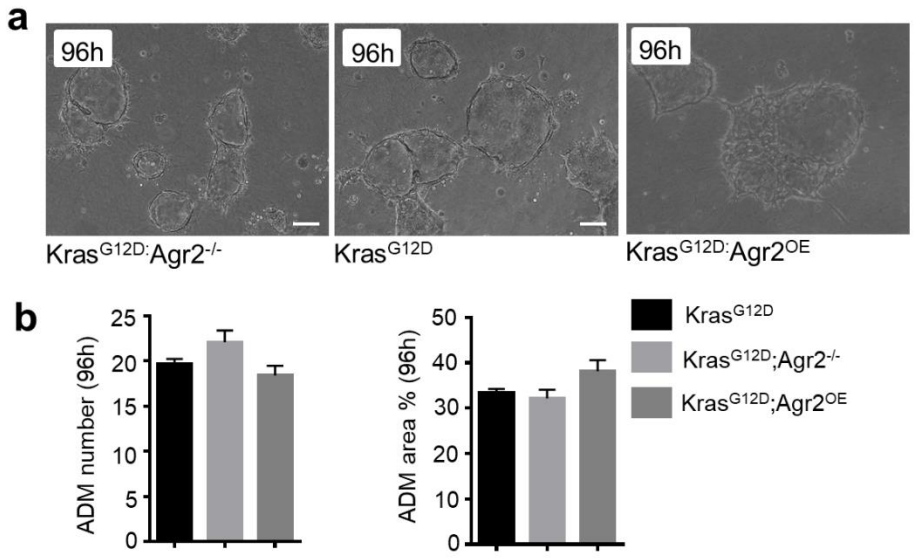


**Figure 22: Agr2 has no effect in acinar-to-ductal metaplasia in vitro.** (a) Representative pictures show the morphology of ADM derived from Kras$^{G12D}$; Agr2$^{OE}$,

$Kras^{G12D}$; $Agr2^{-/-}$ and $Kras^{G12D}$. (b) Quantitative data shows the number of ADM and the percentage of the ADM area. (c) Western blot analysis shows levels of Agr2 and p53 in $Kras^{G12D}$; $Agr2^{OE}$, $Kras^{G12D}$; $Agr2^{-/-}$ and $Kras^{G12D}$ derived ADM.

### 4.6 Agr2 binds to POLR2A and directs its nuclear import via the C-terminal nuclear localization signal.

To determine how Agr2 regulates p53 activity, RNA-sequencing analysis on the $Kras^{G12D}$ mice and $Kras^{G12D}$; $Agr2^{-/-}$ pancreases were performed to search for potential mechanisms. $Kras^{G12D}$ mice were used as controls. Using 0.01 as the statistical cut-off for the false discovery rate (FDR), 437 genes were differentially expressed between two groups (Figure 23 a). Then, the p53 related upregulated genes were selected for gene enrichment analysis (Dysregulated genes were listed in Supplementary list 1). Gene ontology enrichment analysis using Enrich-R for p53 associated genes was performed. The top 15 dysregulated GO categories are shown in figure 23b. The most relevant GO terms are biological processes linked with RNA polymerase II-mediated DNA binding. These data suggest that Agr2 affects the p53 activity by interfering with the RNA polymerase II activity. RNA polymerase II contains 12 subunits (Polr2a-k). Notably, the transcriptional level of p53 was increased (Figure 24).

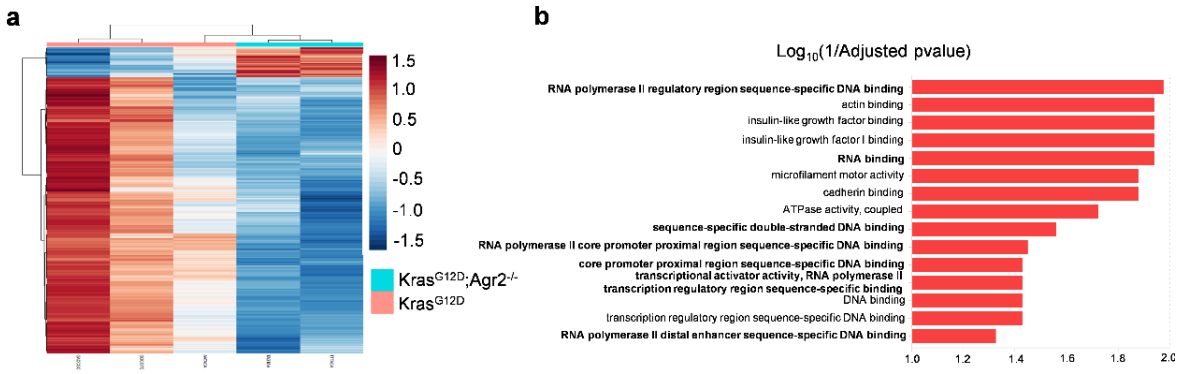


**Figure 23: Study design for RNA-sequencing analysis between $Kras^{G12D}$ and $Kras^{G12D}$; $Agr2^{-/-}$.** (a) A heatmap illustrates the dysregulated genes between $Kras^{G12D}$ and $Kras^{G12D}$; $Agr2^{-/-}$ pancreata 96 hours after caerulein treatment; (**b**) Gene Ontology (GO) term analysis shows enriched biological processes correlated with the p53 activation after Agr2 ablation in $Kras^{G12D}$ pancreata;

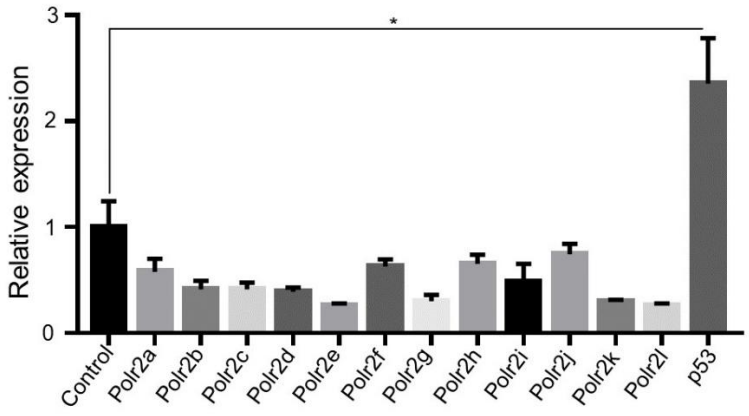


**Figure 24:** (a) QRT-PCR analysis shows the relative mRNA expression of Polr2a, Polr2b, Polr2c, Polr2d, Polr2e, Polr2f, Polr2g, Polr2h, Polr2i, Polr2j, Polr2k, Polr2l and p53 between $Kras^{G12D}$ and $Kras^{G12D}$; $Agr2^{-/-}$ pancreata 96 hours after caerulein treatment.

However, Polr2a's activated form (phosphorylation of the Ser-2/5 site) is significantly decreased in $Kras^{G12D}$; $Agr2^{-/-}$ pancreases (Figure 25 a). IF analysis confirmed deactivation of Polr2a by showing a decreased nuclear staining of p-$Polr2a^{ser2/5}$ in $Kras^{G12D}$; $Agr2^{-/-}$ pancreases (Figure 25 c). Taken together, Agr2 is critical for Pol II activation.

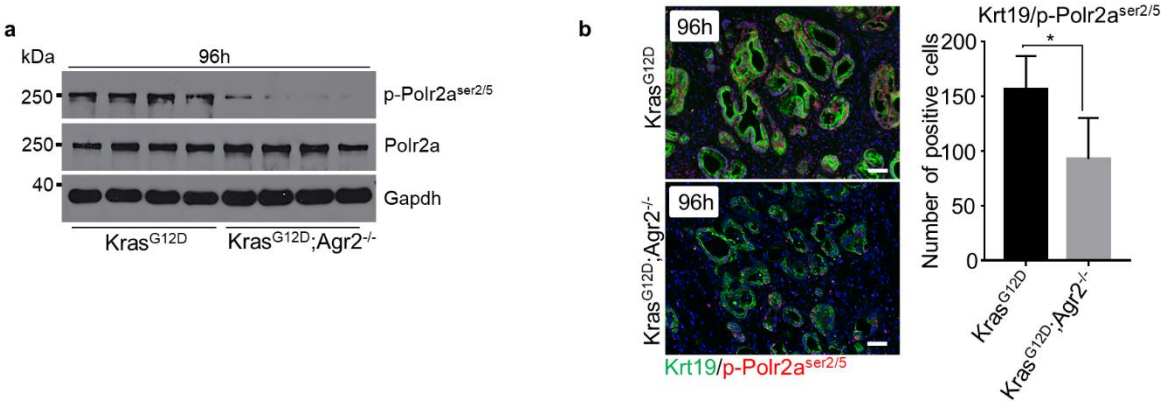


**Figure 25: Loss of Agr2 causes inadequate Pol II activation.** (a) Western blot analysis shows levels of p-$Polr2a^{ser2/5}$ and Polr2a in $Kras^{G12D}$ and $Kras^{G12D}$; $Agr2^{-/-}$ pancreata 96 hours after caerulein treatment. (b) IF pictures show the Krt19/p-$Polr2a^{ser2/5}$ staining in $Kras^{G12D}$ and $Kras^{G12D}$; $Agr2^{-/-}$ pancreata 96 hours after caerulein treatment. Scale bars: 50 mm. Quantitative data shows the number of Krt19/p-$Polr2a^{ser2/5}$ positive cells in $Kras^{G12D}$ and $Kras^{G12D}$; $Agr2^{-/-}$ pancreata 96 hours after caerulein treatment.

To investigate the potential mechanism, we screened human and mouse proteome; As shown in figure 26 a, both human and mouse Polr2a shares a peptide-binding

site consensus of Tx[IL][YF][YF] (aa1173-1177: TAIYY) for Agr2 (Mohtar et al. 2018). The co-immunoprecipitation experiments confirmed this binding between endogenous Agr2 and Polr2a in both mouse and human samples (Figure 26 b, c).

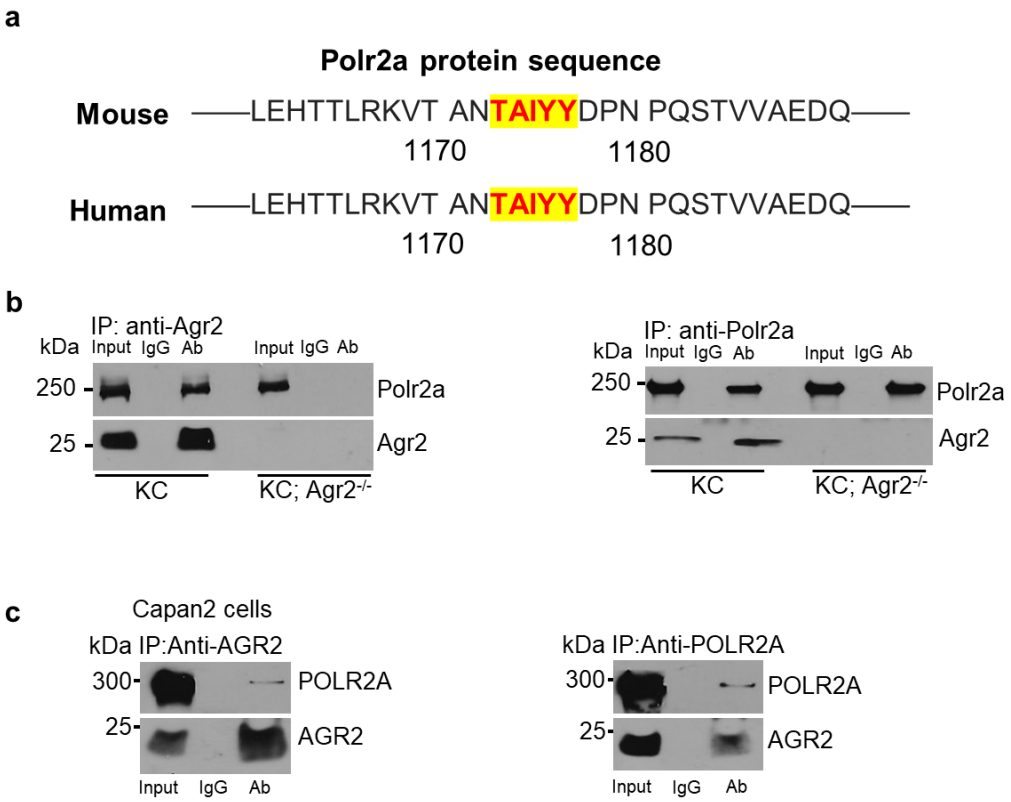


**Figure 26: Agr2 binds to Polr2a.** (a) The protein sequence of human and mouse polr2a; (b) The results of the co-IP assay demonstrate the mutual binding between Agr2 and Polr2a in bulk pancreatic tissues; (**c**) The results of the co-IP assay show the mutual binding between AGR2 and POLR2A in human PDAC cells.

By analysing the full-length protein sequence of AGR2 (http://nls-mapper.iab.keio.ac.jp/cgi-bin/NLS_Mapper_form.cgi), we noticed that AGR2 contains a nuclear localization signal (NLS) at its C-terminus (aa 138-174). Since POLR2A itself is devoid of NLS, it may require the function of AGR2 and mediate its nuclear import in eukaryotic cells. To test this, using a commercially available vector containing human full-length AGR2 cDNA sequence as a template, an expression vector with NLS-deletion (del138-174aa, $AGR2^{\Delta NSL}$) was generated. Using a commercially available vector containing human full-length POLR2A cDNA fused with GFP tag at the C-terminus (POLR2A-GFP) as a template, an expression vector containing a point-mutation at the peptide-binding site of AGR2

(POLR2A$^{Y1177A}$-GFP) was generated. These vectors were sequenced to confirm the introduced mutations (Figure 27).

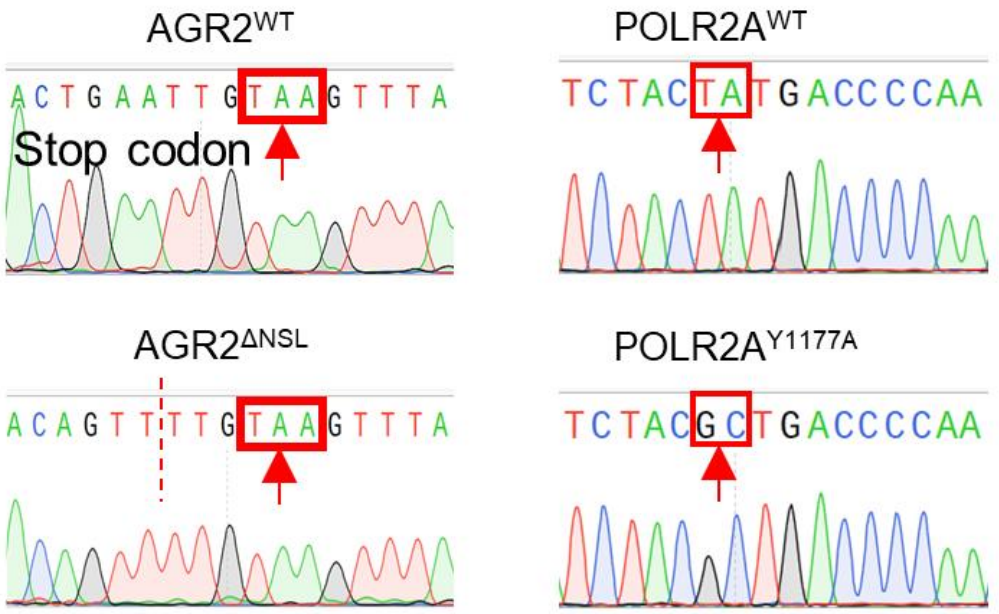


**Figure 27: Generation of AGR2 and POLR2A plasmid.** The picture shows the sequence of AGR2$^{WT}$ and AGR2$^{\Delta NSL}$ plasmid (left panel). The picture shows the sequence of POLR2A$^{WT}$ and POLR2A$^{Y1177A}$ plasmid (right panel).

Then, HEK293 cells were transiently transfected with different combinations of AGR2$^{WT}$, AGR2$^{\Delta NSL}$, POLR2A$^{WT}$-GFP vectors. WB analysis showed that AGR2 could transfer POLR2A into nuclear, while once the NLS sequence at the C-terminus of AGR2 was deleted, both AGR2 and POLR2A cannot be detected in the nuclear (Figure 28a). And coimmunoprecipitation experiments confirmed AGR2$^{\Delta NSL}$ can still bind to POLR2A (Figure 28 b).

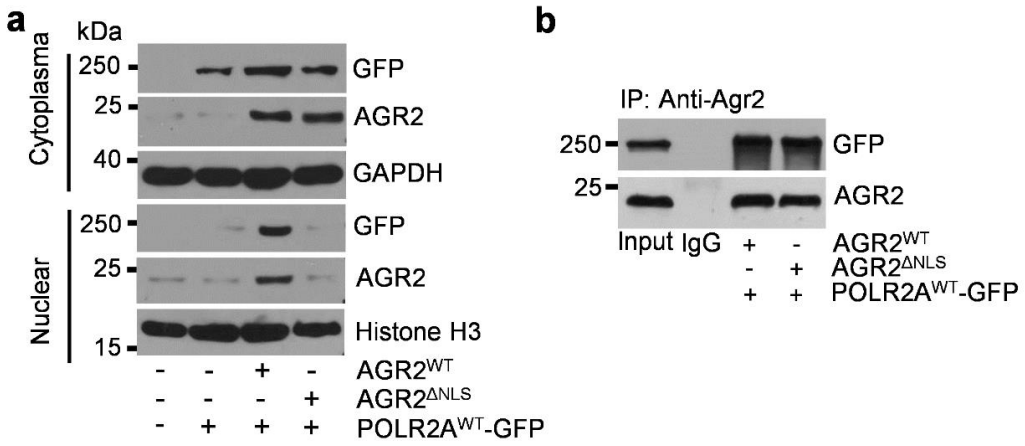


**Figure 28: Agr2 directs Polr2a nuclear import via its C-terminal nuclear localization signal.** (a) Western blot analysis shows levels of GFP, AGR2, GAPDH, and Histone H3 in HEK293 cells. (b) The results of the co-IP assay demonstrate the binding between AGR2 and POLR2A in human PDAC cells.

To test whether the binding between AGR2 and POLR2A is mediated through a specific peptide motif Tx[IL][YF][YF], HEK293 cells were transiently transfected with a different combination of $AGR2^{WT}$, $POLR2A^{WT}$-GFP, and $POLR2A^{Y1177A}$-GFP vectors. WB analysis showed that AGR2 cannot transport mutated POLR2A into the nuclear (Figure 29 a). And coimmunoprecipitation experiments confirmed AGR2 could not bind with mutated POLR2A (Figure 29 b).

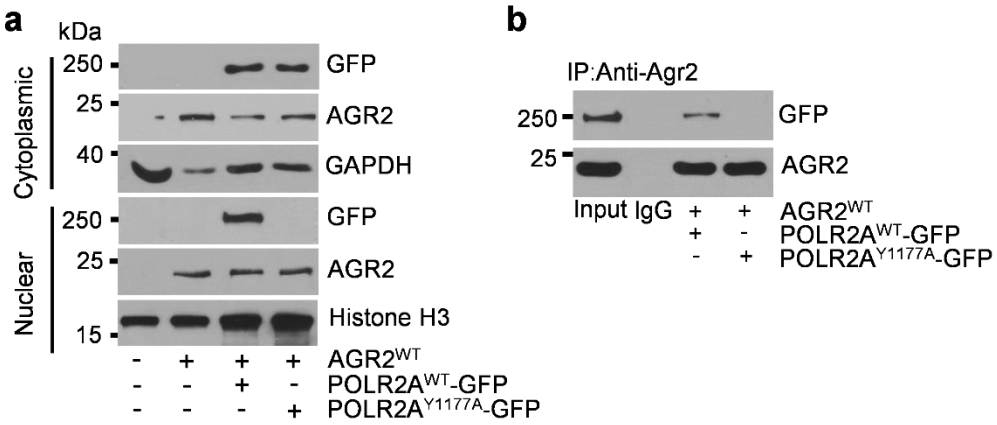


**Figure 29: Agr2 binds to Polr2a through a specific peptide motif.** (a) Western blot analysis shows levels of GFP, AGR2, GAPDH, and Histone H3 in HEK293 cells. (b) The results of the co-IP assay demonstrate the binding between AGR2 and POLR2A in human PDAC cells.

### 4.7 Pol II inactivation resulting in transcriptional stress activates p53 in an ATR-dependent manner

Since Agr2 deficiency leads to Pol II inactivation, and p53 activation. Previous results have shown that Pol II knockdown activated p53 signalling (Hou et al. 2019). And anti-RNA polymerase II antibodies treatment induced phosphorylation of p53 at ser-15 site in an ATM and Rad3-related (ATR)-dependent manner (Derheimer et al. 2007). Thus, WB analysis showed that Agr2 knockout induced the activated form of Atr (p-Atr$^{ser428}$) in Kras$^{G12D}$ mice (Figure 30 a). To specifically inhibit Pol II activity, a specific Pol II inhibitor (α-Amanitin) was used. Human pancreatic cancer cell line HPAC and Capan2 were treated with α-Amanitin showed decreased total POLR2A and p-POLR2A$^{ser2/5}$; In the meantime, the level of p-ATR$^{ser428}$ and p-p53$^{ser15}$ increased significantly (Figure 30 b, c). Then, to identify whether ser15 phosphorylation induced by α-Amanitin is mediated by the ATR kinase. To inhibit the ATR kinase, ATR siRNA was used. ATR siRNA fully abrogated the ATR-dependent phosphorylation of p53 at Ser-15 after α-Amanitin treatment (Figure 30 b, c). Taken together, these results suggest that Pol II inactivation resulting in transcriptional stress activates p53 in an ATR-dependent manner.

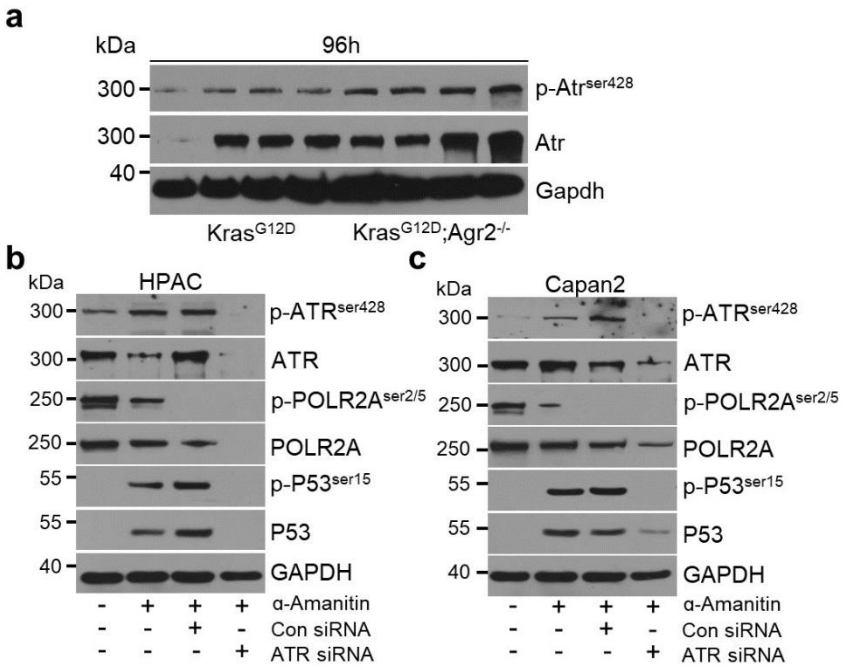

**Figure 30: Pol II inactivation resulting in transcriptional stress activates p53 in an ATR-dependent manner.** (a) Western blot analysis shows levels of p-Atr$^{ser428}$, and Atr in Kras$^{G12D}$ and Kras$^{G12D}$; Agr2$^{-/-}$ mice 96 hours after caerulein treatment. (b) Western blot analysis shows levels of p-ATR$^{ser428}$, ATR, p-POLR2A$^{ser2/5}$, POLR2A, p-p53$^{ser15}$, p53 in HPAC cell treated with α-amanitin and ATR siRNA. (c) Western blot analysis shows levels of p-ATR$^{ser428}$, ATR, p-POLR2A$^{ser2/5}$, POLR2A, p-p53$^{ser15}$, p53 in Capan2 cell treated with α-amanitin and ATR siRNA.

## 4.8 Agr2 knockdown significantly sensitizes PDAC cell lines with wild-type p53 to a specific Polr2a inhibitor.

Here, the AGR2 siRNA treatment potently inhibited POLR2A function and activated p53 in Capan2 and HPAC (with wild-type p53) cell lines (Figure 31 a, b), while AGR2 siRNA treatment also inhibited POLR2A function in PDAC cell lines (PANC-1, and SU.86.86) with p53 mutations (p53$^{R273H}$ and p53$^{G245S}$), however, it didn't activate p53 function (Figure 31 c, d). We hypothesize that the Agr2 knockdown sensitizes PDAC cells to a specific Pol II inhibitor by co-diminishing the activated form of Pol II. To test this, we treated Capan2 and HPAC cells with the Agr2 siRNA in combination with/without a specific Pol II inhibitor-α-amanitin. Compellingly, the Agr2 knockdown significantly enhanced the cytotoxicity of α-amanitin in vitro (Figure 31 e, f). Besides, no such effect was observed in PDAC cell lines carrying mutated p53 (Figure 31 g, h).

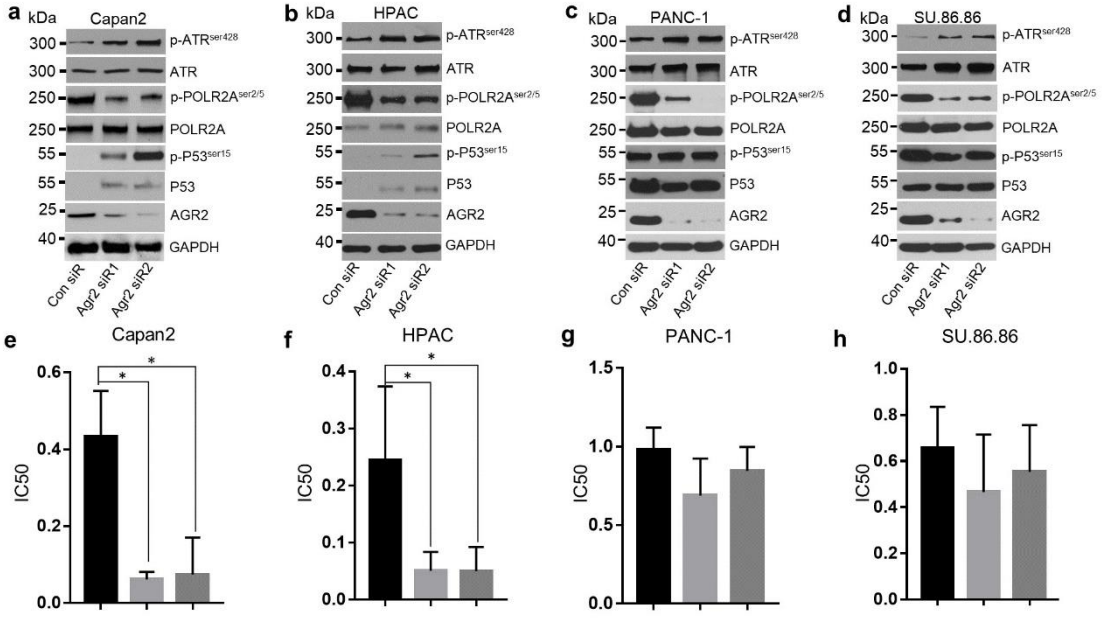


**Figure 31: Agr2 knockdown significantly sensitizes PDAC cell lines and with wild-**

**type p53 to a specific Polr2a inhibitor.** (a-d) Western blot analysis shows levels of p-POLR2A$^{ser2/5}$, POLR2A, p-p53$^{ser15}$, p53, and AGR2 in Capan2, HPAC, PANC1, and SU.86.86 cell treated with AGR2 siRNA. (e-h) The results of the MTT assay demonstrate the dose-dependent changes in the cell viability of Capan2, HPAC, PANC1, and SU.86.86 cells treated with AGR2 siRNA and α-amanitin.

# 5.0 Discussion

The progression of pancreatic acinar cells to premalignant PanIN lesions with intermediary step (ADM) has been an established model of early pancreatic tumorigenesis(Ji et al. 2009). Recently, the natural course of caerulein-induced pancreatitis in wild-type mice was defined in three phases: inflammation, regeneration, and refinement. Mice harbouring $Kras^{G12D}$ mutation displayed a persistent inflammatory phase (Kong et al. 2018). Gene expression analysis of wild-type mice and $Kras^{G12D}$ mice in the regeneration phase identified Agr2 as the only gene that was increased. Here, the biological function of Agr2 in pancreatic carcinogenesis and PDAC cell lines was studied.

## 5.1 Ductal obstruction promotes the formation of preneoplastic lesions from the pancreatic ductal compartment

Murine derived acinar cells have been proved resistant to oncogenic Kras-mediated transformation alone, while they become susceptible in the presence of Kras and inflammation (Guerra et al. 2007, Morris et al. 2010, Kong et al. 2018). Part of pancreatitis is caused by ductal obstruction which can be induced by a mechanic (e.g. ductal structure) or functional causes (e.g. protein plugs due to ductal dysfunction) (Kleeff et al. 2017, Yamaguchi et al. 2017). Here in this study, ductal obstruction has been identified as an essential mechanism to induce the transformation of the pancreatic ductal compartment into preneoplastic lesions. The previous study has shown that $Kras^{G12D}$ alone can only induce a senescence program but not sufficient in initiating preneoplastic lesions (Bailey et al. 2016). This study proved that ductal obstruction leading to acinar compartment atrophy in p53-dependent pathway and causes persistent inflammation-induced transient compartment proliferation in wild-type mice. Duct-specific oncogenic $Kras^{G12D}$ co-opted this transient proliferative response in the ductal compartment and inflammation to construct a permissive scenario specifying preneoplastic lesion formation from the pancreatic ductal compartment. As the $Sox9^{CreERT2}$ line

recombines the Centro-acinar compartment—albeit at a low penetrance—exactly delineate the cell of origin of these preneoplastic cells need further studies (e.g. normal duct vs. Centro-acinar cells).

However, this study has proved that caerulein-induced pancreatitis was not sufficient to initiate early precursor lesions of PDAC from ductal cells. And acinar cells were susceptible to oncogenic $Kras^{G12D}$ and caerulein-induced pancreatitis (Kopp et al. 2012). ADM is defined as a default and reversible metaplasia process in which acinar cells transiently adopt a ductal phenotype with progenitor-like features and the capability of re-differentiating into acinar cells (Kong et al. 2011). ADM lesions progress into PanIN lesions and PDAC in the presence of oncogenic Kras signalling and caerulein-induced pancreatitis (Guerra et al. 2007, Morris et al. 2010, Kopp et al. 2012). In order to better differentiate between these putative subtypes of PDAC, this murine ductal obstruction- and caerulein-induced pancreatitis model will serve as a good platform.

**5.2 Agr2 is crucial for PanIN formation by inhibiting p53 activation**

This study hypothesized that Agr2 is an essential factor required for early carcinogenesis. Using an acinar cell-specific mouse model, this study demonstrated that Agr2 deletion in adult pancreatic acinar cells reduces spontaneous $Kras^{G12D}$-induced PanIN formation. This is consistent with previous reports(Dumartin et al. 2017, Milewski et al. 2017). Interestingly, spontaneously accelerated ADM and PanIN lesions formation were observed with the Agr2 over-expression in the presence of $Kras^{G12D}$. This study confirmed that the Agr2 overexpression by ptf1a-Cre in the embryonic stage might alter exocrine cell properties. Thus, to exclude such influences by Agr2 over-expression, $Ptf1\alpha^{CreERT2}$ mice were used, which was confirmed to have normal homeostasis in adult pancreatic tissue. Agr2 accelerates early pancreatic carcinogenesis in $Kras^{G12D}$ with $Ptf1\alpha^{CreERT2}$. On the other hand, consistent with previous reports(Dumartin et

al. 2017), Agr2, which is usually absent in acinar cells, was expressed in the cytoplasm of acinar cells during pancreatitis and was maintained during ADM and $Kras^{G12D}$-induced PanIN formation. These data support that Agr2 is required for oncogenic $Kras^{G12D}$-induced PanIN formation.

As Agr2 is a p53 suppressor(Pohler et al. 2004, Hrstka et al. 2016). Thus, this study checked the expression of TP53 by qRT-PCR and WB, and it was upregulated in the Agr2 deleted mice 96 hours after caerulein-induced pancreatitis. p53 plays a vital role in the cell cycle and is the most critical tumour suppressor(Joerger and Fersht 2016). During the past years, a significant number of studies on p53 have revealed the complexity and connectivity of the p53 pathway in tumour metabolic regulation, and development(Joerger and Fersht 2016). While p53 protein is frequently inactivated in most cancers, through either mutation in the TP53 gene or deregulation of its associated pathways(Joerger and Fersht 2016), we showed that the ratio of active, phosphorylated p53 at Ser-15 site is up-regulated after Agr2 deletion in vivo. As elevated p53 induces cell growth arrest in the G1 phase of cell cycle or directly induce apoptosis in some transformed cells(Yang et al. 1996). And progenitor-like cell proliferation is the important character of $Kras^{G12D}$-induced pancreatic carcinogenesis(Kong et al. 2018). And the mechanism that couples increased ductal phenotype and increased cellular proliferation during ADM is unknown. Our results demonstrated that Agr2 deletion decreased ADM and PanIN proliferation. These data suggest that Agr2 deletion activates p53 signalling and inhibits ADM and PanIN formation.

### 5.3 AGR2 binds to POLR2A and directs its nuclear import via C-terminal nuclear localization signal

Polr2a is the gene of interest detected by the RNA-sequencing and validated by qRT-PCR and WB, and it is increased in the Agr2 deleted mice 96 hours at mRNA levels after caerulein-induced pancreatitis. We showed that the ratio of active, phosphorylated Polr2a (serine 2/5) to total Polr2a is reduced after Agr2 deletion in

*vivo* and *in vitro*. POLR2A is a member of the family RNA polymerase II complex, contains a C-terminal domain consisting of many repeats (52 in humans) of the heptapeptide YSPTSPS that is phosphorylated(Lian et al. 2008). PoI II takes part in every component of eukaryotic transcription, from pre-initiation to splicing and other post-transcriptional modifications(Clark et al. 2016). The phosphorylated at serine 5 indicates early elongation of PoI II by kinase activity of the transcription factor TFIIH; And the phosphorylation at serine 2 shows the late stages of elongation of PoI II which is the mark of progression of PoI II (Lian et al. 2008). α-Amanitin, a specific inhibitor of POLR2A, causes extensive cell death, and no homozygous deletion of POLR2A was observed (Lindell et al. 1970). Several studies have shown that POLR2A suppression by small interfering or α-Amanitin-based antibody-drug conjugates significantly inhibits proliferation, survival and tumorigenic potential of colorectal cancer and breast cancer (Liu et al. 2015, Xu et al. 2019) Also, we show that endogenous Agr2 can bind to the Polr2a through a specific peptide-binding site consensus of Tx[IL][YF][YF], which is accordance with previous studies (Murray et al. 2007, Mohtar et al. 2018). And a single mutation in POLR2A (Y1177A) abolished its binding to AGR2 in cells.

As PoI II takes part in synthesizing mRNA and several non-coding RNA in nuclear, it's essential for PoI II nuclear import in cells (Forget et al. 2010). And previous studies have shown that the mechanism of nuclear protein import depends on the function of NLS which can be recognized by cytoplasmic importins(Sorokin et al. 2007). Then importins bind to NSL sequences through the α subunit of importin α/β dimers (Tseng et al. 2005). While the POLR2A amino acid sequence doesn't contain NSL (Forget et al. 2010). So POLR2A needs a binding partner which includes NSL. Interestingly, AGR2 contains an NSL at the C-terminus of protein (http://nls-mapper.iab.keio.ac.jp/cgi-bin/NLS_Mapper_form.cgi). Thus, we hypothesized that the C-terminal NSL of AGR2 is important for POLR2A nuclear import. Then, we generated the AGR2 plasmid in which the C-terminal NSL is deleted. Our results confirmed that POLR2A was not observed in the nuclear, but

in the cytoplasm after AGR2$^{\Delta NSL}$ transfection in HEK293 cells. These results indicate that AGR2 directs PoI II nuclear import via its C-terminal NLS.

### 5.4 PoI II inactivation resulting in transcriptional stress activates p53 in an ATR-dependent manner

Also, previous studies have confirmed that blockage of transcription through microinjected anti-RNA polymerase antibodies lead to the accumulation and phosphorylation of p53 in the absence of initial DNA damage (Mellon et al. 1986, Derheimer et al. 2007); And phosphorylation of p53 at Ser-15 was induced especially when elongating RNA polymerases were inhibited through replication protein A (RPA) and ATR-dependent manner (Derheimer et al. 2007). Our results confirmed that the ratio of active, phosphorylated Atr$^{ser428}$ to total Atr is increased after Agr2 deletion in vivo. Consistent with these findings, pancreatic cancer cells treated with PoI II inhibitor, α-Amanitin, significantly increased phosphorylated p53$^{ser15}$ and phosphorylated Atr$^{ser428}$ expression, while ATR siRNA decreased activated p53. Altogether, these findings highlight the function of Polr2a/Atr/p53 signalling in the adult pancreas.

### 5.5 Combined inhibition of Agr2 and PoI II reduces tumour cell survival

As illustrated in the introduction, one of the major reasons leading to PDAC-related death is lack of effective therapies. A significant part of human PDAC (around 30%) contains an intact p53 pathway (Cancer Genome Atlas Research Network. Electronic address and Cancer Genome Atlas Research 2017). However, there is no effective p53-based therapy succeed in patients(Cheok et al. 2011, Camp et al. 2013). Thus, it's crucial to find a specific treatment for PDAC with wild-type p53. In this study, we confirmed that both Agr2 deletion and Polr2A inhibition activate p53. Thus, we combined Agr2 siRNA and α-Amanitin at human PDAC cell lines. Agr2 knockdown significantly sensitizes PDAC cell lines with wild-type p53 to α-Amanitin, but not in PDAC cell lines with mutated p53. Recently, a new antibody against

AGR2 (target orphan glycosylphosphatidylinositol-linked receptor C4.4A) was generated, administration of antibody significantly decreased growth and metastasis of xenograft tumours (Arumugam et al. 2015). Similarly, an antibody against AGR2 named 18A4Hu I was designed by Guo and co-authors by using the pHAb-FAST system, mouse xenograft result showed that 18A4Hu I reduced xenograft growth(Guo et al. 2016). Additional research was performed by Negi and co-authors, xenograft tumour models treated with anti-AGR2 monoclonal antibody mAb18A4 significantly reduced tumour size and increased p53 expression(Negi et al. 2019), which exerted no adverse side effects on the major organs and blood in mice. A peptide named H10 can inhibit cancer cell migration in breast and prostate cancer cell lines by inhibiting AGR2 function(Garri et al. 2018). However, these treatments need to be validated by further clinical trials. Therefore, Agr2 targeted treatment on human PDAC requires further investigations.

## 6.0 SUMMARY

In this study, we investigated the role of Agr2 in the genetically engineered mouse model and PDAC cell line. We observed that p53 is transiently suppressed during the phenotypic progression from acinar-to-ductal metaplasia to pancreatic intraepithelial neoplasia-like lesions. The pancreas-specific Agr2 ablation inhibits this phenotypic progression with concomitant p53 activation. Further investigation proved that Agr2 binds the peptide motif (Tx[IL][YF][YF]) of POLR2A. Also, Agr2 directs Pol II nuclear import via its C-terminal nuclear localization signal. Agr2 knockdown sensitizes PDAC cell lines with wild-type p53 to a specific Pol II inhibitor: α-Amanitin.

Therefore, we answered the questions raised in the “Aim of study” as follow:

**Question 1:** What is the effect of regeneration in the early pancreatic carcinogenesis?

**Conclusion 1:** Our data uncovered molecular interactions mediating the proliferative transition from progenitor-like to acinar cells during organ regeneration, and those maintaining persistent proliferation of progenitor-like cells in early carcinogenesis. And pancreatic ductal obstruction causes p53-dependent acinar compartment atrophy but promotes transient ductal compartment proliferation with persistent inflammation in wild-type mice. This transient proliferative response in the ductal compartment and inflammation is co-opted by duct-specific oncogenic Kras to construct a permissive scenario specifying preneoplastic lesion formation from the pancreatic ductal compartment.

**Question 2:** What is the effect of Agr2 deletion on murine pancreatic carcinogenesis driven by $Kras^{G12D}$ and caerulein-induced inflammation?

**Conclusion 2:** Deletion of Agr2 led to decreased PanIN lesions in the presence of $Kras^{G12D}$, while it has no effects on acinar-to-ductal metaplasia in vitro and in vivo.

**Question 3:** What is the molecular mechanism of Agr2 involved in pancreatic carcinogenesis?

**Conclusion 3:** Agr2 deletion inhibits this phenotypic progression with concomitant p53 activation. Mechanistically, AGR2 binds the peptide motif (Tx[IL][YF][YF]) of POLR2A, which is the catalytic subunit of the Pol I). Besides, AGR2 directs Pol II nuclear import via its C-terminal nuclear localization signal. Loss of AGR2 function causes inadequate Pol II activation, and the resulting transcriptional stress activates p53 in an ATR-dependent manner.

**Question 4:** What is the potential application of Agr2-based interference in pancreatic cancer?

**Conclusion 4:** Since Agr2 plays an essential role in pancreatic carcinogenesis, the application of Agr2 inhibitors (antibodies, peptide, siRNA) would be carried out with caution. In this study, we showed that Agr2 knockdown sensitizes PDAC cell lines and patient-derived PDAC cell lines with wild-type p53 to a specific Pol II inhibitor: α-Amanitin. Thus, Agr2-based treatment needed further investigation.

# 7.0 ABBREVIATIONS

| | |
|---|---|
| ADM | Acinar-to-ductal metaplasia |
| AGR2 | Anterior gradient 2 |
| AMPK | AMP-activated protein kinase |
| BSA | Bovine serum albumin |
| Casp3 | Caspase3 |
| CTCs | Circulating tumour cells |
| DAPI | 4,6-diamidino-2-phenylindole |
| ECM | Extracellular matrix |
| EGFR | Epidermal growth factor receptor |
| ER | Endoplasmic reticulum |
| ERK | Extracellular signal-regulated kinase |
| EMT | Epithelial-mesenchymal transition |
| FBS | Fetal bovine serum |
| FDR | False discovery rate |
| GAPDH | Glyceraldehyde-3-phosphate dehydrogenase |
| GEMM | Genetically engineered mouse model |
| IF | Immunofluorescence |
| IHC | Immunohistochemistry |
| IPMN | Intraductal papillary mucinous neoplasm |
| KCl | Potassium chloride |
| KRAS | V-Ki-ras2 Kirsten rat sarcoma viral oncogene homolog |
| Krt19 | Keratin 19 |
| MCN | Mucinous cystic neoplasm |
| MTT | 3-(4,5-dimethylthiazole-2-yl)2,5-diphenyltetrazolium bromide |
| MUC2 | MUCIN2 |
| P16 | Cyclin-dependent kinase inhibitor 2A |
| P48 | Pancreas specific transcription factor, 1a |
| P53 | Tumour protein p53 |
| PanIN | Pancreatic intraepithelial neoplasia |
| PBS | Phosphate buffered saline |
| PDAC | Pancreatic ductal adenocarcinoma |
| PDI | Pancreas-specific protein disulphide isomerase |
| Pdx1 | Pancreatic and duodenal homeobox 1 |
| PFA | paraformaldehyde |
| POLR2A | RNA polymerase II subunit a |
| PSCs | pancreatic stellate cells |
| SDS | sodium dodecyl sulfate |
| SMAD4 | SMAD family member 4 |
| PSCs | Pancreatic stellate cells |
| UV | ultraviolet |

# 8.0 REFERENCES


Aguirre, A. J., N. Bardeesy, M. Sinha, L. Lopez, D. A. Tuveson, J. Horner, M. S. Redston and R. A. DePinho (2003). "Activated Kras and Ink4a/Arf deficiency cooperate to produce metastatic pancreatic ductal adenocarcinoma." Genes Dev **17**(24): 3112-3126.DOI: 10.1101/gad.1158703.

Aichler, M., C. Seiler, M. Tost, J. Siveke, P. K. Mazur, P. Da Silva-Buttkus, D. K. Bartsch, P. Langer, S. Chiblak, A. Durr, H. Hofler, G. Kloppel, K. Muller-Decker, M. Brielmeier and I. Esposito (2012). "Origin of pancreatic ductal adenocarcinoma from atypical flat lesions: a comparative study in transgenic mice and human tissues." J Pathol **226**(5): 723-734.DOI: 10.1002/path.3017.

Arumugam, T., D. Deng, L. Bover, H. Wang, C. D. Logsdon and V. Ramachandran (2015). "New Blocking Antibodies against Novel AGR2-C4.4A Pathway Reduce Growth and Metastasis of Pancreatic Tumors and Increase Survival in Mice." Mol Cancer Ther **14**(4): 941-951.DOI: 10.1158/1535-7163.MCT-14-0470.

Bailey, J. M., A. M. Hendley, K. J. Lafaro, M. A. Pruski, N. C. Jones, J. Alsina, M. Younes, A. Maitra, F. McAllister, C. A. Iacobuzio-Donahue and S. D. Leach (2016). "p53 mutations cooperate with oncogenic Kras to promote adenocarcinoma from pancreatic ductal cells." Oncogene **35**(32): 4282-4288.DOI: 10.1038/onc.2015.441.

Bapat, A. A., G. Hostetter, D. D. Von Hoff and H. Han (2011). "Perineural invasion and associated pain in pancreatic cancer." Nat Rev Cancer **11**(10): 695-707.DOI: 10.1038/nrc3131.

Bardeesy, N., A. J. Aguirre, G. C. Chu, K. H. Cheng, L. V. Lopez, A. F. Hezel, B. Feng, C. Brennan, R. Weissleder, U. Mahmood, D. Hanahan, M. S. Redston, L. Chin and R. A. Depinho (2006). "Both p16(Ink4a) and the p19(Arf)-p53 pathway constrain progression of pancreatic adenocarcinoma in the mouse." Proc Natl Acad Sci U S A **103**(15): 5947-5952.DOI: 10.1073/pnas.0601273103.

Bardeesy, N., K. H. Cheng, J. H. Berger, G. C. Chu, J. Pahler, P. Olson, A. F. Hezel, J. Horner, G. Y. Lauwers, D. Hanahan and R. A. DePinho (2006). "Smad4 is dispensable for normal pancreas development yet critical in progression and tumor biology of pancreas cancer." Genes Dev **20**(22): 3130-3146.DOI: 10.1101/gad.1478706.

Bardeesy, N. and R. A. DePinho (2002). "Pancreatic cancer biology and genetics." Nat Rev Cancer **2**(12): 897-909.DOI: 10.1038/nrc949.

Brychtova, V., A. Mohtar, B. Vojtesek and T. R. Hupp (2015). "Mechanisms of anterior gradient-2 regulation and function in cancer." Semin Cancer Biol **33**: 16-24.DOI: 10.1016/j.semcancer.2015.04.005.

Brychtova, V., B. Vojtesek and R. Hrstka (2011). "Anterior gradient 2: a novel player in tumor cell biology." Cancer Lett **304**(1): 1-7.DOI: 10.1016/j.canlet.2010.12.023.

Caldas, C. and S. E. Kern (1995). "K-ras mutation and pancreatic adenocarcinoma." Int J Pancreatol **18**(1): 1-6.DOI: 10.1007/BF02825415.

Camp, E. R., C. Wang, E. C. Little, P. M. Watson, K. F. Pirollo, A. Rait, D. J. Cole, E. H. Chang and D. K. Watson (2013). "Transferrin receptor targeting nanomedicine delivering wild-type p53 gene sensitizes pancreatic cancer to gemcitabine therapy." Cancer Gene Ther **20**(4): 222-228.DOI: 10.1038/cgt.2013.9.

Cancer Genome Atlas Research Network. Electronic address, a. a. d. h. e. and N. Cancer Genome Atlas Research (2017). "Integrated Genomic Characterization of Pancreatic Ductal Adenocarcinoma." Cancer Cell **32**(2): 185-203 e113.DOI: 10.1016/j.ccell.2017.07.007.
Cheng, T., Z. Zhang, Z. Jian, S. Raulefs, A. M. Schlitter, K. Steiger, N. Maeritz, Y. Zhao, S. Shen, X. Zou, G. O. Ceyhan, H. Friess, J. Kleeff, C. W. Michalski and B. Kong (2019). "Ductal obstruction promotes formation of preneoplastic lesions from the pancreatic ductal compartment." Int J Cancer **144**(10): 2529-2538.DOI: 10.1002/ijc.31981.
Cheok, C. F., C. S. Verma, J. Baselga and D. P. Lane (2011). "Translating p53 into the clinic." Nat Rev Clin Oncol **8**(1): 25-37.DOI: 10.1038/nrclinonc.2010.174.
Clark, V. E., A. S. Harmanci, H. Bai, M. W. Youngblood, T. I. Lee, J. F. Baranoski, A. G. Ercan-Sencicek, B. J. Abraham, A. S. Weintraub, D. Hnisz, M. Simon, B. Krischek, E. Z. Erson-Omay, O. Henegariu, G. Carrion-Grant, K. Mishra-Gorur, D. Duran, J. E. Goldmann, J. Schramm, R. Goldbrunner, J. M. Piepmeier, A. O. Vortmeyer, J. M. Gunel, K. Bilguvar, K. Yasuno, R. A. Young and M. Gunel (2016). "Recurrent somatic mutations in POLR2A define a distinct subset of meningiomas." Nat Genet **48**(10): 1253-1259.DOI: 10.1038/ng.3651.
Collins, M. A., F. Bednar, Y. Zhang, J. C. Brisset, S. Galban, C. J. Galban, S. Rakshit, K. S. Flannagan, N. V. Adsay and M. Pasca di Magliano (2012). "Oncogenic Kras is required for both the initiation and maintenance of pancreatic cancer in mice." J Clin Invest **122**(2): 639-653.DOI: 10.1172/JCI59227.
Day, J. D., J. A. Digiuseppe, C. Yeo, M. Lai-Goldman, S. M. Anderson, S. N. Goodman, S. E. Kern and R. H. Hruban (1996). "Immunohistochemical evaluation of HER-2/neu expression in pancreatic adenocarcinoma and pancreatic intraepithelial neoplasms." Hum Pathol **27**(2): 119-124.DOI: 10.1016/s0046-8177(96)90364-0.
Derheimer, F. A., H. M. O'Hagan, H. M. Krueger, S. Hanasoge, M. T. Paulsen and M. Ljungman (2007). "RPA and ATR link transcriptional stress to p53." Proc Natl Acad Sci U S A **104**(31): 12778-12783.DOI: 10.1073/pnas.0705317104.
Dumartin, L., W. Alrawashdeh, S. M. Trabulo, T. P. Radon, K. Steiger, R. M. Feakins, M. P. di Magliano, C. Heeschen, I. Esposito, N. R. Lemoine and T. Crnogorac-Jurcevic (2017). "ER stress protein AGR2 precedes and is involved in the regulation of pancreatic cancer initiation." Oncogene **36**(22): 3094-3103.DOI: 10.1038/onc.2016.459.
Ferreira, R. M. M., R. Sancho, H. A. Messal, E. Nye, B. Spencer-Dene, R. K. Stone, G. Stamp, I. Rosewell, A. Quaglia and A. Behrens (2017). "Duct- and Acinar-Derived Pancreatic Ductal Adenocarcinomas Show Distinct Tumor Progression and Marker Expression." Cell Rep **21**(4): 966-978.DOI: 10.1016/j.celrep.2017.09.093.
Fessart, D., C. Domblides, T. Avril, L. A. Eriksson, H. Begueret, R. Pineau, C. Malrieux, N. Dugot-Senant, C. Lucchesi, E. Chevet and F. Delom (2016). "Secretion of protein disulphide isomerase AGR2 confers tumorigenic properties." Elife **5**.DOI: 10.7554/eLife.13887.
Fletcher, G. C., S. Patel, K. Tyson, P. J. Adam, M. Schenker, J. A. Loader, L. Daviet, P. Legrain, R. Parekh, A. L. Harris and J. A. Terrett (2003). "hAG-2 and hAG-3, human homologues of genes involved in differentiation, are associated with oestrogen

receptor-positive breast tumours and interact with metastasis gene C4.4a and dystroglycan." Br J Cancer **88**(4): 579-585.DOI: 10.1038/sj.bjc.6600740.
Forget, D., A. A. Lacombe, P. Cloutier, R. Al-Khoury, A. Bouchard, M. Lavallee-Adam, D. Faubert, C. Jeronimo, M. Blanchette and B. Coulombe (2010). "The protein interaction network of the human transcription machinery reveals a role for the conserved GTPase RPAP4/GPN1 and microtubule assembly in nuclear import and biogenesis of RNA polymerase II." Mol Cell Proteomics **9**(12): 2827-2839.DOI: 10.1074/mcp.M110.003616.
Fritzsche, F. R., E. Dahl, S. Pahl, M. Burkhardt, J. Luo, E. Mayordomo, T. Gansukh, A. Dankof, R. Knuechel, C. Denkert, K. J. Winzer, M. Dietel and G. Kristiansen (2006). "Prognostic relevance of AGR2 expression in breast cancer." Clin Cancer Res **12**(6): 1728-1734.DOI: 10.1158/1078-0432.CCR-05-2057.
Garri, C., S. Howell, K. Tiemann, A. Tiffany, F. Jalali-Yazdi, M. M. Alba, J. E. Katz, T. T. Takahashi, R. Landgraf, M. E. Gross, R. W. Roberts and K. Kani (2018). "Identification, characterization and application of a new peptide against anterior gradient homolog 2 (AGR2)." Oncotarget **9**(44): 27363-27379.DOI: 10.18632/oncotarget.25221.
Guerra, C., A. J. Schuhmacher, M. Cañamero, P. J. Grippo, L. Verdaguer, L. Pérez-Gallego, P. Dubus, E. P. Sandgren and M. Barbacid (2007). "Chronic pancreatitis is essential for induction of pancreatic ductal adenocarcinoma by K-Ras oncogenes in adult mice." Cancer Cell **11**(3): 291-302.DOI: 10.1016/j.ccr.2007.01.012.
Guo, H., H. Chen, Q. Zhu, X. Yu, R. Rong, S. B. Merugu, H. B. Mangukiya and D. Li (2016). "A humanized monoclonal antibody targeting secreted anterior gradient 2 effectively inhibits the xenograft tumor growth." Biochem Biophys Res Commun **475**(1): 57-63.DOI: 10.1016/j.bbrc.2016.05.033.
Haeberle, L. and I. Esposito (2019). "Pathology of pancreatic cancer." Transl Gastroenterol Hepatol **4**: 50.DOI: 10.21037/tgh.2019.06.02.
Hammel, P., F. Huguet, J. L. van Laethem, D. Goldstein, B. Glimelius, P. Artru, I. Borbath, O. Bouche, J. Shannon, T. Andre, L. Mineur, B. Chibaudel, F. Bonnetain, C. Louvet and L. A. P. T. Group (2016). "Effect of Chemoradiotherapy vs Chemotherapy on Survival in Patients With Locally Advanced Pancreatic Cancer Controlled After 4 Months of Gemcitabine With or Without Erlotinib: The LAP07 Randomized Clinical Trial." JAMA **315**(17): 1844-1853.DOI: 10.1001/jama.2016.4324.
Healy, A. R., D. R. Houston, L. Remnant, A.-S. Huart, V. Brychtova, M. M. Maslon, O. Meers, P. Muller, A. Krejci, E. A. Blackburn, B. Vojtesek, L. Hernychova, M. D. Walkinashaw, N. J. Westwood and T. R. Hupp (2015). "Discovery of a novel ligand that modulates the protein–protein interactions of the AAA+ superfamily oncoprotein reptin." Chemical science **6**(5): 3109-3116.DOI: 10.1039/c4sc03885a.
Hezel, B., I. Lesanovsky and P. Schmelcher (2006). "Controlling ultracold Rydberg atoms in the quantum regime." Phys Rev Lett **97**(22): 223001.DOI: 10.1103/PhysRevLett.97.223001.
Hingorani, S. R., E. F. Petricoin, A. Maitra, V. Rajapakse, C. King, M. A. Jacobetz, S. Ross, T. P. Conrads, T. D. Veenstra, B. A. Hitt, Y. Kawaguchi, D. Johann, L. A. Liotta, H. C. Crawford, M. E. Putt, T. Jacks, C. V. Wright, R. H. Hruban, A. M. Lowy and D. A. Tuveson (2003). "Preinvasive and invasive ductal pancreatic cancer and its early

detection in the mouse." Cancer Cell **4**(6): 437-450.DOI: 10.1016/s1535-6108(03)00309-x.
Hosein, A. N., R. A. Brekken and A. Maitra (2020). "Pancreatic cancer stroma: an update on therapeutic targeting strategies." Nat Rev Gastroenterol Hepatol **17**(8): 487-505.DOI: 10.1038/s41575-020-0300-1.
Hou, S., D. Qu, Y. Li, B. Zhu, D. Liang, X. Wei, W. Tang, Q. Zhang, J. Hao, W. Guo, W. Wang, S. Zhao, Q. Wang, S. Azam, M. Khan, H. Zhao, L. Zhang and H. Lei (2019). "XAB2 depletion induces intron retention in POLR2A to impair global transcription and promote cellular senescence." Nucleic Acids Res **47**(15): 8239-8254.DOI: 10.1093/nar/gkz532.
Hrstka, R., P. Bouchalova, E. Michalova, E. Matoulkova, P. Muller, P. J. Coates and B. Vojtesek (2016). "AGR2 oncoprotein inhibits p38 MAPK and p53 activation through a DUSP10-mediated regulatory pathway." Mol Oncol **10**(5): 652-662.DOI: 10.1016/j.molonc.2015.12.003.
Hrstka, R., V. Brychtova, P. Fabian, B. Vojtesek and M. Svoboda (2013). "AGR2 predicts tamoxifen resistance in postmenopausal breast cancer patients." Dis Markers **35**(4): 207-212.DOI: 10.1155/2013/761537.
Hrstka, R., J. Podhorec, R. Nenutil, L. Sommerova, J. Obacz, M. Durech, J. Faktor, P. Bouchal, H. Skoupilova and B. Vojtesek (2017). "Tamoxifen-Dependent Induction of AGR2 Is Associated with Increased Aggressiveness of Endometrial Cancer Cells." Cancer Invest **35**(5): 313-324.DOI: 10.1080/07357907.2017.1309546.
Hruban, R. H., K. Takaori, D. S. Klimstra, N. V. Adsay, J. Albores-Saavedra, A. V. Biankin, S. A. Biankin, C. Compton, N. Fukushima, T. Furukawa, M. Goggins, Y. Kato, G. Kloppel, D. S. Longnecker, J. Luttges, A. Maitra, G. J. Offerhaus, M. Shimizu and S. Yonezawa (2004). "An illustrated consensus on the classification of pancreatic intraepithelial neoplasia and intraductal papillary mucinous neoplasms." Am J Surg Pathol **28**(8): 977-987.DOI: 10.1097/01.pas.0000126675.59108.80.
Hu, Z., Y. Gu, B. Han, J. Zhang, Z. Li, K. Tian, C. Y. Young and H. Yuan (2012). "Knockdown of AGR2 induces cellular senescence in prostate cancer cells." Carcinogenesis **33**(6): 1178-1186.DOI: 10.1093/carcin/bgs141.
Ilic, M. and I. Ilic (2016). "Epidemiology of pancreatic cancer." World J Gastroenterol **22**(44): 9694-9705.DOI: 10.3748/wjg.v22.i44.9694.
Ji, B., L. Tsou, H. Wang, S. Gaiser, D. Z. Chang, J. Daniluk, Y. Bi, T. Grote, D. S. Longnecker and C. D. Logsdon (2009). "Ras activity levels control the development of pancreatic diseases." Gastroenterology **137**(3): 1072-1082, 1082 e1071-1076.DOI: 10.1053/j.gastro.2009.05.052.
Joerger, A. C. and A. R. Fersht (2016). "The p53 Pathway: Origins, Inactivation in Cancer, and Emerging Therapeutic Approaches." Annu Rev Biochem **85**: 375-404.DOI: 10.1146/annurev-biochem-060815-014710.
Kamisawa, T., L. D. Wood, T. Itoi and K. Takaori (2016). "Pancreatic cancer." Lancet **388**(10039): 73-85.DOI: 10.1016/S0140-6736(16)00141-0.
Kleeff, J., D. C. Whitcomb, T. Shimosegawa, I. Esposito, M. M. Lerch, T. Gress, J. Mayerle, A. M. Drewes, V. Rebours, F. Akisik, J. E. D. Munoz and J. P. Neoptolemos (2017). "Chronic pancreatitis." Nat Rev Dis Primers **3**: 17060.DOI:

10.1038/nrdp.2017.60.
Klimstra, D. S., M. B. Pitman and R. H. Hruban (2009). "An algorithmic approach to the diagnosis of pancreatic neoplasms." Arch Pathol Lab Med **133**(3): 454-464.DOI: 10.1043/1543-2165-133.3.454.
Kondo, N., Y. Murakami, K. Uemura, T. Sudo, Y. Hashimoto, A. Nakashima and T. Sueda (2012). "Combined analysis of dihydropyrimidine dehydrogenase and human equilibrative nucleoside transporter 1 expression predicts survival of pancreatic carcinoma patients treated with adjuvant gemcitabine plus S-1 chemotherapy after surgical resection." Ann Surg Oncol **19 Suppl 3**: S646-655.DOI: 10.1245/s10434-011-2140-2.
Kong, B., P. Bruns, N. A. Behler, L. Chang, A. M. Schlitter, J. Cao, A. Gewies, J. Ruland, S. Fritzsche, N. Valkovskaya, Z. Jian, I. Regel, S. Raulefs, M. Irmler, J. Beckers, H. Friess, M. Erkan, N. S. Mueller, S. Roth, T. Hackert, I. Esposito, F. J. Theis, J. Kleeff and C. W. Michalski (2018). "Dynamic landscape of pancreatic carcinogenesis reveals early molecular networks of malignancy." Gut **67**(1): 146-156.DOI: 10.1136/gutjnl-2015-310913.
Kong, B., T. Cheng, C. Qian, W. Wu, K. Steiger, J. Cao, A. M. Schlitter, I. Regel, S. Raulefs, H. Friess, M. Erkan, I. Esposito, J. Kleeff and C. W. Michalski (2015). "Pancreas-specific activation of mTOR and loss of p53 induce tumors reminiscent of acinar cell carcinoma." Mol Cancer **14**: 212.DOI: 10.1186/s12943-015-0483-1.
Kong, B., C. W. Michalski, M. Erkan, H. Friess and J. Kleeff (2011). "From tissue turnover to the cell of origin for pancreatic cancer." Nat Rev Gastroenterol Hepatol **8**(8): 467-472.DOI: 10.1038/nrgastro.2011.114.
Kopp, J. L., G. von Figura, E. Mayes, F.-F. Liu, C. L. Dubois, J. P. Morris IV, F. C. Pan, H. Akiyama, C. V. Wright, K. Jensen, M. Hebrok and S. Maike (2012). "Identification of Sox9-dependent acinar-to-ductal reprogramming as the principal mechanism for initiation of pancreatic ductal adenocarcinoma." Cancer Cell **22**(6): 737-750.DOI: 10.1016/j.ccr.2012.10.025.
Kopp, J. L., G. von Figura, E. Mayes, F.-F. Liu, C. L. Dubois, J. P. Morris IV, F. C. Pan, H. Akiyama, C. V. Wright, K. Jensen, M. Hebrok and M. Sander (2012). "Identification of Sox9-dependent acinar-to-ductal reprogramming as the principal mechanism for initiation of pancreatic ductal adenocarcinoma." Cancer Cell **22**(6): 737-750.DOI: 10.1016/j.ccr.2012.10.025.
Kuleshov, M. V., M. R. Jones, A. D. Rouillard, N. F. Fernandez, Q. Duan, Z. Wang, S. Koplev, S. L. Jenkins, K. M. Jagodnik, A. Lachmann, M. G. McDermott, C. D. Monteiro, G. W. Gundersen and A. Ma'ayan (2016). "Enrichr: a comprehensive gene set enrichment analysis web server 2016 update." Nucleic Acids Res **44**(W1): W90-97.DOI: 10.1093/nar/gkw377.
Li, Z., Q. Zhu, H. Chen, L. Hu, H. Negi, Y. Zheng, Y. Ahmed, Z. Wu and D. Li (2016). "Binding of anterior gradient 2 and estrogen receptor-alpha: Dual critical roles in enhancing fulvestrant resistance and IGF-1-induced tumorigenesis of breast cancer." Cancer Lett **377**(1): 32-43.DOI: 10.1016/j.canlet.2016.04.003.
Li, Z., Q. Zhu, L. Hu, H. Chen, Z. Wu and D. Li (2015). "Anterior gradient 2 is a binding stabilizer of hypoxia inducible factor‐1α that enhances CoCl2‐induced doxorubicin

resistance in breast cancer cells." Cancer Science **106**(8): 1041-1049.DOI: 10.1111/cas.12714.
Lian, Z., A. Karpikov, J. Lian, M. C. Mahajan, S. Hartman, M. Gerstein, M. Snyder and S. M. Weissman (2008). "A genomic analysis of RNA polymerase II modification and chromatin architecture related to 3' end RNA polyadenylation." Genome Res **18**(8): 1224-1237.DOI: 10.1101/gr.075804.107.
Lindell, T. J., F. Weinberg, P. W. Morris, R. G. Roeder and W. J. Rutter (1970). "Specific inhibition of nuclear RNA polymerase II by alpha-amanitin." Science **170**(3956): 447-449.DOI: 10.1126/science.170.3956.447.
Liou, G. Y., H. Doppler, U. B. Braun, R. Panayiotou, M. Scotti Buzhardt, D. C. Radisky, H. C. Crawford, A. P. Fields, N. R. Murray, Q. J. Wang, M. Leitges and P. Storz (2015). "Protein kinase D1 drives pancreatic acinar cell reprogramming and progression to intraepithelial neoplasia." Nat Commun **6**: 6200.DOI: 10.1038/ncomms7200.
Liu, Q. G., Y. J. Li and L. Yao (2018). "Knockdown of AGR2 induces cell apoptosis and reduces chemotherapy resistance of pancreatic cancer cells with the involvement of ERK/AKT axis." Pancreatology **18**(6): 678-688.DOI: 10.1016/j.pan.2018.07.003.
Liu, Y., X. Zhang, C. Han, G. Wan, X. Huang, C. Ivan, D. Jiang, C. Rodriguez-Aguayo, G. Lopez-Berestein, P. H. Rao, D. M. Maru, A. Pahl, X. He, A. K. Sood, L. M. Ellis, J. Anderl and X. Lu (2015). "TP53 loss creates therapeutic vulnerability in colorectal cancer." Nature **520**(7549): 697-701.DOI: 10.1038/nature14418.
Love, M. I., W. Huber and S. Anders (2014). "Moderated estimation of fold change and dispersion for RNA-seq data with DESeq2." Genome Biol **15**(12): 550.DOI: 10.1186/s13059-014-0550-8.
Magnuson, M. A. and A. B. Osipovich (2013). "Pancreas-specific Cre driver lines and considerations for their prudent use." Cell Metab **18**(1): 9-20.DOI: 10.1016/j.cmet.2013.06.011.
Maitra, A. and R. H. Hruban (2008). "Pancreatic cancer." Annu Rev Pathol **3**: 157-188.DOI: 10.1146/annurev.pathmechdis.3.121806.154305.
Maslon, M. M., R. Hrstka, B. Vojtesek and T. R. Hupp (2010). "A divergent substrate-binding loop within the pro-oncogenic protein anterior gradient-2 forms a docking site for Reptin." Journal of molecular biology **404**(3): 418-438.DOI: 10.1016/j.jmb.2010.09.035.
McGuigan, A., P. Kelly, R. C. Turkington, C. Jones, H. G. Coleman and R. S. McCain (2018). "Pancreatic cancer: A review of clinical diagnosis, epidemiology, treatment and outcomes." World J Gastroenterol **24**(43): 4846-4861.DOI: 10.3748/wjg.v24.i43.4846.
Mellon, I., V. A. Bohr, C. A. Smith and P. C. Hanawalt (1986). "Preferential DNA repair of an active gene in human cells." Proc Natl Acad Sci U S A **83**(23): 8878-8882.DOI: 10.1073/pnas.83.23.8878.
Midha, S., S. Chawla and P. K. Garg (2016). "Modifiable and non-modifiable risk factors for pancreatic cancer: A review." Cancer Lett **381**(1): 269-277.DOI: 10.1016/j.canlet.2016.07.022.
Milewski, D., D. Balli, V. Ustiyan, T. Le, H. Dienemann, A. Warth, K. Breuhahn, J. A. Whitsett, V. V. Kalinichenko and T. V. Kalin (2017). "FOXM1 activates AGR2 and causes progression of lung adenomas into invasive mucinous adenocarcinomas."

PLoS Genet **13**(12): e1007097.DOI: 10.1371/journal.pgen.1007097.
Mohtar, M. A., L. Hernychova, J. R. O'Neill, M. L. Lawrence, E. Murray, B. Vojtesek and T. R. Hupp (2018). "The Sequence-specific Peptide-binding Activity of the Protein Sulfide Isomerase AGR2 Directs Its Stable Binding to the Oncogenic Receptor EpCAM." Mol Cell Proteomics **17**(4): 737-763.DOI: 10.1074/mcp.RA118.000573.
Morris, J. P., D. A. Cano, S. Sekine, S. C. Wang and M. Hebrok (2010). "β-catenin blocks Kras-dependent reprogramming of acini into pancreatic cancer precursor lesions in mice." The Journal of clinical investigation **120**(2): 508-520.DOI: 10.1172/JCI40045.
Murray, E., E. O. McKenna, L. R. Burch, J. Dillon, P. Langridge-Smith, W. Kolch, A. Pitt and T. R. Hupp (2007). "Microarray-formatted clinical biomarker assay development using peptide aptamers to anterior gradient-2." Biochemistry **46**(48): 13742-13751.DOI: 10.1021/bi7008739.
Murray, E., E. O. McKenna, L. R. Burch, J. Dillon, P. Langridge-Smith, W. Kolch, A. Pitt and T. R. Hupp (2007). "Microarray-formatted clinical biomarker assay development using peptide aptamers to anterior gradient-2." Biochemistry **46**(48): 13742-13751.DOI: 10.1021/bi7008739.
Negi, H., S. B. Merugu, H. B. Mangukiya, Z. Li, B. Zhou, Q. Sehar, S. Kamle, F. U. Yunus, D. S. Mashausi, Z. Wu and D. Li (2019). "Anterior Gradient-2 monoclonal antibody inhibits lung cancer growth and metastasis by upregulating p53 pathway and without exerting any toxicological effects: A preclinical study." Cancer Lett **449**: 125-134.DOI: 10.1016/j.canlet.2019.01.025.
Nevala-Plagemann, C., M. Hidalgo and I. Garrido-Laguna (2020). "From state-of-the-art treatments to novel therapies for advanced-stage pancreatic cancer." Nat Rev Clin Oncol **17**(2): 108-123.DOI: 10.1038/s41571-019-0281-6.
Parekh, S., C. Ziegenhain, B. Vieth, W. Enard and I. Hellmann (2016). "The impact of amplification on differential expression analyses by RNA-seq." Sci Rep **6**: 25533.DOI: 10.1038/srep25533.
Park, S. W., G. Zhen, C. Verhaeghe, Y. Nakagami, L. T. Nguyenvu, A. J. Barczak, N. Killeen and D. J. Erle (2009). "The protein disulfide isomerase AGR2 is essential for production of intestinal mucus." Proc Natl Acad Sci U S A **106**(17): 6950-6955.DOI: 10.1073/pnas.0808722106.
Patel, P., C. Clarke, D. L. Barraclough, T. A. Jowitt, P. S. Rudland, R. Barraclough and L.-Y. Lian (2013). "Metastasis-promoting anterior gradient 2 protein has a dimeric thioredoxin fold structure and a role in cell adhesion." J Mol Biol **425**(5): 929-943.DOI: 10.1016/j.jmb.2012.12.009.
Persson, S., M. Rosenquist, B. Knoblach, R. Khosravi-Far, M. Sommarin and M. Michalak (2005). "Diversity of the protein disulfide isomerase family: identification of breast tumor induced Hag2 and Hag3 as novel members of the protein family." Mol Phylogenet Evol **36**(3): 734-740.DOI: 10.1016/j.ympev.2005.04.002.
Pohler, E., A. L. Craig, J. Cotton, L. Lawrie, J. F. Dillon, P. Ross, N. Kernohan and T. R. Hupp (2004). "The Barrett's antigen anterior gradient-2 silences the p53 transcriptional response to DNA damage." Mol Cell Proteomics **3**(6): 534-547.DOI: 10.1074/mcp.M300089-MCP200.

Ramachandran, V., T. Arumugam, H. Wang and C. D. Logsdon (2008). "Anterior gradient 2 is expressed and secreted during the development of pancreatic cancer and promotes cancer cell survival." Cancer Res **68**(19): 7811-7818.DOI: 10.1158/0008-5472.CAN-08-1320.

Redston, M. S., C. Caldas, A. B. Seymour, R. H. Hruban, L. da Costa, C. J. Yeo and S. E. Kern (1994). "p53 mutations in pancreatic carcinoma and evidence of common involvement of homocopolymer tracts in DNA microdeletions." Cancer Res **54**(11): 3025-3033. Retrive from https://pubmed.ncbi.nlm.nih.gov/8187092/

Rosenbaum, J., S. H. Baek, A. Dutta, W. A. Houry, O. Huber, T. R. Hupp and P. M. Matias (2013). "The emergence of the conserved AAA+ ATPases Pontin and Reptin on the signaling landscape." Sci Signal **6**(266).DOI: 10.1126/scisignal.2003906.

Rosty, C., J. Geradts, N. Sato, R. E. Wilentz, H. Roberts, T. Sohn, J. L. Cameron, C. J. Yeo, R. H. Hruban and M. Goggins (2003). "p16 Inactivation in pancreatic intraepithelial neoplasias (PanINs) arising in patients with chronic pancreatitis." Am J Surg Pathol **27**(12): 1495-1501.DOI: 10.1097/00000478-200312000-00001.

Saif, M. W., I. Merikas, S. Tsimboukis and K. Syrigos (2008). "Erlotinib-induced skin rash. Pathogenesis, clinical significance and management in pancreatic cancer patients." JOP **9**(3): 267-274. Retrieved from https://pubmed.ncbi.nlm.nih.gov/18469438/

Scoggins, C. R., I. M. Meszoely, M. Wada, A. L. Means, L. Yang and S. D. Leach (2000). "p53-dependent acinar cell apoptosis triggers epithelial proliferation in duct-ligated murine pancreas." Am J Physiol Gastrointest Liver Physiol **279**(4): G827-836.DOI: 10.1152/ajpgi.2000.279.4.G827.

Singhi, A. D., E. J. Koay, S. T. Chari and A. Maitra (2019). "Early Detection of Pancreatic Cancer: Opportunities and Challenges." Gastroenterology **156**(7): 2024-2040.DOI: 10.1053/j.gastro.2019.01.259.

Sive, H. L., K. Hattori and H. Weintraub (1989). "Progressive determination during formation of the anteroposterior axis in Xenopus laevis." Cell **58**(1): 171-180.DOI: 10.1016/0092-8674(89)90413-3.

Smeenk, H. G., T. C. Tran, J. Erdmann, C. H. van Eijck and J. Jeekel (2005). "Survival after surgical management of pancreatic adenocarcinoma: does curative and radical surgery truly exist?" Langenbecks Arch Surg **390**(2): 94-103.DOI: 10.1007/s00423-004-0476-9.

Sorokin, A. V., E. R. Kim and L. P. Ovchinnikov (2007). "Nucleocytoplasmic transport of proteins." Biochemistry (Mosc) **72**(13): 1439-1457.DOI: 10.1134/s0006297907130032.

Tseng, S. F., C. Y. Chang, K. J. Wu and S. C. Teng (2005). "Importin KPNA2 is required for proper nuclear localization and multiple functions of NBS1." J Biol Chem **280**(47): 39594-39600.DOI: 10.1074/jbc.M508425200.

Vanderlaag, K. E., S. Hudak, L. Bald, L. Fayadat-Dilman, M. Sathe, J. Grein and M. J. Janatpour (2010). "Anterior gradient-2 plays a critical role in breast cancer cell growth and survival by modulating cyclin D1, estrogen receptor-alpha and survivin." Breast Cancer Res **12**(3): R32.DOI: 10.1186/bcr2586.

Wang, Z., Y. Hao and A. W. Lowe (2008). "The adenocarcinoma-associated antigen,

AGR2, promotes tumor growth, cell migration, and cellular transformation." Cancer Res **68**(2): 492-497.DOI: 10.1158/0008-5472.CAN-07-2930.
Watanabe, S., K. Abe, Y. Anbo and H. Katoh (1995). "Changes in the mouse exocrine pancreas after pancreatic duct ligation: a qualitative and quantitative histological study." Arch Histol Cytol **58**(3): 365-374. Retrieved from https://pubmed.ncbi.nlm.nih.gov/8527243/
Xu, J., Y. Liu, Y. Li, H. Wang, S. Stewart, K. Van der Jeught, P. Agarwal, Y. Zhang, S. Liu, G. Zhao, J. Wan, X. Lu and X. He (2019). "Precise targeting of POLR2A as a therapeutic strategy for human triple negative breast cancer." Nat Nanotechnol **14**(4): 388-397.DOI: 10.1038/s41565-019-0381-6.
Yamaguchi, M., M. C. Steward, K. Smallbone, Y. Sohma, A. Yamamoto, S. B. Ko, T. Kondo and H. Ishiguro (2017). "Bicarbonate‐rich fluid secretion predicted by a computational model of guinea‐pig pancreatic duct epithelium." The Journal of physiology **595**(6): 1947-1972.DOI: 10.1113/JP273306.
Yang, B., J. R. Eshleman, N. A. Berger and S. D. Markowitz (1996). "Wild-type p53 protein potentiates cytotoxicity of therapeutic agents in human colon cancer cells." Clin Cancer Res **2**(10): 1649-1657. Retrieved from https://pubmed.ncbi.nlm.nih.gov/9816112/

# 9.0 LIST OF FIGURES

## 10.0 ACKNOWLEDGEMENTS

I am appreciative of the executive committee of Technische Universität München to carry out my dissertation within the framework of the Doctor Med program. The research work was performed between 09.2016 and 12.2019.

At this point, I would like to thank all those who are directly or indirectly involved in contributed to the development of my dissertation and supported me in the project.

Firstly, I would like to thank Univ. Prof. Dr. med. Helmut Friess for his support of this project.

My special thanks to PD. Dr. Bo Kong for the opportunity and scientific support the preparation of my dissertation in his working group, participation at numerous national and international conferences that are very motivating, understanding, discussion-friendly support.

I would like to thank Prof. Bernhard Holzmann, Prof. Klaus-Peter Janssen, and PD. Melanie Laschinger for helpful advice.

Many thanks to PD. Dr. Bo Kong and Dr. Kathleen Schuck for discussing, reading and correcting the final dissertation.

Many thanks to Ms. Nadja Maeritz for her intensive scientific and dedicated support for the practical part of the work, which is crucial to success and has completed this work.

I would like to thank Dr. Susanne Raulefs for her kindly help and scientific suggestion.

I would like to thank Prof. Dr. Klaus-Peter Janssen who provided HEK293 cells and kindly provided cell lines authentic results.

I would like to thank Dr. Öllinger Rupert and Dr. Thomas Engleitner who performed the RNA-sequencing analysis.

Many thanks to my colleagues of the pancreas research group, Dr. Susanne Raulefs, Dr. Ligong Chang, Dr. Tao Cheng, Dr. Ziying Jian, Dr. Simone Benitz, Yamin Zhao, Jing Cao, Yuanyuan Yu for their kindly supports during my work.

Many thanks to the Scholarship Council of the Ministry of Education of China for funding my study.

Finally, I want to thank my family. I am especially grateful to my beloved father Mr.

Chunfu Zhang, beloved mother Mrs. Yuanhua Li, and kind girlfriend Yuhong Yang who has always been helping me out of difficulties, supporting without a word of complaint, and giving me great confidence all these years.